Masters Theses 1911 - February 2014

2008

Miniaturization of Microstrip Patch Antennas for Gps Applications

Steven S. Holland
University of Massachusetts Amherst

MINIATURIZATION OF MICROSTRIP PATCH ANTENNAS FOR GPS APPLICATIONS

A Thesis Presented

by

STEVEN S. HOLLAND

Submitted to the Graduate School of the
University of Massachusetts Amherst in partial fulfillment
of the requirements for the degree of

MASTER OF SCIENCE IN ELECTRICAL AND COMPUTER ENGINEERING

May 2008

Electrical and Computer Engineering

MINIATURIZATION OF MICROSTRIP PATCH ANTENNAS FOR GPS APPLICATIONS

A Thesis Presented

by

STEVEN S. HOLLAND

Approved as to style and content by:

_____

Daniel H. Schaubert, Chair

_____

David M. Pozar, Member

_____

Marinos N. Vouvakis, Member

_____

C. V. Hollot, Department Head
Electrical and Computer Engineering

To my parents.

ACKNOWLEDGMENTS

ABSTRACT

**MINIATURIZATION OF MICROSTRIP PATCH ANTENNAS FOR GPS
APPLICATIONS**

MAY 2008

STEVEN S. HOLLAND, B.S.E.E., MILWAUKEE SCHOOL OF ENGINEERING

M.S.E.C.E., UNIVERSITY OF MASSACHUSETTS AMHERST

Directed by: Professor Daniel H. Schaubert

The desire to incorporate multiple frequency bands of operation into personal communication devices has led to much research on reducing the size of antennas while maintaining adequate performance. GPS is one such application, where dual frequency operation, bandwidth and circular polarization pose major challenges when using traditional miniaturization techniques. Various loading methods have been studied to reduce the resonant frequency of the antenna – high permittivity dielectric loading, slot loading and cavity loading – while examining their effects on bandwidth and gain. The objective of this thesis is to provide guidelines on what is achievable using these miniaturization methods and insight into how to implement them effectively.

TABLE OF CONTENTS

LIST OF TABLES

LIST OF FIGURES

xvi

CHAPTER 1

INTRODUCTION

1.1 Background of Microstrip Antennas

The microstrip patch antenna first took form in the early 1970's [1], and interest

was renewed in the first microstrip antenna proposed by Deschamps in 1953 [2]. Some

of the benefits of microstrip patch antennas include [4] small profile, low weight and

inexpensive fabrication. Additionally, by changing the shape of the structure, versatility

in resonant frequency, polarization, pattern, and impedance can be achieved. Many

feeding mechanisms are possible for feeding the microstrip patch structure, such as probe

feeds, aperture feeds, microstrip line feeds and proximity feeds, where each method has

advantages depending on the application. Despite these advantages, microstrip antennas

present major challenges to the designer due to an inherently narrow bandwidth, poor

polarization purity and tolerance problems [3]. Much research has been done to

overcome these limitations, notably in increasing the bandwidth.

The compact size of the microstrip patch antenna is advantageous for the

reception of GPS (Global Positioning System) signals by personal communication

devices since it is planar, and does not extend vertically from its mounting surface. The

radiation pattern of the microstrip antenna has broad coverage in the E-plane with a

maximum at broadside [4], which allows good coverage of signals from broadside down

to near the horizon. When two orthogonal modes are excited on the antenna to produce

circular polarization (required for GPS), the broad E-plane patterns are also orthogonally

orientated in space, providing broad coverage in both major planes. This creates an

approximately hemispherical pattern, which is ideal for use in GPS, where multiple satellites are required to accurately determine location [5].

1.2   Motivation for this Study

The motivation for this study evolved from the desire to design a GPS antenna with VSWR 2:1 bandwidth greater than 5MHz at L1 (1.575GHz) and L2 (1.227GHz) when matched to a source impedance Z_o of 50Ω. The gain bandwidth is defined with respect to gain flatness, here required as having a maximum ripple of $\pm$1dB across a bandwidth of at least 20MHz for both L1 and L2, with a goal of 30MHz. Since GPS systems use circular polarization to maximize the received signal, reception of circular polarization is desired with an axial ratio of less than 3dB over the specified gain bandwidth at each band.   The size was to be made as small as possible with a goal of 31.8$\times$31.8$\times$5mm (1.25$\times$1.25$\times$0.2") as a total volume. Some recent work has been done investigating miniaturized microstrip GPS antennas, such as Zhou et al [6] with a 31mm$\times$31mm$\times$12.8mm stacked patch design, Zhou et al [7] with a 38mm$\times$38mm$\times$20mm design, and Guo [8] with a 36$\times$80$\times$6mm antenna. None of these designs met all of the desired specifications.

1.3   GPS Antenna Challenges

While miniaturization of microstrip antennas, in general, is a process of critically choosing performance trade-offs, GPS presents some specific challenges. One challenge is the production of circular polarization with low axial ratio, which limits potential design choices, since many miniaturization methods only support a single linear

polarization. A single probe feeding arrangement on a diagonal axis to generate

orthogonal modes is not suitable, due to its inherently low axial ratio bandwidth – which

becomes even narrower as the bandwidth of each mode is decreased through

miniaturization. The polarization specification, therefore, probably requires a two-axis

symmetric geometry, with two feeds orientated orthogonally in space and fed in

quadrature in order to generate clean circular polarization over a wide bandwidth.

Another family of techniques that do not satisfy the polarization requirements are

modified patch shapes that excite multiple modes. The higher order modes these patch

shapes excite can have drastically varying gain patterns, which in general are different

than that of the fundamental mode of the patch. The two orthogonal probes may also lose

isolation when higher order modes are excited. When multiple resonances are formed

through different path lengths, such as U shaped slots, or E-shaped patches, the patterns

of these resonances are often out of alignment, and the radiation pattern tends to rotate

and shift with changing frequency, limiting them to applications that only require a linear

polarization.

Another limitation posed by GPS antennas is the bandwidth required. While the

actual GPS data occupies a very narrow bandwidth, the signal is encoded using spread

spectrum, resulting in a transmit signal with a bandwidth of approximately 20MHz. At

L1 and L2, this bandwidth translates to (assuming 2:1 VSWR) a fractional bandwidth of

1.26% and 1.63%, respectively. This is obtainable by a standard patch, but such

bandwidths become extremely difficult to obtain when the antenna size is limited. As

discussed in Chapter 2, there is a direct relationship between the bandwidth and the

volume occupied by an antenna. Consequently, many of the methods used to increase the

bandwidth of a patch antenna rely on more efficient use of the antenna volume, or an increase in this volume through stacked patches, coplanar parasitic resonator patches and thick substrates.

Finally, for a GPS system it is desired to have gain of at least isotropic (0dB). GPS relies on spread spectrum, and in addition to the wide bandwidth needed, the signal is at a low power level of -130dBm [9], which is below the noise power of most systems. As a result, loading the antenna with lossy materials, either as dielectric materials with high loss tangents (tanδ) or lumped resistors, are not viable bandwidth enhancement methods for this application.

1.4   Overview of Thesis

In this thesis, studies were conducted to examine three miniaturization methods that have been used to generate potential design solutions for an L1, L2 band GPS system. The loading methods explored are high permittivity dielectric materials, slots in the patch layer, and metallic backing cavities.

Chapter 2 provides a theoretical overview of the derived limits on the Q factor of antennas, starting with the Chu analysis and comparing his solution to exact solutions carried out by Collin and McLean. Some of the gain implications for small antennas are discussed, and finally a comparison is presented between the theoretical limits and the bandwidths achieved with the successful designs from this study.

Chapter 3 presents studies undertaken to characterize some of the effects of the three loading methods, and provides optimized designs using each loading method to show what is achievable by using one or more of these loading methods to miniaturize the

4

patch antenna. Included are both simulation results and measured results from prototypes

that were built and tested over the course of this study

CHAPTER 2

SMALL ANTENNA CONSIDERATIONS

It is well known that the size of the antenna will impact its performance, specifically in terms of bandwidth and gain. In general, antennas can be split into two main types – resonant structures (e.g. microstrip patch antennas, dipoles, loops) and travelling wave structures (e.g. horns, helixes, spirals). Travelling wave antennas range in size from a wavelength up to many 10's of wavelengths in size, and in general have wider bandwidths. This increased bandwidth results from the antennas creating a smooth transition to couple energy from a guided wave to free space radiation as it propagates through the structure. Their larger size also allows for more directive antennas. Conversely, resonant antennas couple energy to free space via a structure proportionate to the operating wavelength, and only efficiently over limited frequency ranges. These antennas typically have dimensions on the order of $\lambda/2$ and multiples thereof. Since their size is less than λ, they also tend to have lower directivity, due to the smaller aperture size. At very small sizes, a class of antennas are known as "electrically small", commonly defined as one that occupies a volume of less than a "radian sphere" (a sphere of radius a $= \lambda_o/2\pi$) [4], equivalent to the definition that ka < 1, where stored energy dominates. Since this study involved antennas operating at a minimum of 1.227GHz, a radian sphere has radius equal to r $= \lambda_o/2\pi = 3.9$cm – much larger than any of the antennas considered in this study. A discussion of some pertinent performance considerations provides useful benchmarks on what is fundamentally possible for the designer.

2.1   Quality Factor Considerations

Bandwidth is often one of the most important design specifications to consider

when an antenna has a size restriction. A helpful figure of merit is the concept of the

"quality factor", also referred to as simply "Q", of a circuit – in this case an antenna.

Fundamentally, in antenna design Q is defined as the ratio of the total time averaged

energy stored in a given volume to the power radiated (i.e. power "loss") [11], and is

defined as

$$
Q = \begin{cases} \dfrac{2\omega\overline{W_e}}{\overline{P_f}} & \overline{W_e} > \overline{W_m} \\[2ex] \dfrac{2\omega\overline{W_m}}{\overline{P_f}} & \overline{W_m} > \overline{W_e} \end{cases}
\tag{2.1}
$$

where $\overline{W_e}$ and $\overline{W_m}$ are the time averaged stored electric and magnetic energies,

respectively, and $\overline{P_f}$ is the power dissipated in radiation. For an antenna, Q is important

because it helps define inherent limits on the physical size of the antenna with respect to

antenna bandwidth and gain. A High Q implies that there is a large amount of energy

stored in the reactive near field [12], which induces large currents on the antenna

structure – leading to high ohmic losses and narrow bandwidth.

The limits of small antenna performance were first analyzed by Wheeler in 1947

using lumped inductor and capacitor modeling [13]. Then, in 1948, Chu [14] developed a

ladder network model relating the Q of an antenna to its physical size, which has been

widely cited as the theoretical limitation to the bandwidth obtainable by antennas of a

given size.   The model enclosed an imaginary sphere of radius "a" around the entire

antenna structure, shown in Figure 1, and expanded the fields generated outside of this sphere in spherical harmonics, essentially the modes of free space.
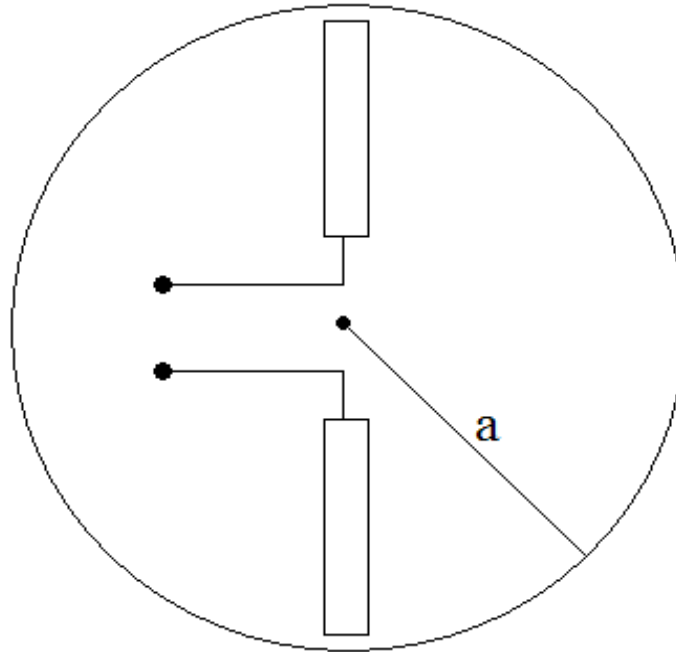
Figure 1 - Sphere enclosing an antenna structure.

A linear antenna with an omnidirectional pattern was assumed inside the sphere, therefore requiring only the set of TM_{n0} modes. Further, the infinite set of discrete spherical TM modes were modeled as a ladder network of L and C components terminated in a resistor R (representing power flow in radiation), shown in Figure 2. This model was extracted from the continued fraction generated by the Legendre polynomials used to expand the fields. This separation into lumped components is possible since the modes outside the sphere are orthogonal, and there is no power coupling between modes – each mode can be considered individually and its contribution superimposed with the other modes.

(a)

(b)
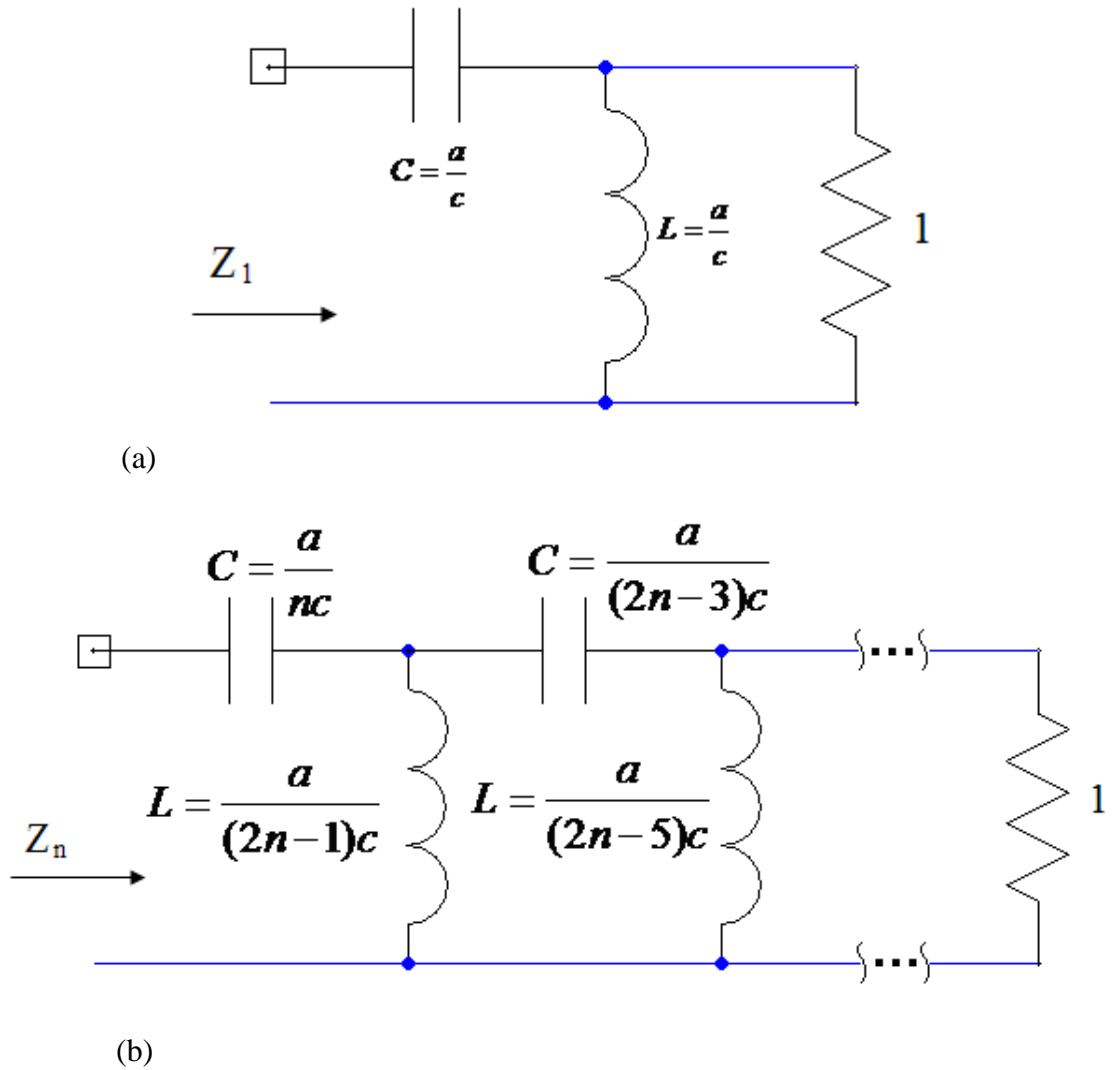
Figure 2 - Circuit Schematic representation of the spherical TM modes, with (a) the TM$_{01}$ mode, and (b) the set of TM$_{n0}$ modes.

These circuits show the TM modes to be high-pass in nature, and, since each L and C are proportional to $\dfrac{a}{c}$ (c = speed of light), increasing the size of the enclosing sphere is analogous to raising the frequency, resulting in more average power coupled to free space. Since, as Chu states, Q is extremely tedious to calculate for the higher order modes, he instead used a simple second order RLC circuit to model all of the TM$_{n0}$ antenna modes around a small frequency range. It was shown in [14] that as ka decreases

below a mode number index, the Q becomes extremely large. This led to the realization

that the lowest order modes, TM_{10} and TM_{10} have the lowest possible Q, since any of the

higher order modes increase the stored energy substantially when ka < 1. The results of

his analysis show that the minimum Q can be approximated as shown in equation 2.2

[15].

$$Q \approx \begin{cases} \dfrac{1+2(ka)^2}{(ka)^3(1+(ka)^2)} \\ \dfrac{1}{(ka)^3} \quad \text{for } ka \ll 1 \end{cases} \tag{2.2}$$

This shows that the Q factor of the antenna is approximately proportional to the inverse

of the volume it occupies. This Q is also only accurate when a single resonance is

considered. However, derivations have been performed using more direct methods of

calculating the Q of an antenna, instead of using the circuit approximation employed by

Chu. In 1964, Collin [12] calculated the exact Q of the first three TM modes by

subtracting the energy associated with the power flow (radiated power) from the total

energy, thereby finding the electric and magnetic stored energies. More recently, in 1996,

McLean [15] found the exact Q of the TM_{10} using a similar subtraction of the propagating

energy from the total energy, except he based his Q calculation solely on the stored

electric energy found. Their calculations arrived at an equivalent expression for the Q of

the TM_{10} mode, equation 3 (see Appendix A for derivation).

$$Q = \frac{1}{k^3 a^3} + \frac{1}{ka} \tag{2.3}$$

Interestingly, this same expression can be obtained by using the circuit approximation for

the TM_{10} shown in Figure 2a, from Chu. This analysis assumes a lossless, ideal antenna,

but can be modified to reflect the reduction in Q from losses by multiplying the Q by the

antenna efficiency [16]

$$Q = \eta_r \left(\frac{1}{k^3 a^3} + \frac{1}{ka} \right) \tag{2.4}$$

where η_r is the antenna radiation efficiency. It is important to account for the loss, as an

antenna can readily be loaded via lumped resistors or lossy materials to achieve

bandwidths that exceed the limits given for a lossless antenna, and may otherwise

mistakenly appear to invalidate the calculated Q limits. Figure 3 shows the effect of

efficiency on the Q limits.
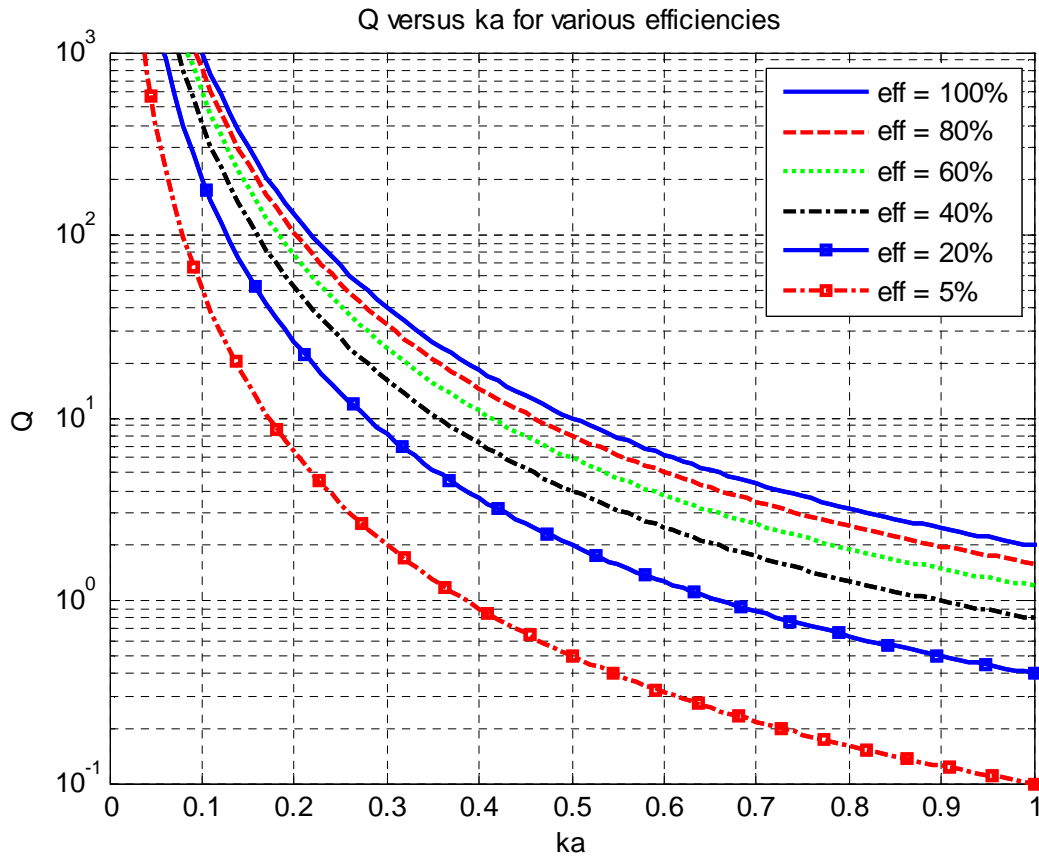
Figure 3 – The minimum Q for various levels of efficiency.

Up to this point, it has been assumed that a linear antenna occupied the volume enclosed by the sphere, but as noted by Chu [14], Wheeler [13], Collin [12] and McLean [15], the antenna Q for dual polarizations exciting TE and TM modes is approximately half that of a single polarization (at very small ka <<1, $Q^{TE+TM} \approx 1/2(ka)^3$). McLean [15] has an especially lucid treatment of this phenomenon, showing that the contribution to stored electric energy increases a slight amount when both the TE_{10} and TM_{10} modes are excited, whereas the radiated power doubles. This derivation (see Appendix A) results in equation 2.5.

$$Q = \frac{1}{2}\left(\frac{1}{k^3 a^3} + \frac{2}{ka}\right) \qquad (2.5)$$

This applies more appropriately for antennas with a single feed, and antennas with high cross-pol, as an equation in [17] provides the more general Q relationship as

$$Q = \eta_r\left(\frac{1}{1+\gamma}\right)\left(\frac{1}{k^3 a^3} + \frac{2}{ka}\right) \qquad (2.6)$$

where γ is the ratio of power in the two polarizations. For this study, where circular polarization is achieved using two orthogonal feeds with quadrature phasing, the Q of each port is only affected by a single linear polarization, thus power is radiated in only one polarization and stored in only one polarization per port, and the VSWR bandwidth seen at the input of each port does not increase. A comparison of the approximate Chu solution and the exact solutions are shown in Figure 4.
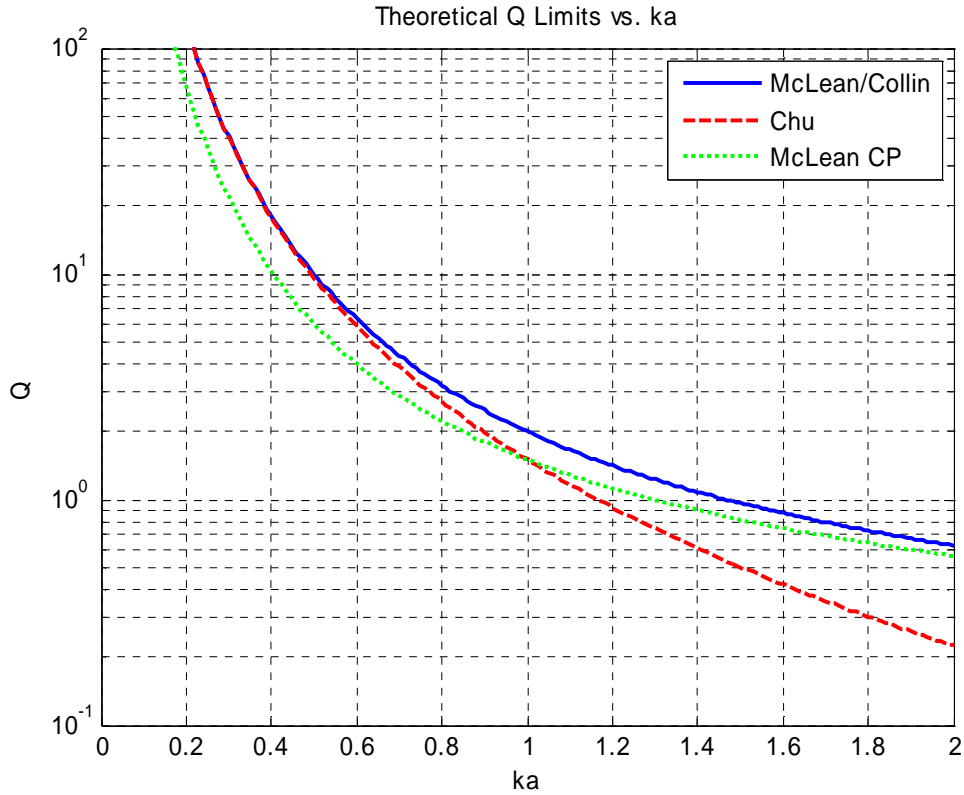
Figure 4 - Comparison of the approximate (Chu) and exact (McLean, Collin) Q limits.

The approximate Chu limit and the exact solution given by McLean and Collin have very good agreement when ka $\ll$ 1, but begin to diverge as ka nears 1. Interestingly, the TM_{01} mode should have the lowest Q out of all of the modes, as Chu found, but the approximation that takes into account higher order modes gives a lower Q than the exact – stressing the limitations of the approximation used by Chu in his derivation.

One method of estimating an antenna's quality factor is to use the input impedance at the terminals of a tuned antenna as it varies with frequency. In [18], Yaghjian and Best developed an approximate relationship between the impedance $Z(\omega) = R(\omega) + jX(\omega)$ of an antenna and the Q of an antenna defined as

$$Q(\omega_o) \approx \frac{\omega_o}{2R(\omega_o)} \sqrt{R'(\omega_o)^2 + \left(X'(\omega_o) + \frac{|X(\omega_o)|}{\omega_o} \right)^2} \qquad (2.7)$$

where $R'(\omega_o)$ and $X'(\omega_o)$ are the frequency derivatives of the resistive and reactive

components. For single band antennas (and for Q >> 1), the Q is often used to

approximate the fractional 3dB bandwidth [4] as shown in equation 2.8.

$$\text{fractional bandwidth} = \frac{f_{upper} - f_{lower}}{f_o} = \frac{\Delta f}{f_o} = \frac{1}{Q} \qquad (2.8)$$

The 3dB bandwidth is equivalent to a VSWR bandwidth of 5.828:1, but for evaluating

the Q with bandwidths defined by different VSWR levels, equation 2.9 can be used [16]

$$Q(\omega_o) \approx \frac{2\sqrt{\beta}}{FBW_V(\omega_o)} \qquad where \quad \sqrt{\beta} = \frac{s-1}{2\sqrt{s}} \leq 1 \qquad (2.9)$$

where FBW_V is the desired bandwidth at s:1 VSWR.

The bandwidth of the antenna is therefore fundamentally bound by theoretically derived

limits, with the linear polarization cases shown in Figure 5.
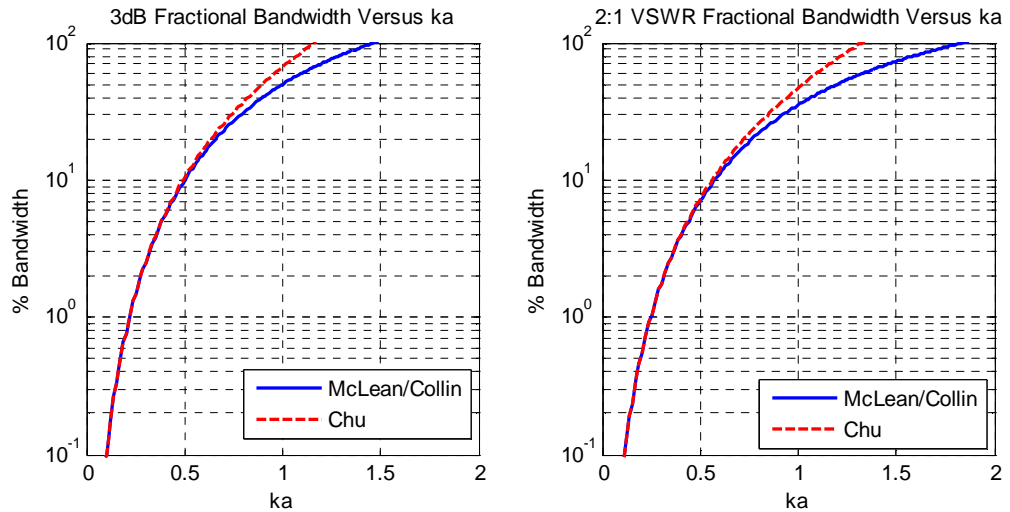
Figure 5 – The theoretical limits on the 3dB and 2:1 VSWR fractional bandwidths versus ka.

2.2 Gain Considerations

Fundamental to antenna theory is the relationship between the radiating aperture size and gain – specifically, that a large aperture will generate higher directivity (and therefore, assuming equal loss, higher gain) than a smaller aperture. The effective aperture of an antenna relates how large of an area over which an antenna efficiently accepts an incoming signal, and is related to the size of an antenna.   It is related to directivity (and therefore gain), and is defined as [10]

$$D = \frac{4\pi}{\lambda^2} A_{eff} \tag{2.10}$$

While for small antennas the effective aperture size is, in general, larger than the physical aperture size, as operating frequency decreases for a fixed antenna size, the effective aperture size will also decrease. For miniaturized antennas, the directivity will be lower than that of a regular antenna, and will have a directivity pattern that broadens, and looks more like an omnidirectional antenna as size is further reduced. However, this is not the only factor working against the gain of small antennas.   The currents of the antenna are confined to a smaller area on the antenna surface, contributing to conductive losses, and stronger fields near the antenna contribute to the stored energy. This increases the Q of the antenna [19], reducing the bandwidth.

An additional reduction in gain is caused by the decreasing radiation resistance as the size of the antenna is reduced, making ohmic losses even more important as they become a sizable fraction of the overall input resistance of an antenna. The radiation efficiency can be expressed as [10]

$$\eta_r = \frac{R_r}{R_r + R_L} \tag{2.11}$$

15

where R_r represents the radiation resistance and R_L represents the losses in the antenna. The losses are typically a result of the conductors and dielectric materials, which are minimized using dielectric materials with as low loss as possible and high-quality conductors. An example of a small antenna with low radiation efficiency is that of an infinitesimal dipole, which has a radiation resistance given by [4]

$$R_r = 80\pi^2 \left(\frac{l}{\lambda}\right)^2 \tag{2.12}$$

Thus, for a range of dipole lengths between $\lambda/1000$ and $\lambda/20$ ($0.001 < l/\lambda < 0.05$), the radiation resistance is a maximum of 2Ω, and a minimum of 0.0008Ω, shown in Figure 6. This small radiation resistance is also important when the loss of the antenna structure is taken into account. Staying with the example of an infinitesimal dipole, the same antenna length variation is considered, but the efficiency is calculated using four different equivalent loss impedances in the antenna model, as shown in Figure 7.
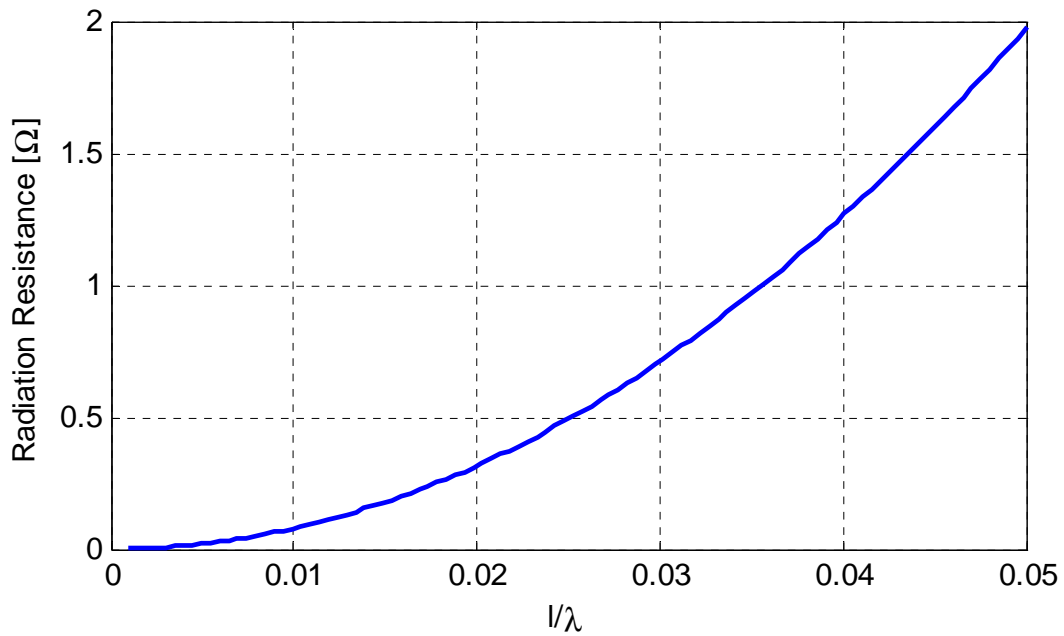
Figure 6 - Radiation Resistance for infinitesimal dipole versus length.
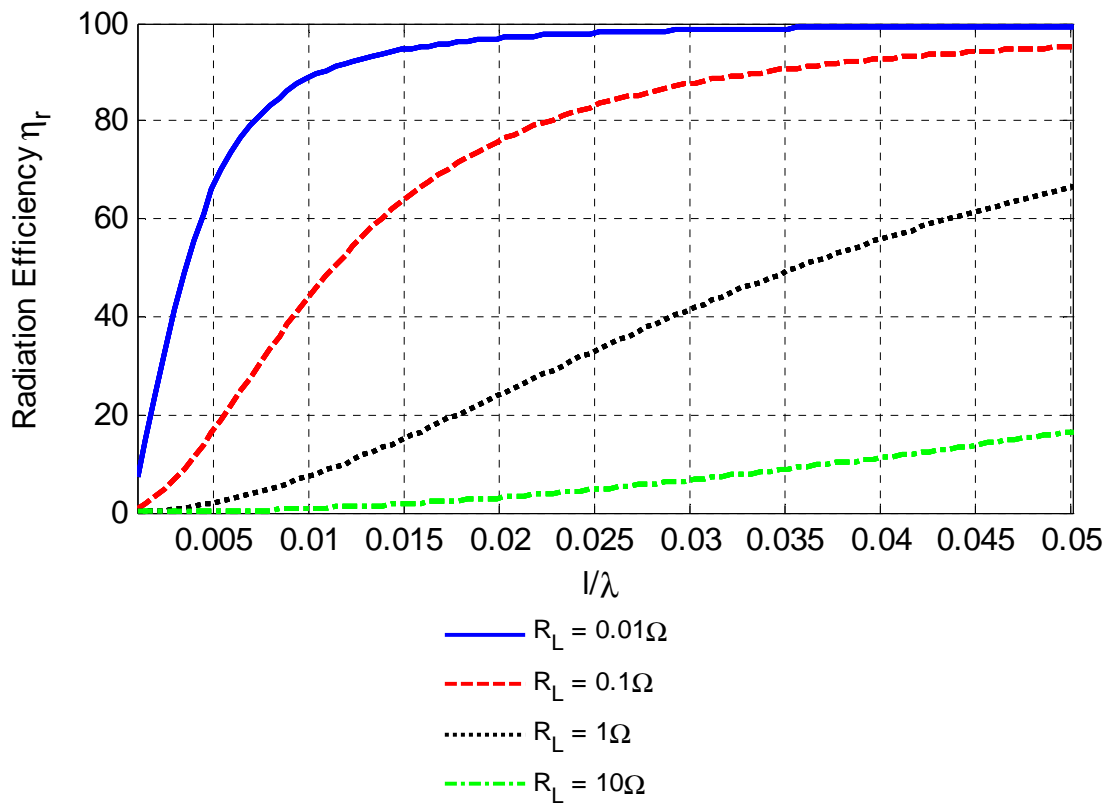
Figure 7 – The effect on of loss resistance R_L on radiation efficiency versus the length of an infinitesimal dipole relative to operating wavelength.

This efficiency problem will impact the gain, and it will also contribute to the noise temperature of the antenna. The gain will already be limited by the size of the antenna and the reduced radiation resistance, so for successful miniaturization of an antenna, losses in the antenna should be minimized. Gain can be traded for bandwidth fairly easily by loading an antenna with lossy material, or a lumped resistor, which lowers the Q and increases the bandwidth, but reduces the gain. As a result, methods of miniaturization often seek solutions that optimize bandwidth by making the most efficient use of the volume enclosed by the antenna, ideally maximizing both gain and bandwidth.

2.3   Recent Research on Electrically Small Antennas

There has been much interest in reducing the size of antennas. Hum et al [20] studied the effects of resistively loading a microstrip patch antenna, with the objective to find loading locations that provided the best tradeoff between reduction in gain and increase in bandwidth. Karmaker [21] developed a design for a cavity backed circular microstrip patch antenna that incorporated an air gap between the substrate and ground plane, an LC matching network, a loading capacitor and a ferrite loading bead to reduce the size of the antenna and retain fairly good bandwidth performance. Wang and Tsai [22] investigated the use of meander-line loading of the patch antenna which effectively increases the length of the current paths, but does so over a small area. The use of meander lines parallels the phenomenon behind slot loading, which is discussed in section 3.2. Zhou et al has produced a number of small GPS antenna designs, with a 33mm×14mm (diameter × height) circular stacked patch configuration in [23], and a

18

31×31×12.4 stacked patch design [6], both of which cover L1, L2 and L5 by reducing

constraints on the VSWR bandwidth. It is noted that while much of the research

presented in this section has led to successful designs, none accomplished a match of 2:1

over the bands of interest, which was one of the design motivations for this study.

As a comparison, some of the more successful design approaches in this study are

plotted, showing their proximity to the bandwidth limits in Figure 8 and Figure 9.

Included are two antennas of Zhou, shown for comparison. None of the designs approach

the line, but this is mainly due to the patch geometry only filling a fraction of the sphere

enclosing the antenna- all of these antennas are planar.

Figure 8 shows that Zhou's antenna, [23], has the largest 3dB bandwidth of all of

the antennas considered, 95MHz. Figure 9 shows that for the same antenna, neither band

has a 2:1 VSWR match, and emphasizes the difference between the antennas presented in

this thesis and those in the literature. There are many designs in the literature that achieve

the wide gain bandwidths required for GPS, notably the two designs of Zhou, et al, shown

for comparison, but they achieve their large bandwidths via a poor match at the bands of

interest. The Bode-Fano criteria indicates that the 3dB bandwidth can be broadened at

the expense of a good impedance match. In antenna design it is normally desired to have

a match of at least 2:1 VSWR, especially in a GPS system where noise considerations

require a proper match. All of the optimized designs presented in this thesis obtain 2:1

VSWR matches at both L1 and L2 bands.
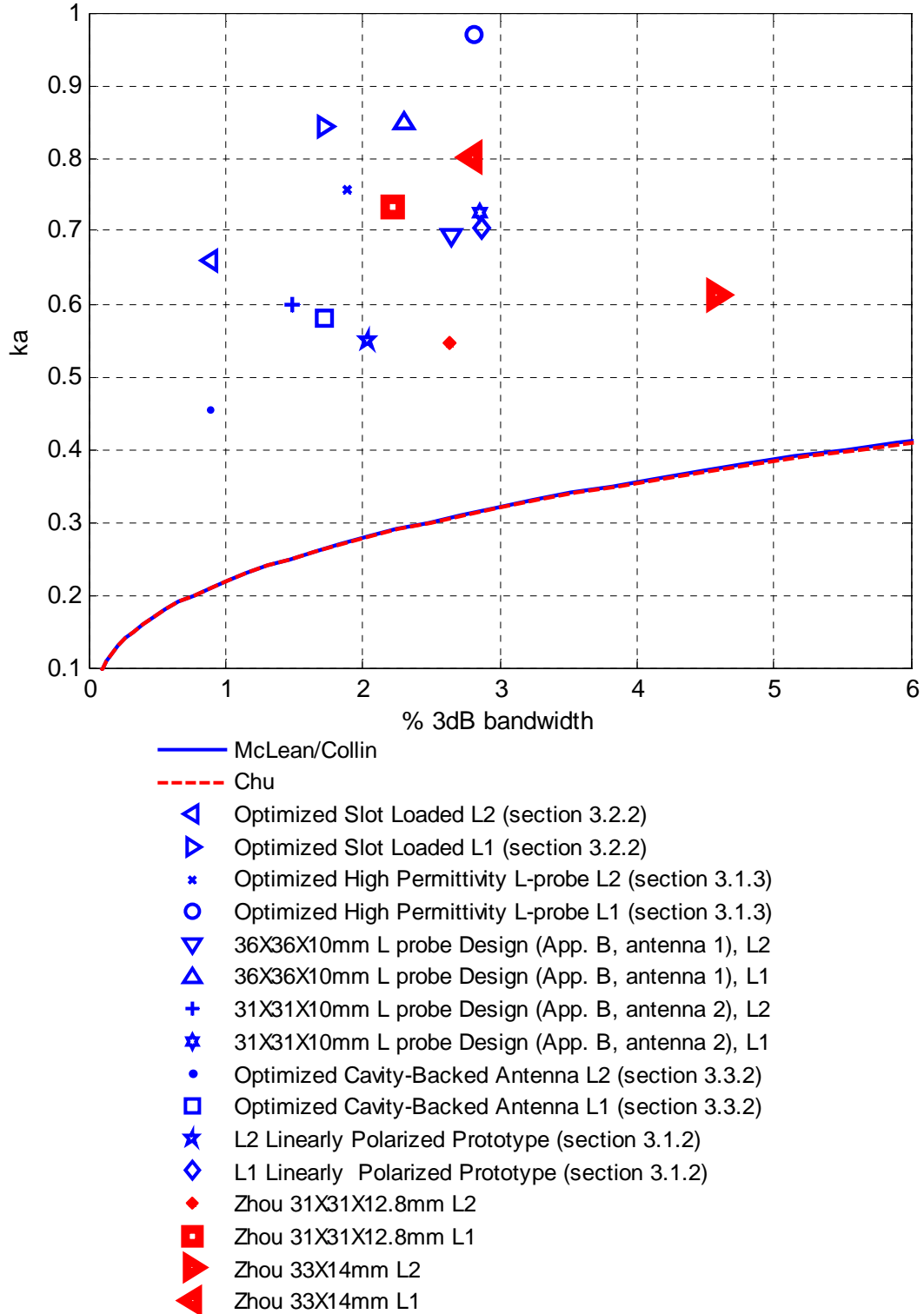
Figure 8 – Comparison of designs developed throughout this study and the theoretical 3dB bandwidth limits. The antennas are denoted by the symbols in the legend.
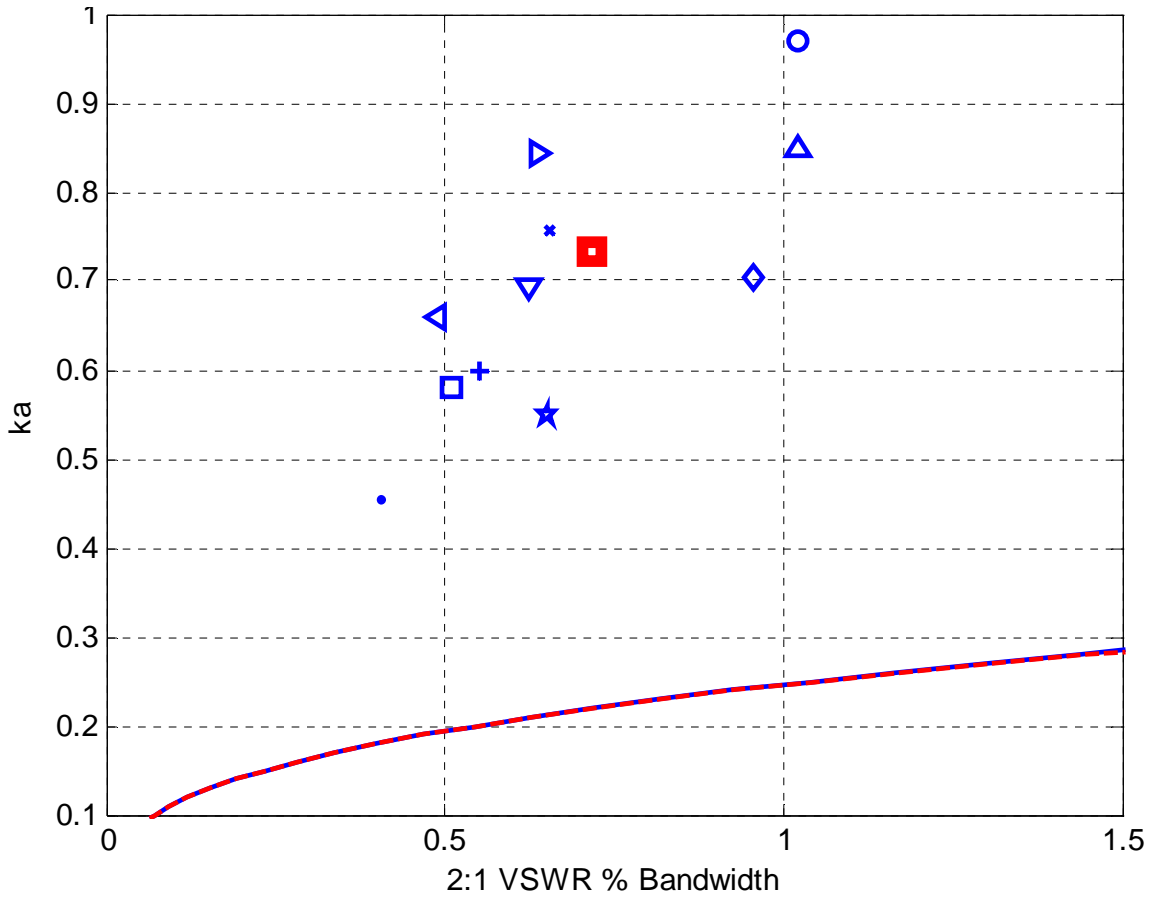
Figure 9 - Comparison of designs developed throughout this study and the theoretical 2:1 VSWR bandwidth limits. The antennas are denoted by the symbols in the legend.

CHAPTER 3

LOADING METHODS

3.1   High Permittivity Dielectric Loading

One of the most direct means of reducing the size of a microstrip antenna is to increase the relative permittivity (ε_r) of the dielectric used for the substrate material. The lowering of resonant frequency results from the relationship between the speed of light and the dielectric permittivity, shown in equation 3.1.

$$c = \frac{1}{\sqrt{\varepsilon\mu}} = \frac{c_o}{\sqrt{\varepsilon_r\mu_r}} \tag{3.1}$$

Thus, as the relative permittivity is increased, the speed of light decreases. For a resonant structure, this slower speed means an object loaded with dielectric materials of $\varepsilon_r > 1$ will have a lower resonant frequency than an unloaded identical size structure. Therefore, these loaded structures are said to be "electrically larger" than their unloaded counterparts of the same physical size.

The performance of a microstrip patch antenna can be approximated using a transmission line model, where the patch radiator length is modeled as a length L of transmission line, and the radiating edges are modeled as slots with an admittance $Y = G_r + jB$, Figure 10 [24]. The conductance, G_r, accounts for the radiation from the slot, whereas the susceptance, jB, accounts for the capacitance formed between the edge of the patch and the ground plane.
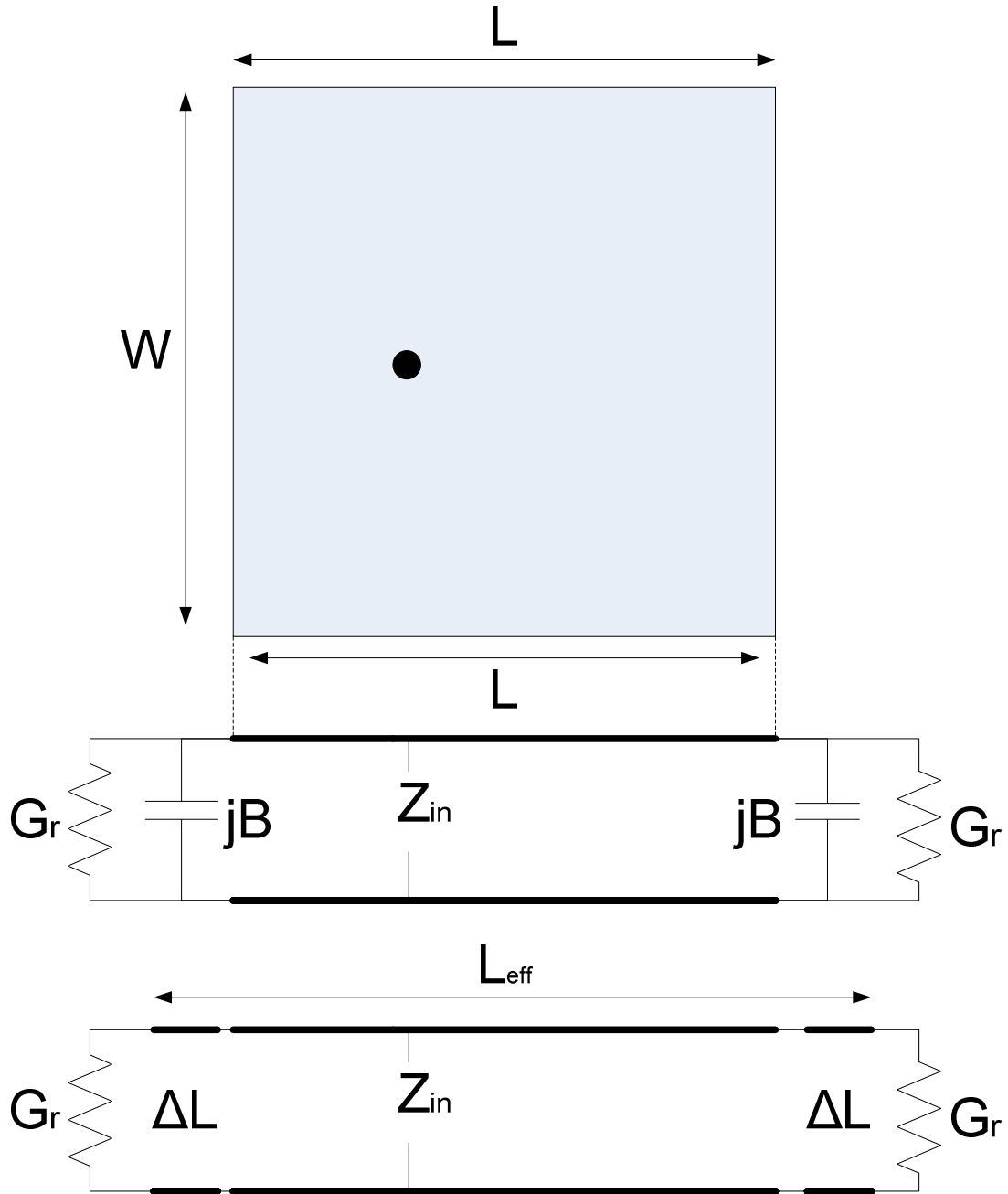
Figure 10- Transmission line model of microstrip patch antenna, showing the equivalent representation of the slot susceptance as an extension to the length of the transmission line.

The resonant frequency of the antenna can be calculated from this model using equations

3.2-3.5 [4], [25]. Equation 3.2 represents an effective relative permittivity ϵ_{reff}, which is a

modified relative permittivity value that accounts for the fields fringing in the air above the substrate material.

$$\varepsilon_{reff} = \frac{\varepsilon_r + 1}{2} + \frac{\varepsilon_r - 1}{2} \frac{1}{\sqrt{1 + 12\frac{h}{W}}} \qquad (3.2)$$

This modified relative permittivity value is then used to find the length extension ΔL that accounts for the fringing fields at the each of the radiating edges.

$$\Delta L = h0.412 \frac{\left(\varepsilon_{reff} + 0.3\right)\left(\frac{W}{h} + 0.264\right)}{\left(\varepsilon_{reff} - 0.258\right)\left(\frac{W}{h} + 0.8\right)} \qquad (3.3)$$

The effective length L_{eff} can be calculated using the results of equation 3.3.

$$L_{eff} = L + 2\Delta L \qquad (3.4)$$

This allows the resonant frequency to be calculated using the new effective length, as shown in equation 3.5.

$$f_r = \frac{c_o}{2\left(L_{eff}\right)\sqrt{\varepsilon_{reff}}} \qquad (3.5)$$

Equation 3.5 denotes the resonant frequency of the dominant TM_{001}, typically the excited mode for patch antennas. The resonant frequency and the permittivity are inversely related, such that increasing the permittivity decreases the resonant frequency of the patch antenna. This allows an antenna to be miniaturized significantly, without adding complexity to the metal patch, since a simple rectangular patch can be etched onto high permittivity substrate to realize a smaller size for a given operating frequency, requiring no modification to its shape. This can be beneficial for manufacturing and for mechanical robustness.

As the size of the antenna decreases, by increasing substrate permittivity or by the other loading methods discussed below, bandwidth and gain will be adversely affected. Chapter 2 provided a theoretical basis for this intrinsic relationship and this chapter contains examples of loading methods that show the balance between size and performance. As the size of the antenna decreases, the effective aperture size is reduced, lowering directivity. There have been some efforts to use high permittivity superstrate loading (in the range of $\varepsilon_r = 80$) of microstrip antennas to recover some of the gain lost by the reduction in size [26]. While the results presented do in fact show an increase in gain, they involve miniaturizing the patch radiator itself but not the actual substrate around the patch. The result is that the higher permittivity superstrate increases the aperture size by utilizing the large substrate around the patch antenna. For true miniaturization, the substrate size must also be reduced.

Another set of drawbacks for high permittivity materials involve their mechanical properties and material tolerances. Often high permittivity dielectric materials are ceramic, which are brittle, fragile materials. This weakens the robustness of the antenna, which traditionally is one of the advantages in using a microstrip antenna. The ceramic materials can be difficult to work with compared to more common substrate materials such as Duroid, or FR4, adding complexity to the manufacturing process. Also, loss in the dielectric material tends to be higher for the ceramic dielectrics. For example, Rogers TMM10 ($\varepsilon_r = 9.2$) has a loss tangent $\tan\delta=0.0022$ (at 10GHz), whereas Rogers 5880 (PTFE) has a loss tangent of $\tan\delta=0.0009$ (at 10GHz). The tolerances on the relative permittivity become more significant as the permittivity is increased. For Rogers 5880, the relative permittivity is specified as $\varepsilon_r = 2.2$ +/- 0.02, which is a tolerance of 0.9%.

25

Conversely, TMM10 has a relative permittivity specified as $\varepsilon_r = 9.2 +/- 0.230$, which is a tolerance of 2.5%. This is a large variation, and can generate significant differences between predicted and measured performance. TMM10 is only a modest increase in permittivity, whereas dielectric materials of $\varepsilon_r = 30, 40, 50$, and higher will have larger tolerances of the actual permittivity.

3.1.1 High Permittivity Performance Trends

To show the relationships between permittivity, bandwidth, and resonant frequency, a study considered relative permittivity between $\varepsilon_r = 1$ and $\varepsilon_r = 25$. The antennas are identical in size, with a 100×100×3mm substrate and a 27×27mm square patch, with and without a 100×100×3mm superstrate as indicated, Figure 11. The results were generated through HFSS simulations, in Figure 12 and Figure 13.
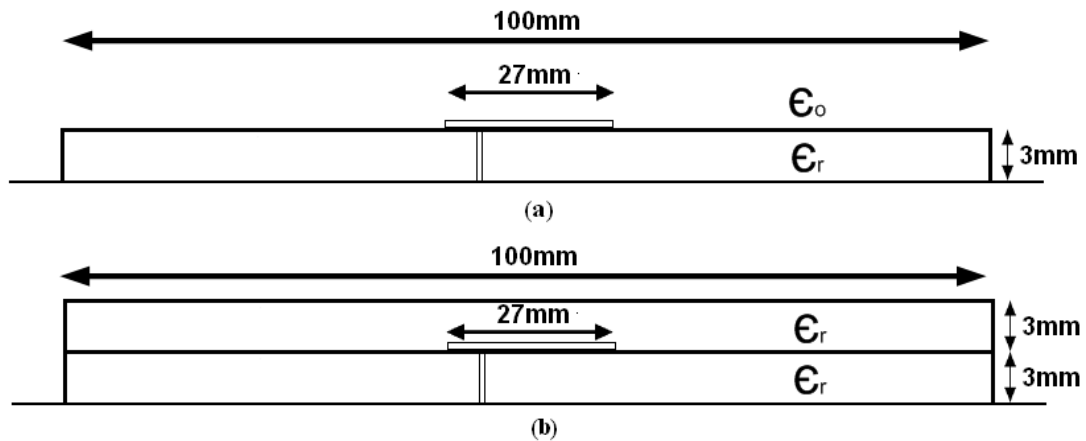
Figure 11 - Geometry of the 27×27mm square patch antenna model used for the permittivity variation, (a) without a superstrate, and (b) with a superstrate. Substrate and superstrate are 100×100×3mm.
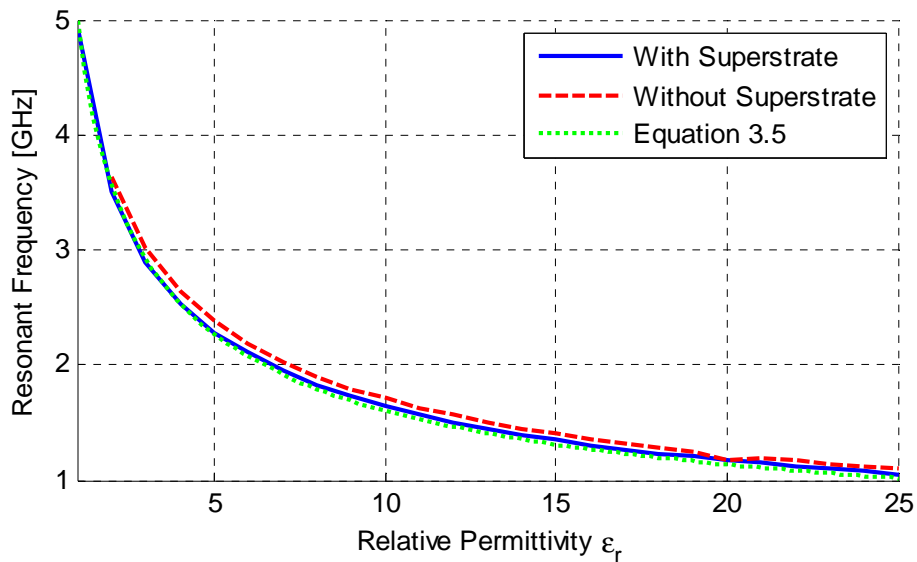
Figure 12 - Change in resonant frequency with relative permittivity. Antennas are
27×27mm on 31×31×3mm substrates and, as indicated, have 31×31×3mm superstrates.
Predicted Frequency from equation 3.5 is shown for comparison.
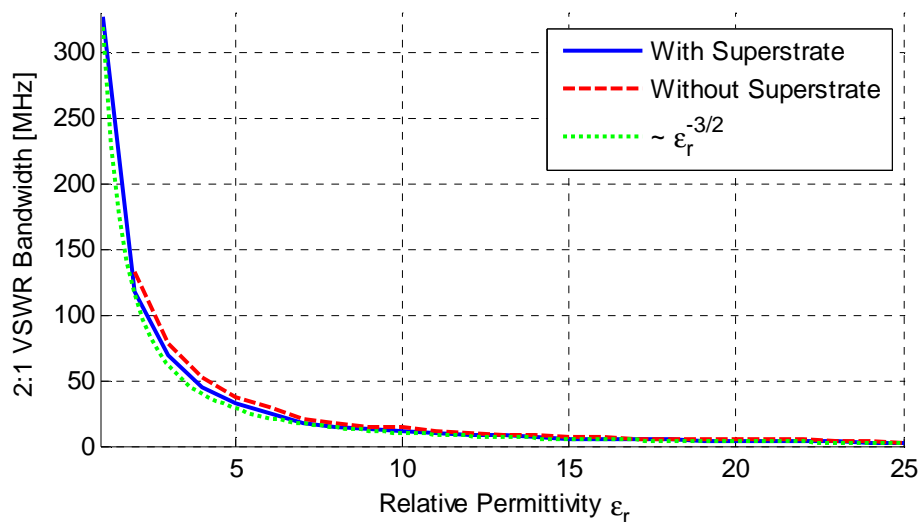
Figure 13 - Change in 2:1 VSWR bandwidth with relative permittivity. Antennas are
27×27mm on 31×31×3mm substrates and, as indicated, have 31×31×3mm superstrates.

As the permittivity is increased in Figure 12, the resonant frequency decreases at a rate

proportional to $1/\sqrt{\varepsilon_r}$. The resonant frequency was calculated using equation 3.5 and is

plotted for comparison, showing good agreement with the simulations. The frequencies

calculated with equation 3.5 are consistently lower than those of the HFFS simulations,

since an infinite extent substrate is assumed in the equation. Truncated substrates are used

in the HFSS simulations, which results in a lower effective ϵ_r. Further, the simulations

performed with superstrates show less reduction in effective ϵ_r compared to the

simulations without superstrates, since the patch element has the same permittivity

dielectric both above and below. Figure 13 shows that the bandwidth decreases at a rate

proportional to $\epsilon_r^{-3/2}$, which can be explained by equation 2.2, which states that the Q (and

therefore bandwidth) is proportional to the inverse of the volume of the antenna, or B~

$(ka)^3$. With increasing permittivity for an antenna of fixed size, the bandwidth decreases

at a faster rate than the resonant frequency.

High ε_r materials have been used as a substrate and a superstrate to take advantage

of this miniaturization, where both configurations make the patch electrically smaller. A

few designs successfully employed this method, one of which is shown in Figure 14.
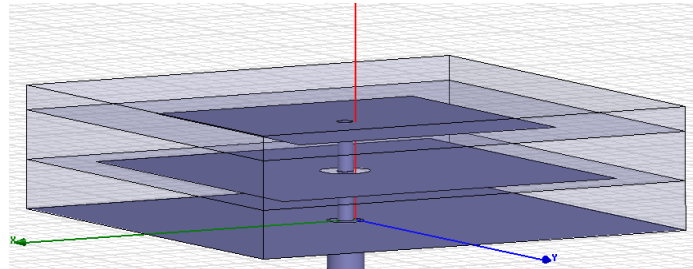
Figure 14 -Stacked patch design using dielectrics with $\varepsilon_r = 50$. Dimensions: top patch =
11.5×11.5mm, bottom patch = 15×15mm, dielectrics =19×19mm with 5mm total
thickness of all three layers.

The antenna was miniaturized to a very small size (19×19×5mm total volume) with the

use of such a high relative dielectric constant, but exhibited extremely narrow bandwidth,

as seen in Figure 15.
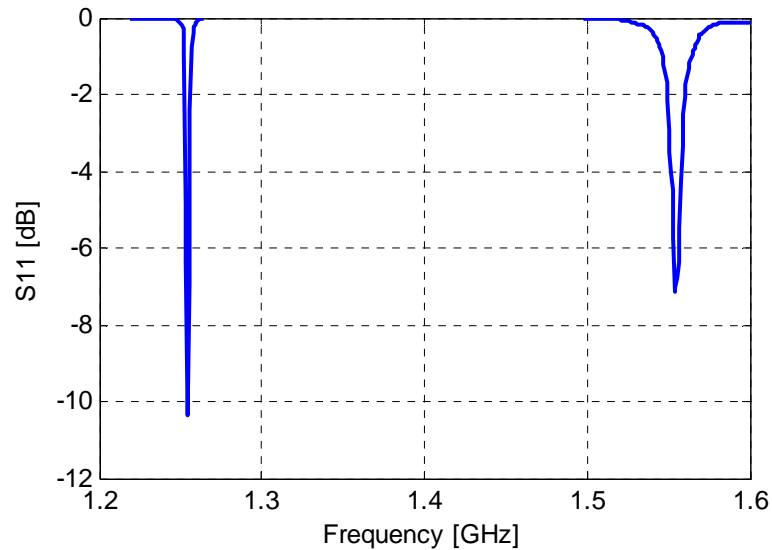
Figure 15 - Return loss for antenna on $\varepsilon_r = 50$. Dimensions: top patch $= 11.5 \times 11.5$mm, bottom patch $= 15 \times 15$mm, dielectrics $= 19 \times 19$mm with 5mm total thickness of all three layers.

Many designs were attempted using very high permittivity dielectrics ($\epsilon_r = 50$ in this example) and were found to be too narrowband for this application. However, many examples using lower relative permittivities of $\varepsilon_r = 9.2$-30 have shown some promise, and have been explored for use in two prototypes.

3.1.2   Optimized Linearly Polarized Prototype Design

Initially, high permittivity dielectric materials with $\varepsilon r = 40$-50 were investigated as potential means of miniaturization. After many design attempts realized 2-3MHz 2:1 VSWR bandwidths in the best cases, more modest relative permittivities were considered. From this study a linearly polarized prototype was designed and built, where resonances at the L1 and L2 bands were obtained by tuning one of the bands on each of the orthogonal TM_{010} and TM_{100} modes of a rectangular patch, shown in Figure 16.
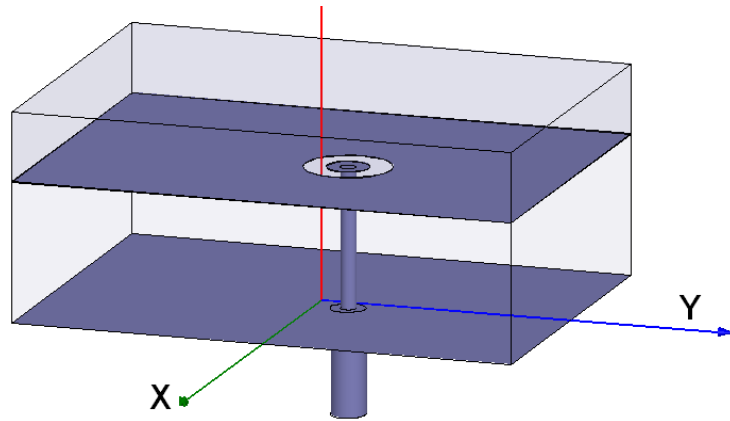
Figure 16 - Linearly polarized GPS antenna on high permittivity materials of $\varepsilon_r = 25$ and $\varepsilon_r = 38$.

The substrate is $\varepsilon_r = 25$ dielectric, and the superstrate is $\varepsilon_r = 38$ dielectric. The substrate dielectric was chosen to provide miniaturization while not decreasing the bandwidth as severely as the higher permittivity materials. The $\varepsilon_r = 38$ dielectric layer was then added as a loading superstrate to further decrease the resonant frequency, and also to provide a better match between the patch and the free space impedance. The substrate was truncated to be the same width and length as the patch itself in order to minimize the potential for surface wave excitation due to the high permittivity dielectric and thick substrate. With the patch tuned in this configuration, the substrate thickness was then increased incrementally to 8mm until a bandwidth of at least 5MHz 2:1 VSWR was obtained at both the L1 and L2 bands. Finally, a capacitive feed element, a disc coplanar with the patch, was added to tune out the inductance caused by the long feed probe in the thick substrate, and was optimized in size to provide a good impedance match to 50Ω over the widest bandwidth. The dimensioned antenna is shown in Figure 17.
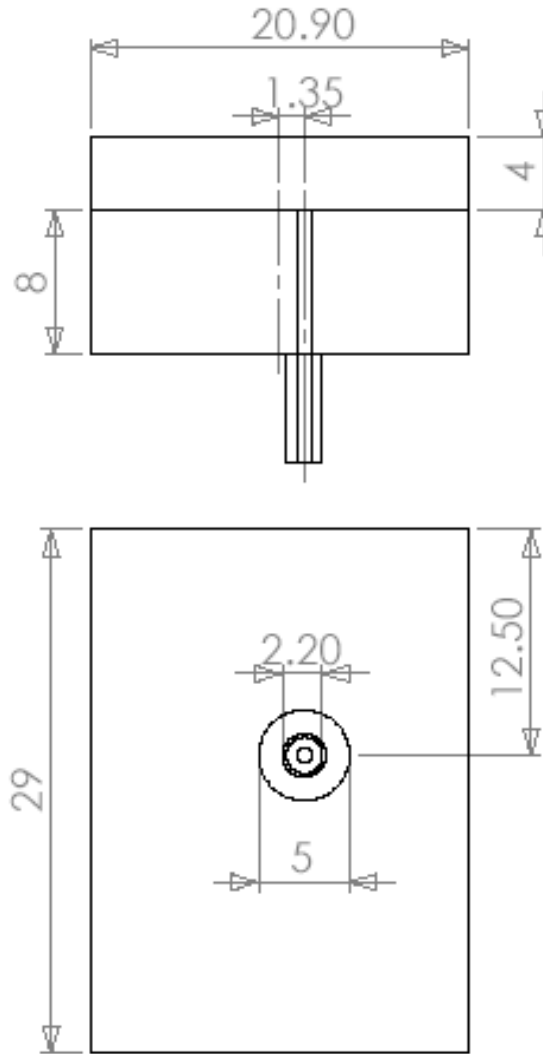
Figure 17 - Design layout of the high permittivity, linearly polarized GPS antenna prototype. All dimensions are in millimeters.

The antenna was simulated using Ansoft HFSS using PEC metallic surfaces (see Appendix C), and on an infinite ground plane. The antenna is shown to have a 2:1 VSWR bandwidth of 8MHz at L2, and 15MHz at L1. One advantage of a single feed design is the freedom of tuning without the potential for coupling to another feed port, especially when using capacitive discs, where close proximity of the clearance holes can lead to coupling between adjacent probes.
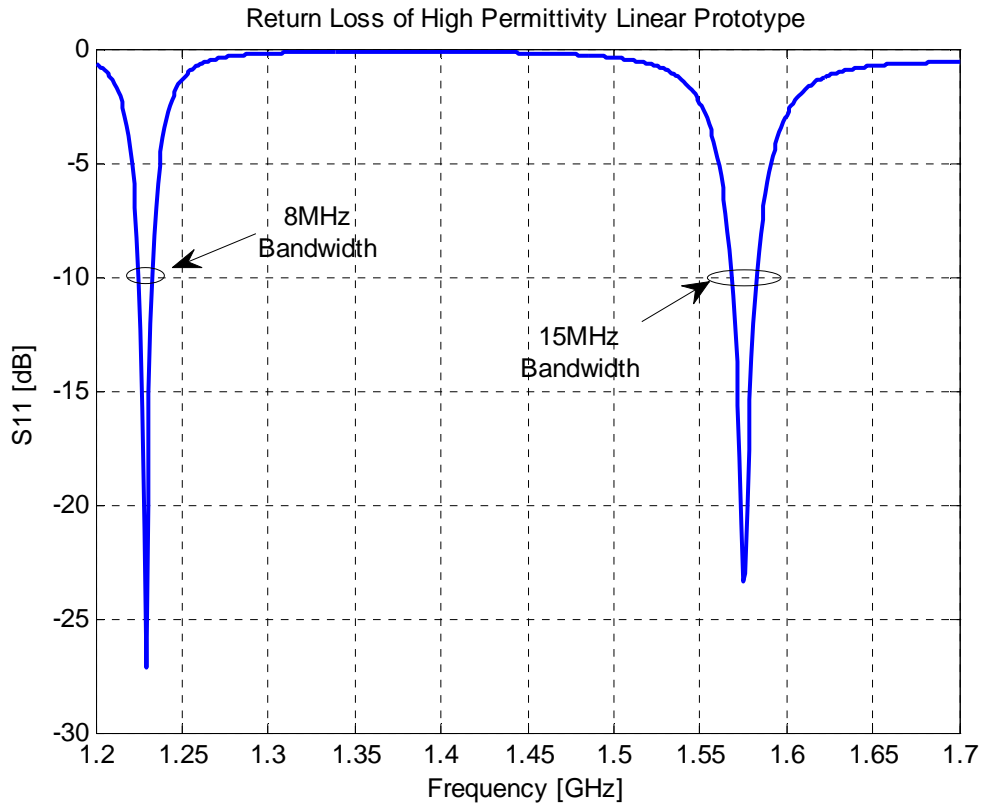
Figure 18 - Return loss performance of the linearly polarized 29×21×12mm GPS antenna on high permittivity dielectric materials.

The broadside realized gain is shown in Figure 19 for both the x-polarization and y-polarization (see Figure 16 for coordinate axis orientation), which takes into account mismatch losses. Figure 19 shows that at L2 the gain flatness bandwidth of +/-1dB is 19MHz, and at L1 the gain flatness bandwidth is 33MHz, both above 3.2dB over each band. The maximum gain is 5dB at each band, and the cross-pol is shown to be below -16dB over both bands. Since each band utilizes a different orthogonal mode on the patch, the polarizations of the gain are also on two orthogonal axes. An additional GPS link budget consideration for this antenna is the 3dB reduction in signal when the linearly polarized antenna is used to receive a CP signal, which is not taken into account on this gain calculation.
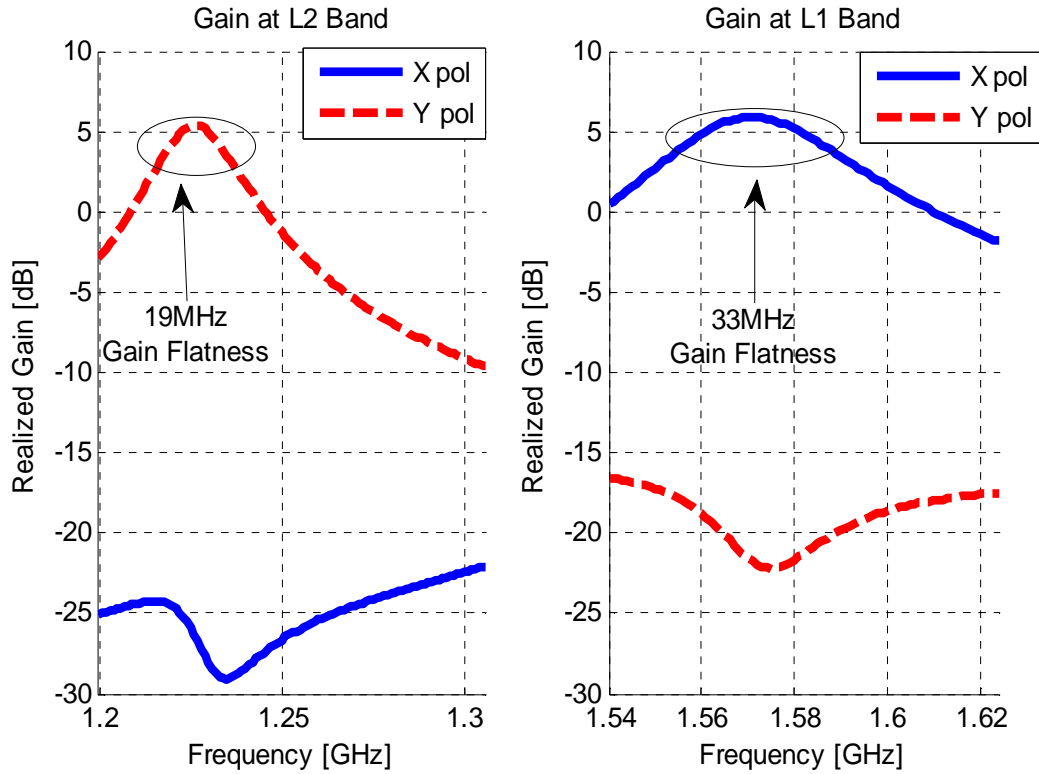
Figure 19 - Simulation results for the broadside gain across both L2 and L1 bands.

In addition to the simulations used in designing the structure, prototype antennas were fabricated and tested at Tyco Electronic Systems Division. Multiple prototypes were fabricated, some using the AF-126 bonding epoxy ($\epsilon_r = 4.5$) to adhere the dielectric layers together, and some without the bonding epoxy layers, held together instead with tape. Figure 20 shows the location of the bonding layers in the prototype antennas.
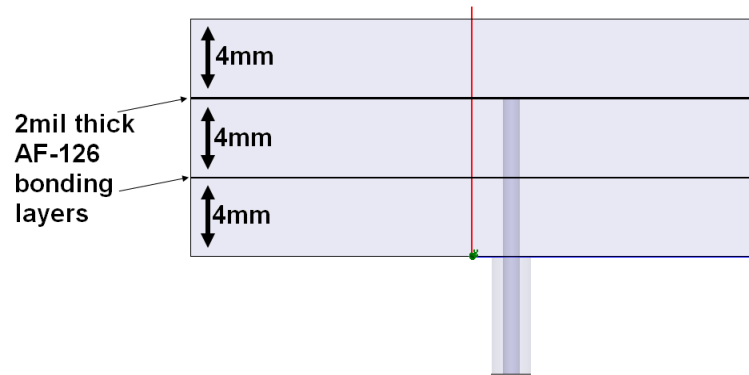
Figure 20 - Diagram of the location and thickness of the AF-126 bonding epoxy layers used in fabrication of the linear prototype antenna.

A comparison between the measured and simulated VSWR for the prototype with epoxy bonding layers and without the epoxy layers is presented in Figure 21.
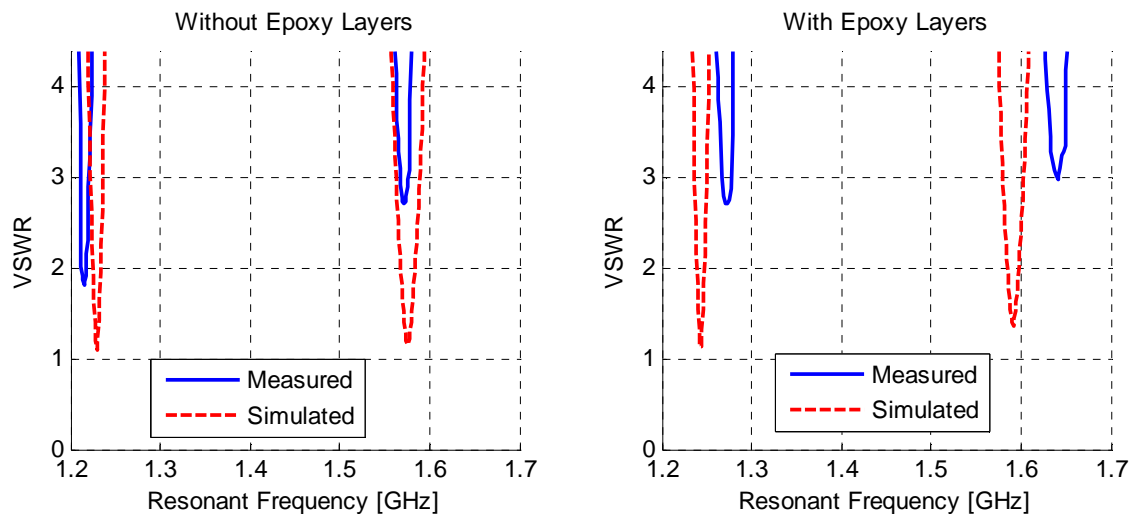
Figure 21 - Comparison between the measured and simulated VSWR for the linear prototype antenna on high permittivity dielectric.

The resonant frequencies for the prototype built without the epoxy layer match up closely with the HFSS simulation, but the impedance matching of the prototype antenna differs drastically from the simulation. At L2 the measured result shows the VSWR dips just below 2:1, but is not nearly the same bandwidth as the simulation predicted. At L1 the

match is very poor, with the measured VSWR result only reaching 3:1 over a small bandwidth, clearly not covering the same bandwidth as the simulation. For the prototype with the bonding layers, the resonant frequency is tuned slightly higher than that of the simulation at both L1 and L2 bands, and the match is also much different than that of the simulations. These prototypes showed that the bonding layers shift the resonant frequency upward, and the simulation does not fully account for their effects. The impedance match of both prototypes is not what the simulations predicted, and this may be a result of two factors: the dielectric materials were only modeled with the relative permittivity value (as was done with the epoxy), ignoring the dielectric losses, and there may be further uncertainty in the actual relative permittivity of the material used; and the prototypes may have some mechanical tolerances associated with them, such as uneven bonding of the dielectric layers, or air pockets in the epoxy layers that are not accounted for in the simulation. All of these are unknowns that would require further adjustment in subsequent prototype versions when working with this high permittivity material, such as tuning the resonant frequency of the simulated antennas to be slightly lower than desired, to compensate for the increase in frequency from the epoxy layers.

The gain patterns were measured, and are plotted at the resonant frequencies indicated in Figure 21, and compared to the HFSS simulated patterns, the results of which are shown in Figure 22 and Figure 23. Note that the HFSS simulations were performed on an infinite ground plane, so there is no comparison for the back-lobe radiation. The prototypes without epoxy bonding layers were also only measured over -90° < θ < 90°.

L2 E Plane Gain Pattern With Epoxy

L2 E-Plane Gain Pattern Without Epoxy
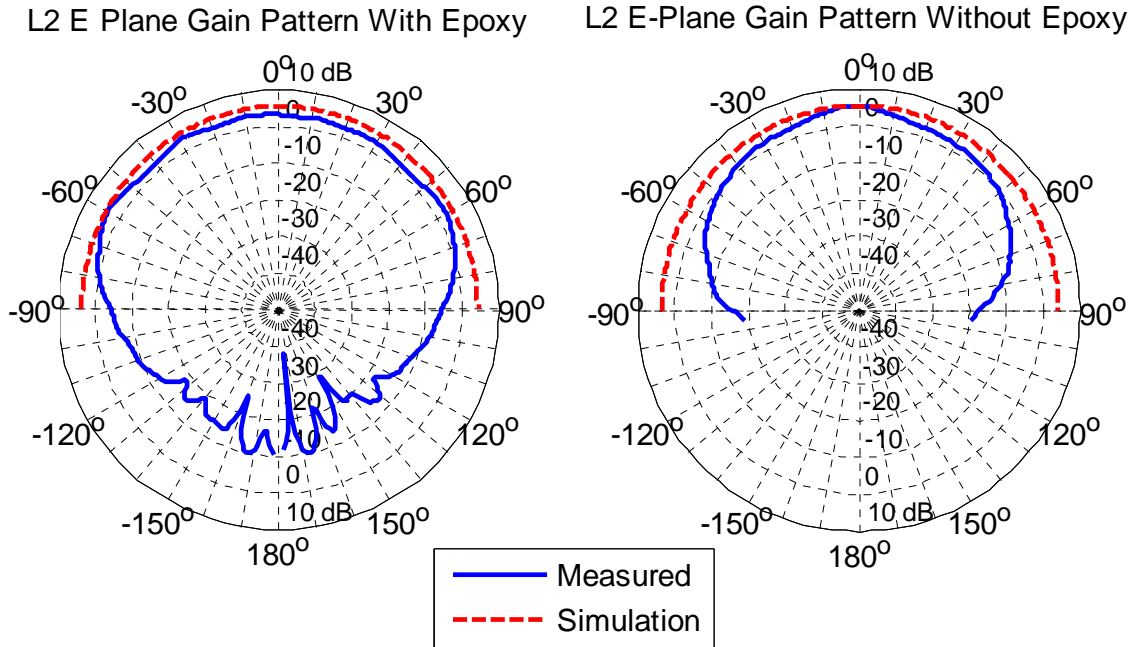
Figure 22 - Measured and simulated gain patterns at L2 band for linear prototype antenna.

L1 E-Plane Gain Pattern With Epoxy

L1 E-Plane Gain Pattern Without Epoxy
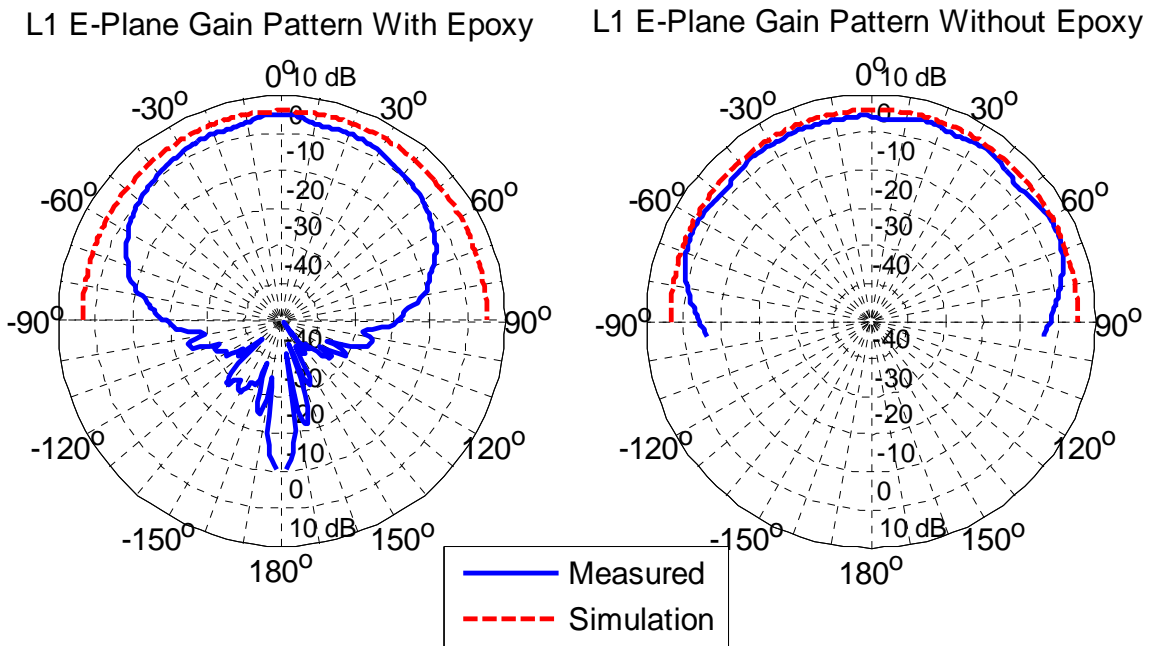
Figure 23 - Measured and simulated gain patterns at L1 band for linear prototype antenna.

The patterns shown are typical of the E-plane pattern of microstrip antennas, with a broad

beamwidth and a hemispherical pattern.   At L2 there is approximately 3dB maximum

36

gain at broadside, and at L1 approximately 5dB maximum gain at broadsize, with significant back-lobe radiation for the measured results. The measured and simulated gains have good agreement at broadside. Even though the match is not the same over each band for measured and simulated results, a 3:1 VSWR match is an insertion loss of only 1.3dB, which explains why the maximum gain is still fairly close to the simulation at both L1 and L2 bands. Normally, circular polarization is desired for a GPS antenna, but on some portable handsets, such as cell phones or tablet PCs, linear polarization can be tolerated when propagation effects such as multipath are the dominant form of signal reception due to a lack of line-of-sight, such as in a city with large buildings on all sides.

3.1.3   Optimized L-probe, CP Stacked Patch Prototype

The next design took advantage of the more stable properties of the Rogers TMM10 material, which was also used for many of the other antennas in this study. This design began in a form similar to that of the linear prototype, where a second patch was added to the linear prototype of section 3.1.2 to tune the L1 frequency and L2 frequency, as shown in Figure 24. The stacked patch antenna structure was made into a square such that a probe along each of the principle axis could be used to tune both L1 and L2 on each probe, providing the opportunity for CP operation when the proper phasing is applied to the feeds. Then the substrate thickness was reduced to 6.5mm to approach the 5mm thickness goal, and the length and width of the antenna was increased to tune L1 and L2, since a lower permittivity material is used for the substrate.
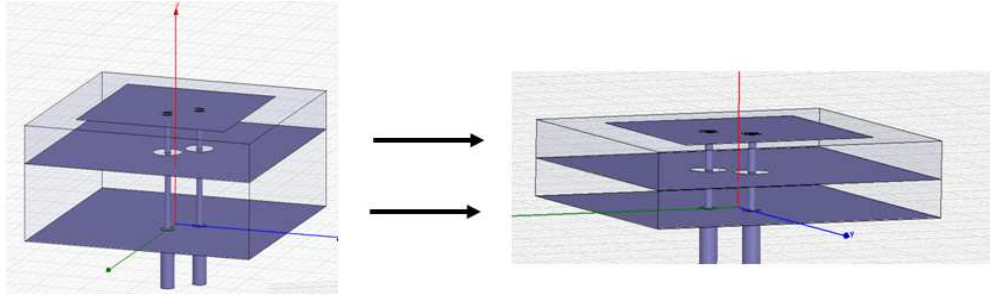
Figure 24 - A step in the transformation from the linear antenna prototype to the CP version, showing the addition of an orthogonal feed and thinner, but longer substrates.

The set of size iterations further optimized the tuning and resonant frequencies, and resulted in an antenna occupying a volume of 41.5×41.5×6.50mm, and is shown in Figure 25.
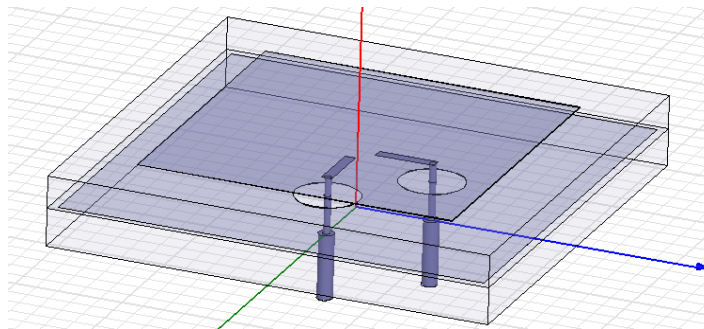
Figure 25 - Circularly polarized GPS prototype antenna on TMM10 dielectric material. The top patch is 29.6mm×29.6mm in size, and the lower patch is 40×40mm.

The antenna uses an "L" shaped feeding probe, fed through a hole in the lower patch, with the horizontal section situated between the two patches. This configuration allows for an extra degree of freedom in the tuning of the antenna, providing the opportunity to match both bands over a large of bandwidth. Figure 26 shows a detailed dimensioned drawing of the stacked patch antenna.
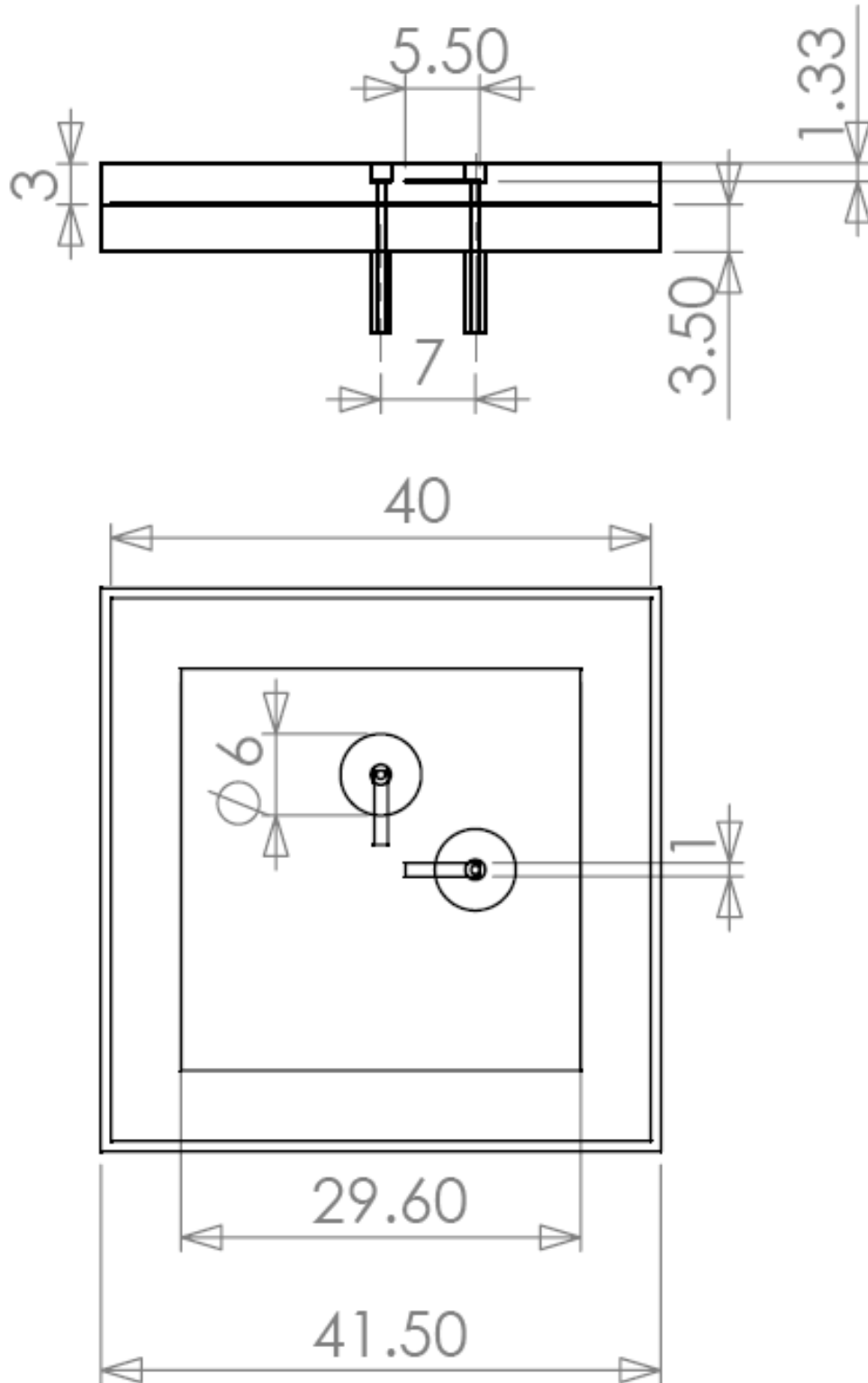
Figure 26 - Drawing of the circularly polarized, stacked patch prototype GPS antenna. Horizontal "L" probes are 1mm×5.5mm. All dimensions are in millimeters.

Ansoft HFSS was used to analyze the performance of the antenna, with PEC metallic

surfaces. A 2:1 VSWR bandwidth of 8MHz was achieved at L2, and a bandwidth of

16MHz was achieved at L1, as shown in Figure 27.
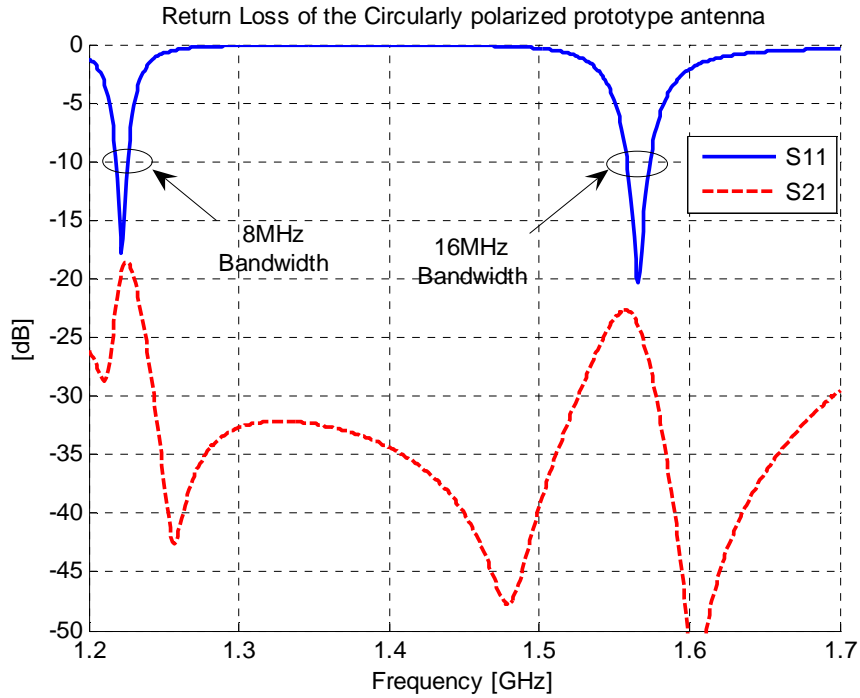
Figure 27 - Simulated return loss for the 41.5×41.5×6.5mm circularly polarized Antenna.

In addition to adequate bandwidth over both bands, the isolation between the probes is

better than 18dB over both bands. This indicates low power loss through coupling

between the orthogonal feeds, and this also correlates to good cross-pol performance, as

the two modes are well isolated and orthogonal. For orthogonal feed structures, coupling

of fields between the probes can indicate high cross-pol, since, in order to couple between

the probes, currents (and fields) must have components in both principle axis directions

on the patch. The gain is shown in Figure 28 over each band, where two probes were fed

in quadrature, resulting in right hand circular polarization (RHCP).
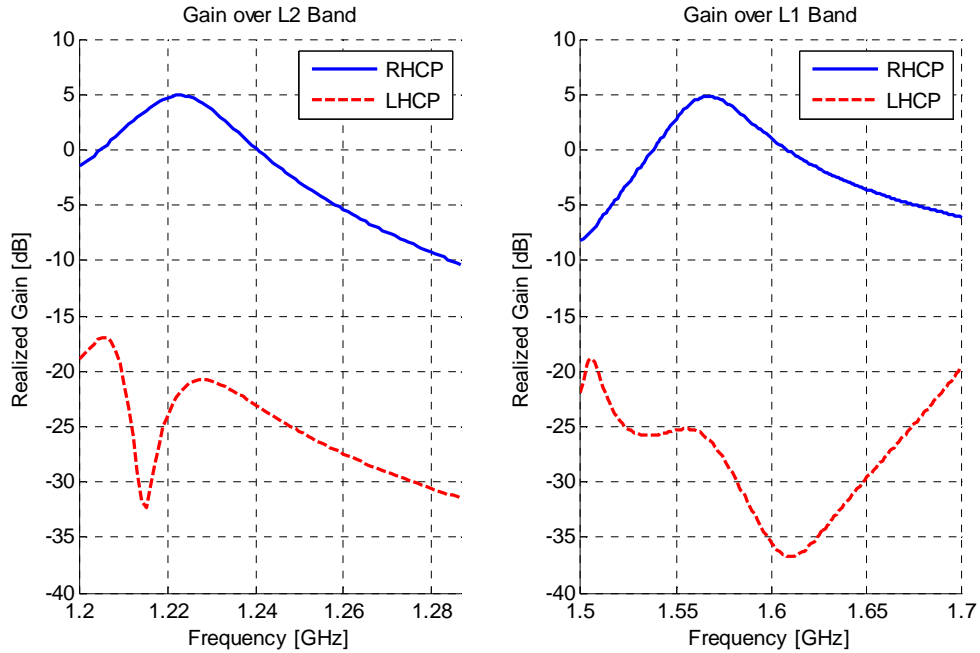
Figure 28 - Simulated broadside gain performance for the 41.5×41.5×6.5mm circularly polarized, stacked patch antenna.

The results indicate a gain flatness bandwidth of +/- 1dB of 19MHz over L2, and 33MHz over L1. These gain bandwidths are large enough to satisfy the requirements of the GPS system. Also, over each gain bandwidth the LHCP gain component is below -20dB, which indicates very low cross polarization and, therefore, very low axial ratio. The axial ratio is shown in Figure 29.
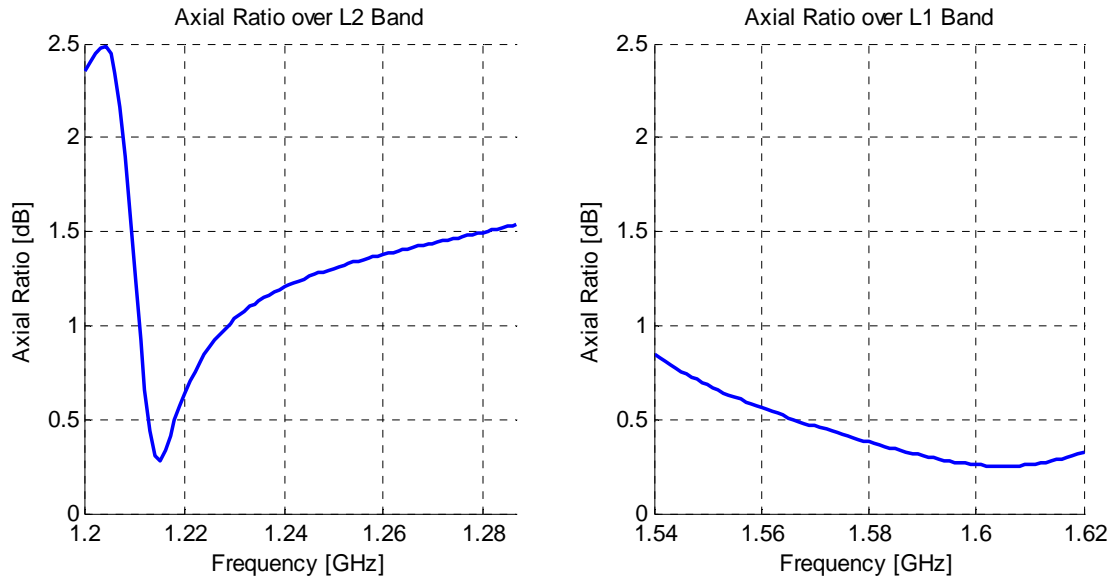
Figure 29 - Axial ratio for the circularly polarized, stacked patch prototype antenna for both L2 and L1 bands.

Over both bands, the antenna has better than 3dB axial ratio, which is desirable

polarization purity for GPS operation. This antenna meets all of the electrical

specifications of the design criteria that were the basis for this investigation, but is larger

than the desired size of 31×31×5mm. Given the performance of 3dB of gain over the

gain flatness bandwidth, a 2:1 VSWR of better than 8MHz over each band and axial ratio

below 3dB, literature searches at this time have failed to find an antenna of comparable

size that exceeds this performance.

In addition to the simulations performed in the design of this antenna, a prototype

was built and tested by Tyco Electronic Systems Division, and the results are shown

compared to the HFSS simulations. The antenna return loss measurements in Figure 30

show the resonant frequency at the L1 band to be shifted approximately 100MHz above

the design frequency range of 1.575GHz, while the resonant frequency at the L2 band was

close to the simulated design data and is properly centered around 1.227GHz. The

addition of epoxy layers does not impact the tuning of the L2 band, namely because the dielectric substrate beneath the L2 patch is homogeneous, and there is only an epoxy layer on top of the patch. L1 was strongly affected, since it has two epoxy layers holding together the substrate below it creating an inhomogeneous substrate. The large shift in resonant frequency for the simulated and measured prototypes with and without epoxy layers are compared in Figure 30. A 2:1 VSWR bandwidth of 18MHz was measured at L2, and 64MHz bandwidth at L1, exceeding the impedance bandwidth requirement of 5MHz at each band.
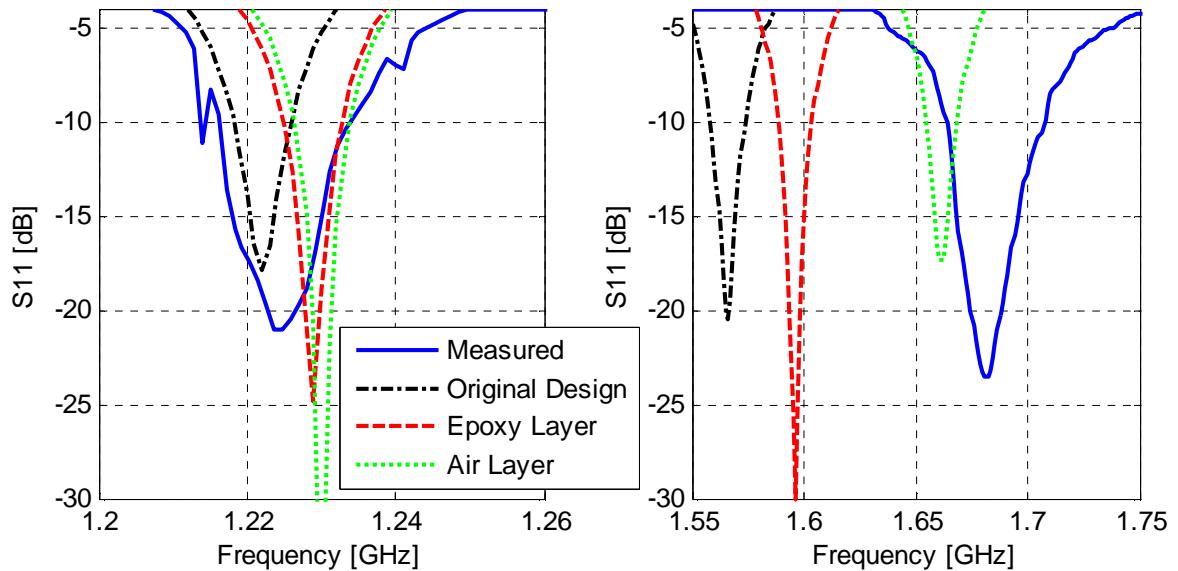
Figure 30 - Comparison of the measured and simulated return loss performance of the circularly-polarized, stacked patch prototype antenna. The antennas shown are the measured prototype, the HFSS design simulations, and an HFSS simulated antenna modeling the epoxy boding layers, and an HFSS simulation modeling the whole top epoxy layer as an air layer.

In order to account for the shift in frequency, the two AF-126 (ε_r = 4.5) epoxy layers that were used to fabricate the antenna were modeled in HFSS, shown in Figure 31, and the results are shown in Figure 30 along with the measured data.
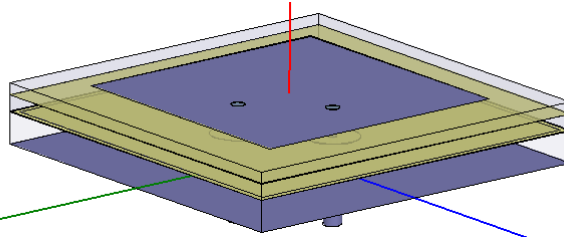
Figure 31 - HFSS model of the circularly polarized, stacked patch prototype antenna including the two 2mil thick AF-126 epoxy layers used to fabricate the antenna, one at the lower patch and one at the layer with the horizontal section of the L probes.

Even with the epoxy layers in the model, the antenna simulations did not tune to as high a resonant frequency as the measurements. The next step was to run simulations assuming an air bubble was present at the top patch epoxy layer, shown in Figure 30, where the top epoxy layer was assumed to be an air volume ($\varepsilon_r = 1$). This approaches the resonant frequency measured, and it is likely there is an air bubble in this epoxy layer, or perhaps a larger thickness epoxy layer than the 2mil estimated, that is tuning the frequency of the L1 band up by 100MHz.

The gain response was measured with the antennas mounted on a 4ft ground plane. Spin-linear pattern plots were taken in order to measure the axial ratio of the circular polarization over all elevation angles along with the gain. Figure 32 shows that the axial ratio measured is on the order of 6dB at broadside, increasing to approximately 10dB at $\theta=60°$, and 20dB at the horizon. This is much higher than the simulated axial ratio, and it was noted by Tyco Electronic Systems Division that the measurements taken had a poorly tuned 90° hybrid that may explain the poor axial ratio. Further measurements were not available to confirm the source of the poor axial ratio performance. The antenna is shown to have a broad pattern, typical of a patch antenna, and the ripples on the pattern are a result of the finite sized ground plane used to measure

44

the gain. The back lobe radiation is low, below -10dB, and multiple lobes are present for

theta angles greater than 90° due to scattering off the edges of the ground plane.

Otherwise, the measured gain envelope is fairly close to the simulated gain pattern,

showing good agreement.
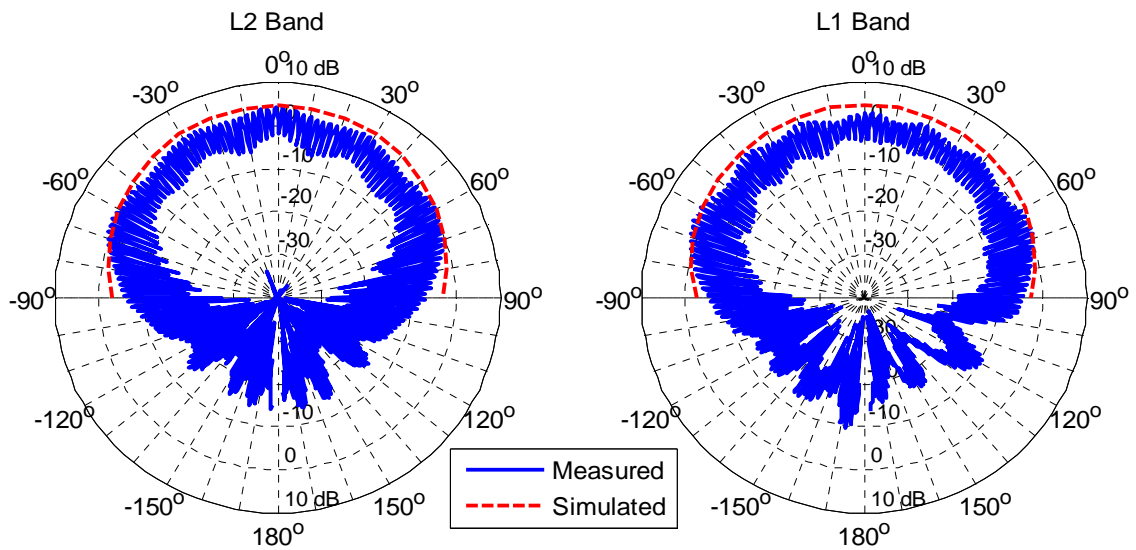
Figure 32 - Spin-linear E-plane gain patterns for the L-probe fed, stacked patch GPS
prototype at both L1 and L2 bands, for both measured and simulated antennas. The
patterns were taken at the center frequency of each gain bandwidth.

These patterns show that with the axial ratio improved, the antenna would have a wide

field of view, since it has such a broad beamwidth. The maximum gain was measured at

broadside for the L1 and L2 bands to show the gain roll-off with frequency. Figure 33

shows that the L2 band gain peaked at 5dBi, and the gain at L1 peaked at 3.5dBi.
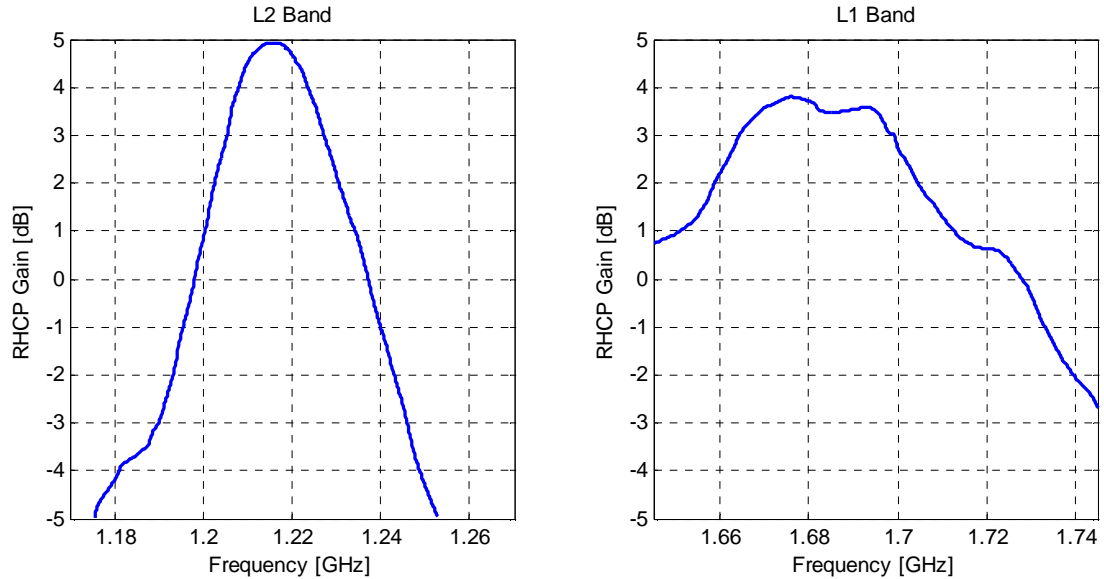
Figure 33 - Broadside RHCP gain vs. Frequency over both the L1 and L2 bands for the L-feed, stacked patch GPS antenna prototype.

At L2 the +/-1dB gain flatness bandwidth is 22MHz, and at L2 the gain flatness bandwidth is 47MHz, once again exceeding the minimum 20MHz gain flatness bandwidth. Both the VSWR and gain bandwidths were measured to be larger than the simulations predicted, and the axial ratio and L1 resonant frequency were also different than the simulations. This indicates that developing designs on TMM10 with the epoxy layers may require the simulation model to incorporate better models of the epoxy layers in the design stage to account for their effect as the design progresses.

Overall this antenna was one of the best candidates designed throughout this study, surpassing the electrical specifications set forth that motivated this study, while approaching the physical size specifications. Also, literature searches have failed to find similar sized antennas meeting the same VSWR, gain flatness, axial ratio and dual band operation in an antenna of this size, and variations on this design appear in section 3.2.2,

as well as section 2.4, where the area occupied by the antenna was reduced to produce even smaller versions of this design at somewhat decreased performance.

3.2   Slot Loading

The TM_{100} mode that develops on the patch has a resonant frequency dependant on the length of the patch. While a high permittivity substrate will make the metal patch look electrically larger by changing the wave propagation speed, another method used in tuning a microstrip antenna is loading the patch with slots.

There are two helpful models that can be used to explain change in resonant frequency. For a visual, intuitive explanation, the slots can be viewed as obstructions to the path of the current, forcing a longer physical distance for the current to travel.   Figure 34a shows the current distribution on a patch surface with no slots, exciting the TM_{100} mode where the antenna is operating at a frequency of 1.730GHz.
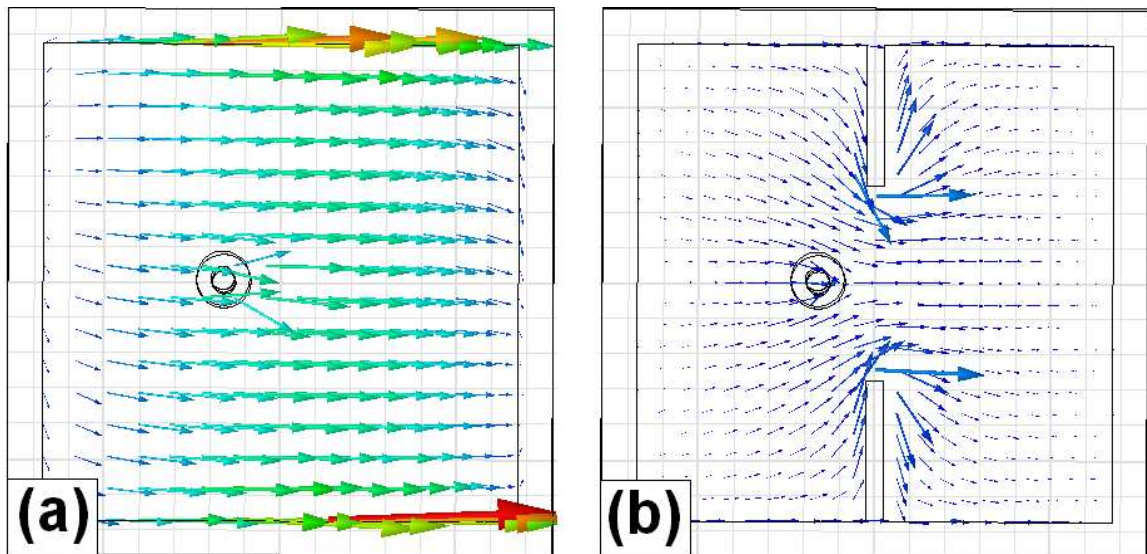
Figure 34 - Current distributions on the patch layer when the TM_{100} mode is excited (a) without slots and (b) with slots.

47

The patch without slots allows a straight path across the patch, whereas the slots force

currents to take a longer path, as in Figure 34b. This longer path corresponds to a longer

resonant length, thereby tuning the patch to 1.464GHz, a reduction in the resonant

frequency of 280MHz. Here the slots are placed at the midpoint of the patch, but they

can be located anywhere along the patch if they change the current paths. One important

consideration in placement of the slots is the polarization desired, as asymmetric slot

placement can potentially cause cross-polarization levels to rise. For asymmetric slots,

resonant current paths can develop off the main axes of the patch, such as along a

diagonal axis, producing radiation components along both of the main axes instead of

only one axis. Increased cross-polarization will result in poor axial ratio for circular

polarization, and coupling between the two orthogonal feeds will increase.

Another representation of the slots is that of a lumped circuit inductor, placed in

series with the transmission line model for the patch antenna, as done in [27]-[29], shown

in Figure 35.
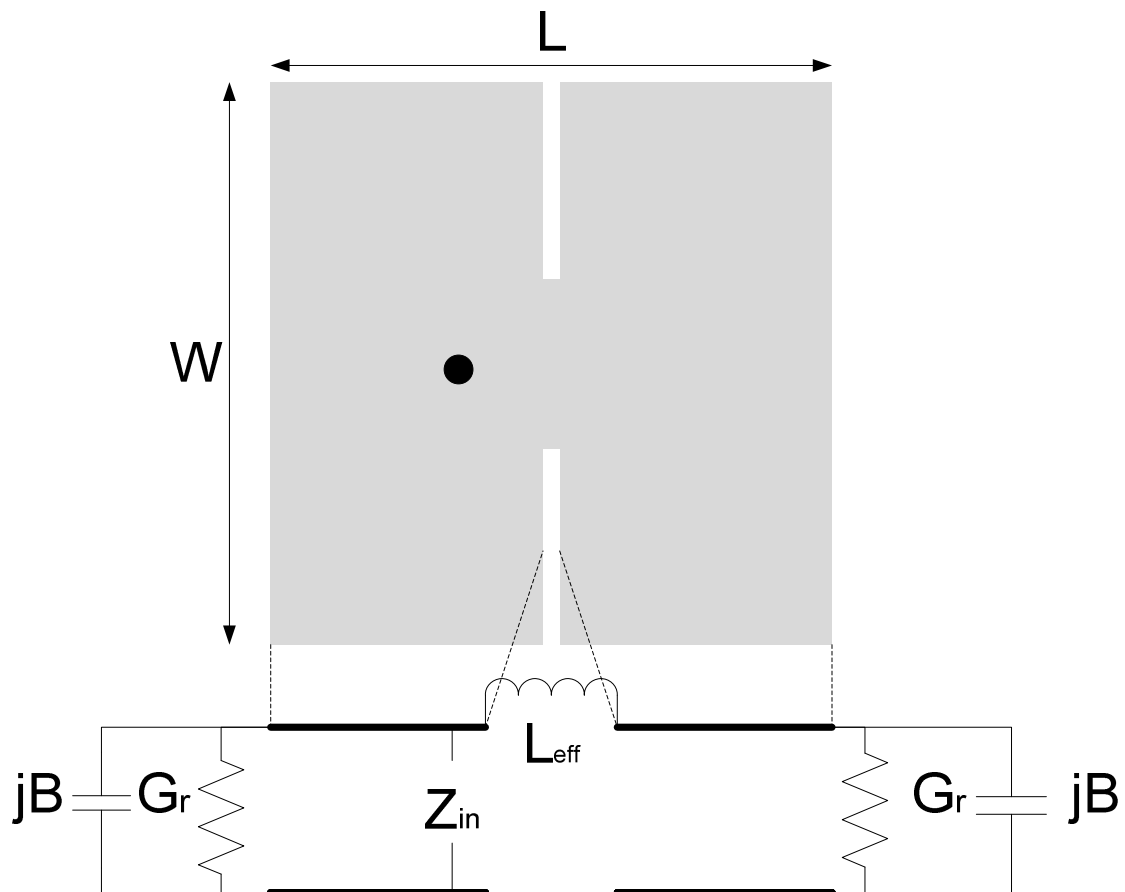
Figure 35 - Transmission line model of the slots, where the series inductance approximates the slot field behavior.

The reasoning behind the inductive model is that the slots cause a concentration of the magnetic field interior to the slots, due to the currents forced to flow along the edge of each slot (see Appendix D). From this lumped model, an inductor stores magnetic energy and resists phase changes in the current flow, introducing a phase delay between the voltage and current, similar to the physical model where the currents are delayed by taking a longer path around the slot. Unfortunately, as [28] shows, a single lumped inductor is only a very coarse approximation, since the inductance changes over the length of the slot. To make this approximation better, many inductances have to be placed in the circuit, and solved using a multiport network model as done in [29] and

49

shown in Figure 36. This yielded good agreement between experiment and simulation in [29], but does not simplify to an analytic solution, and must be solved numerically. Despite the shortcomings of the lumped inductance model shown in Figure 35, it does provide insight into the tuning achieved with the slots from a circuit perspective. Both of these lumped inductance models assume a very thin slot, and do not account for the capacitance from the displacement current in the slot.
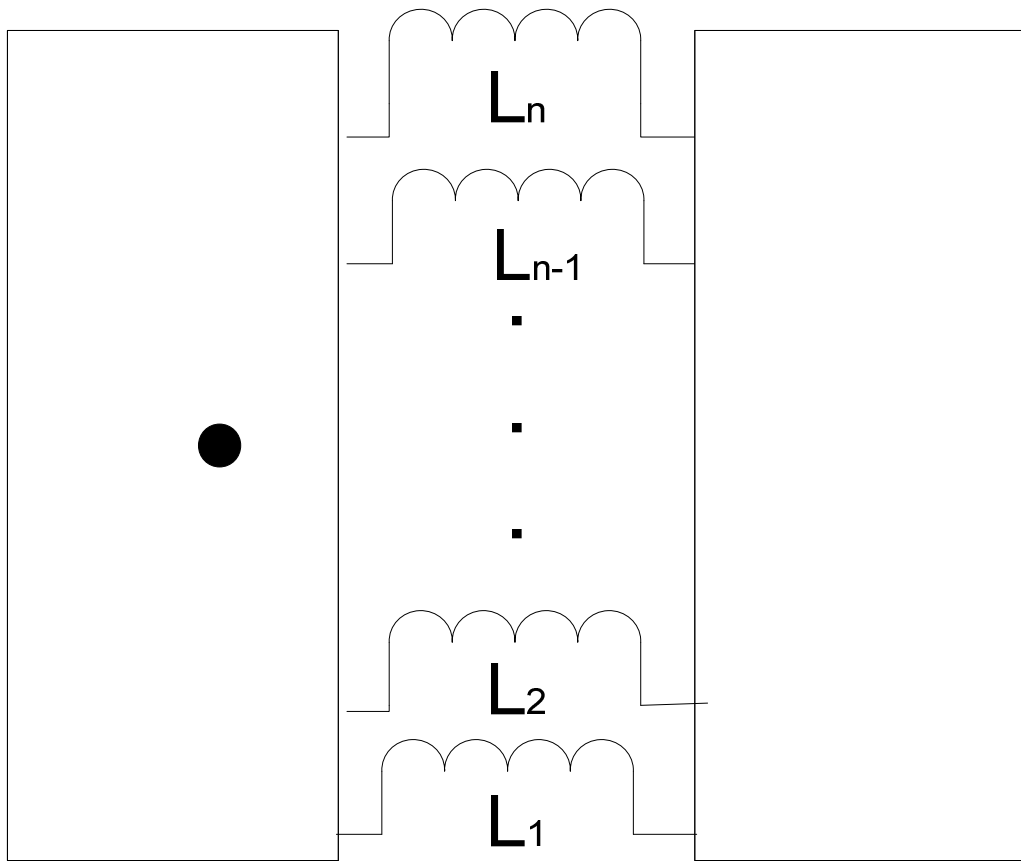
Figure 36 - N-port lumped inductor approximation for the slotted patch.

3.2.1   Slot Loading Performance Trends

A study was undertaken to observe the effects on bandwidth, resonant frequency and gain of a patch antenna when loaded with slots. A 27×27mm patch with a 31×31×3.175mm TMM10 (ε_r = 9.2) substrate, Figure 37, was simulated in HFSS with four slots of varying length τ and a fixed width ζ = 1mm. Prototype antennas were also fabricated (Appendix E) to validate the simulation data. The results are shown in Figure 38.
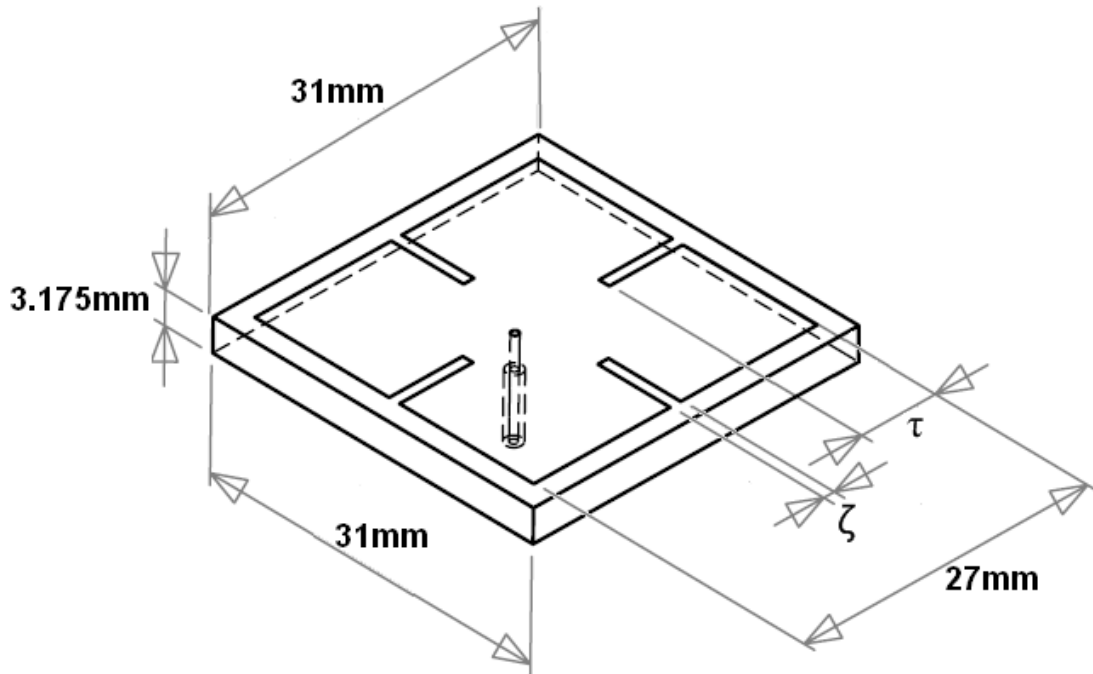
Figure 37 - 27×27mm patch antenna on a 31×31×3.175mm TMM10 substrate, with four slots cut into the patch surface, with length τ and width ζ = 1mm.
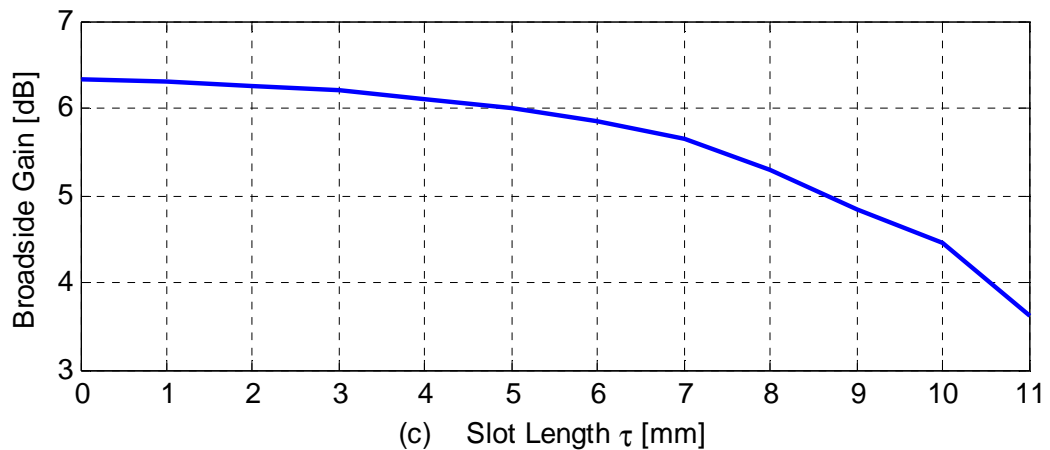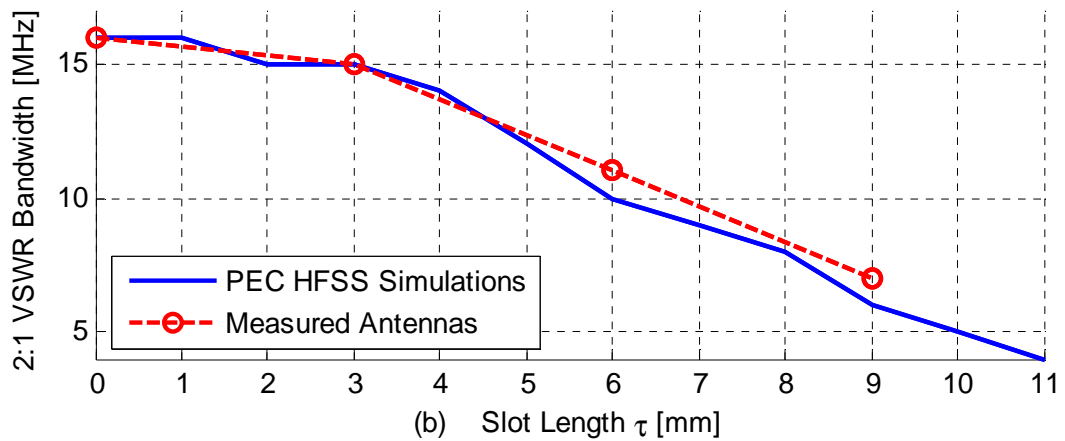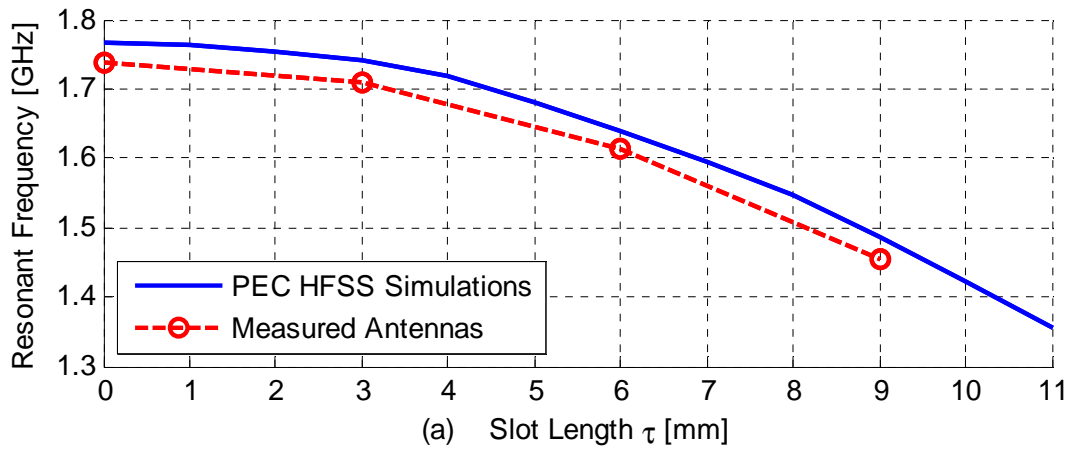
Figure 38 – Change in (a.) the resonant frequency, (b.) bandwidth, and (c.) gain with variation of slot length τ. Patch is 27×27mm square with a 31×31×3.175 mm substrate of TMM10 (ε_r = 9.2). The slot widths are all ζ = 1mm.

For slot lengths greater than 4.5mm the resonant frequency drops off

approximately linearly, Figure 38a, with the longest slot length of $\tau = 11$mm decreasing

the resonant frequency by 500MHz compared to the patch without a slot. The reduction in

resonant frequency with increasing slot length agrees with both the lumped inductor

model and the resonant path length model. The approximate bandwidth also drops off

linearly, Figure 38b, (the stair-stepping is a result of using whole number MHz

frequencies for the bandwidth). The bandwidth decreases similar to the resonant

frequency because the antenna volume is fixed, and the antenna looks electrically smaller

as the resonant frequency decreases, increasing the Q. The measured data show good

agreement with the simulation results. Broadside gain performance, Figure 38c, behaves

very similar to the resonant frequency as the slot length is increased. The aperture is fixed

in size, so as resonant frequency decreases, the aperture looks electrically smaller.

Next, for the antenna in Figure 37, the slot widths ζ are varied, with a fixed slot

length of $\tau = 9$mm. The resonant frequency decreases with increasing slot width ζ, shown

in Figure 39a, with the maximum slot width of $\zeta = 6$mm decreasing the resonant

frequency by 200MHz compared to the $\zeta = 1$mm antenna. As in the slot length study, the

bandwidth, Figure 39b, and broadside gain, Figure 39c, decrease similar to the resonant

frequency for increasing slot widths ζ. The measured data also shows good agreement.

While the reduction in frequency with increasing slot width agrees with the model

that the slots force the resonant path of the current to lengthen, it is unclear from the

lumped inductor model what impact of slot width will have, since the model assumes

very narrow slots. In [27], a rule of thumb is provided such that the impedance of the

series gap capacitance is negligible, in comparison, with the impedance of the slot

inductance when the width of the slot is less than the substrate thickness, which was true in the study on slot lengths (1mm wide slot vs. 3mm thick substrate).
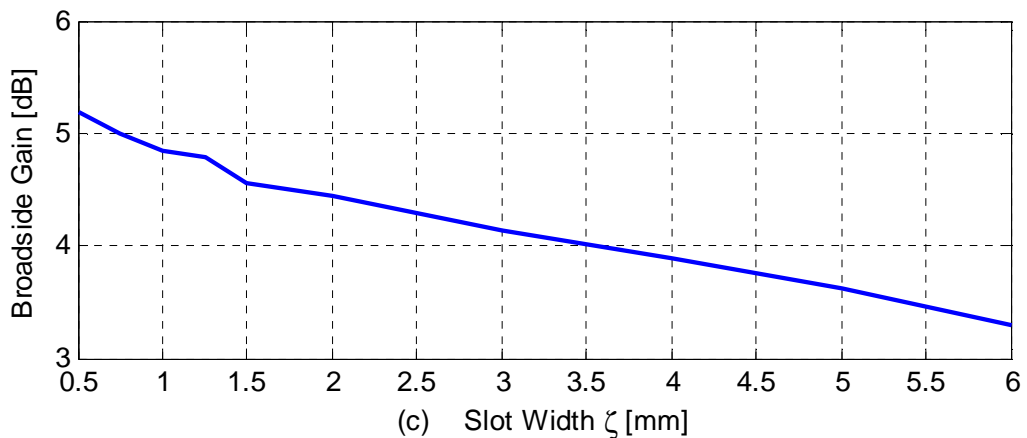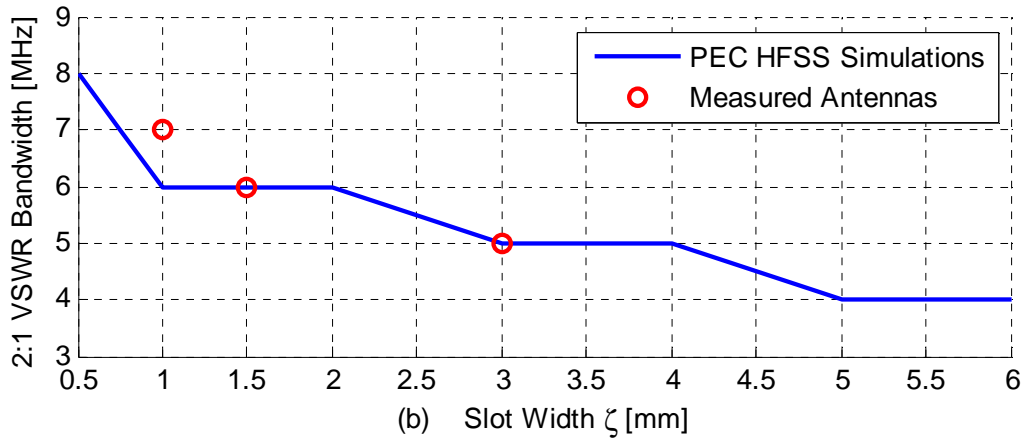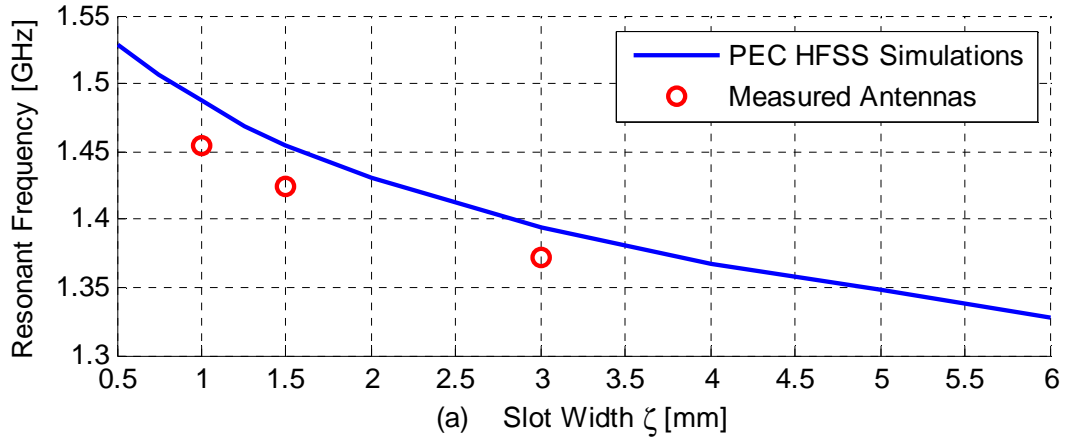
Figure 39 – Change in (a) the resonant frequency, (b) bandwidth, and (c) gain with variation of slot width ζ. Patch is 27×27mm square with a 31×31×3.175 mm substrate of TMM10 ($\varepsilon_r = 9.2$). The slot lengths are all $\tau = 9$mm.

Appendix F shows a modified transmission line circuit for the slot loaded patch when the slot is wide compared to the substrate thickness, using approximations given in [30]. As the slot width is increased, shunt capacitance on either side of the slot increases between the patch and ground, and a series capacitance connecting the two sides of the slot decreases. The ratio between the slot width and the substrate thickness determines when these capacitances are significant, namely when the slot width is on the order of the substrate thickness or larger.

While a previous study varied the width of the slot on a fixed thickness substrate, varying the substrate thickness with a fixed width slot is also of interest, since it also affects the capacitances. A 27×27mm patch with and without four 9mm long, 1mm wide slots was analyzed on a 100×100mm square TMM10 (ε_r =9.2) substrate, ranging in thickness from t = 0.5-5mm, with a 100×100×3mm TMM10 (ε_r =9.2) superstrate. The large substrate size was chosen to approximate an infinite substrate, to avoid the effects of substrate truncation.
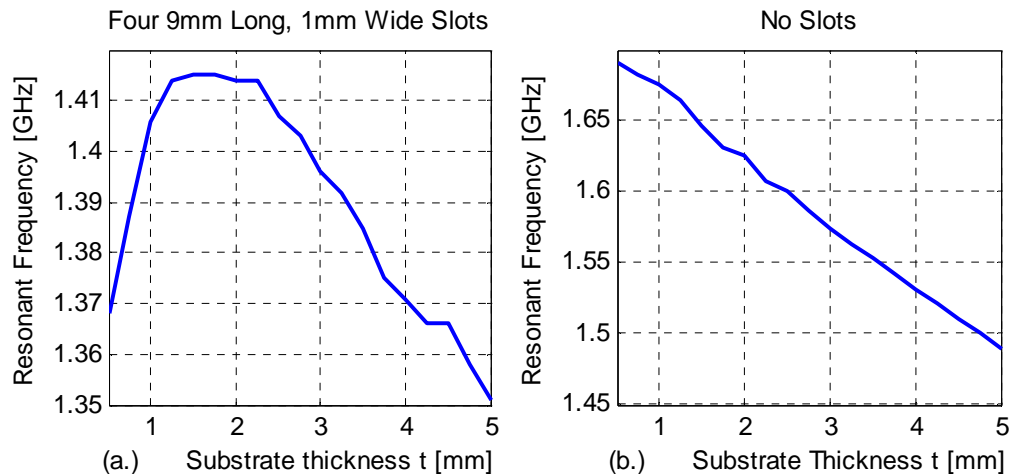
Figure 40 - Change in resonant frequency for a 27×27mm patch vs. substrate (ε_r =9.2) thickness t, (a.) with slots, and (b.) without slots in the patch surface.

For the thinnest substrate in Figure 40a, the shunt capacitance is relatively large since the separation between the ground and patch is small. This leads to a low resonant frequency. As the substrate thickness increases, the shunt capacitance decreases and the resonant frequency increases until $\frac{t}{w} \approx 2$. After this point the slot is narrow with respect to the substrate thickness, and the shunt and series capacitances no longer dominant. The frequency then decreases with increasing substrate thickness, as in the traditional microstrip antenna, Figure 40b.

Another study involves moving the slots along the length of the patch to observe the effect of slot placement. The antenna consists of a 27mm square patch, on a 31×31×3mm square substrate of TMM10 ($\varepsilon_r = 9.2$), with no superstrate. Two slots, arranged symmetrically on the patch, are moved from -13mm to +13mm along the resonant length of the patch.
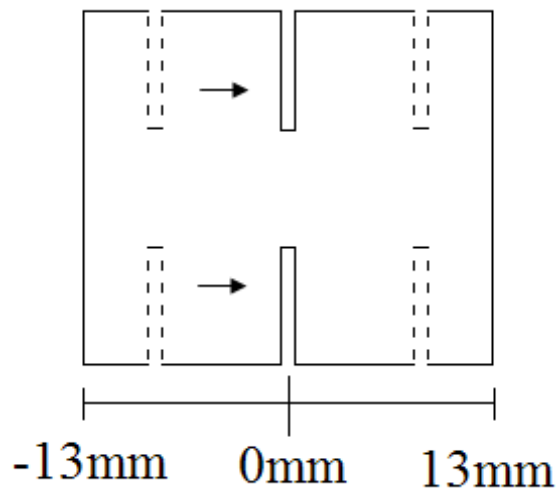
Figure 41 - Diagram of patch surface with slot positions varied along the resonant length of the antenna.
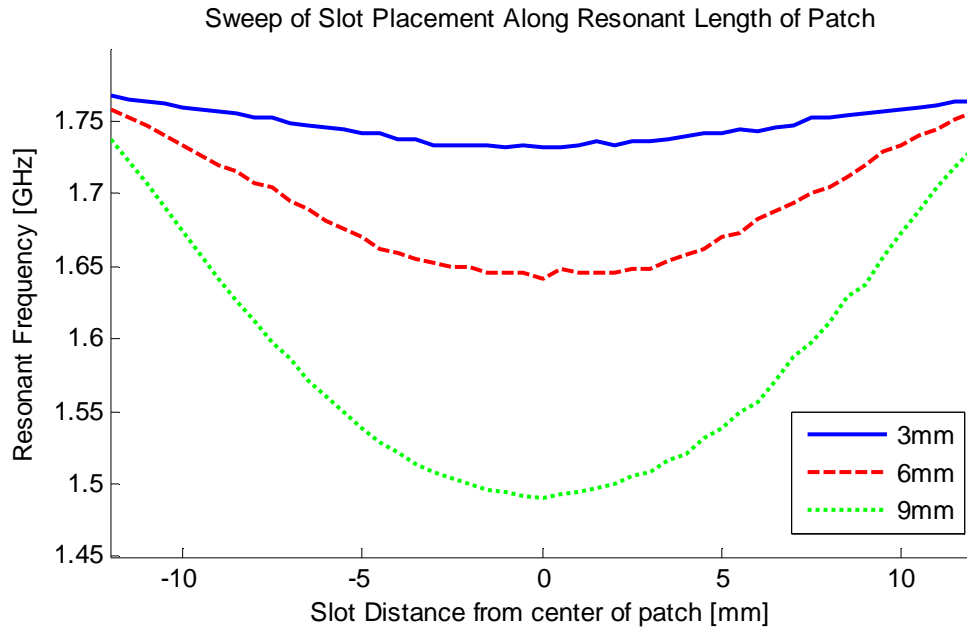
Figure 42 – Resonant frequency vs. slot position showing the change in resonant frequency for three different slot lengths of 3mm, 6mm, and 9mm. The patch is 27×27mm on a 31×31×3mm substrate ($\varepsilon_r = 9.2$).

This study confirms that placing the slot at the center of the patch, where the largest currents are, has the most impact on performance. From a circuit theory perspective, the inductance will have the most affect when there is high current involved. As the slots are moved away from the center of the patch, in either direction, the resonant frequency rises symmetrically (independent of which direction the slots are moved). In fact, the resonant frequency tuning curve maps out the cosine current distribution that develops on the patch with respect to length, except as an inverted cosine, since the lowest frequency tuning is at the current maximum, and the highest frequency tunings are where the lowest levels of current are. There may be situations where placing the slots off of the midpoint of the patch has an advantage, such as less conflict between placement of the feeding probe and the slot. Additionally, multiple slots can be utilized, although

with the knowledge that the slots will have less effect as they move away from the central axis.

Slot shapes are another aspect of slot loading that was studied. Previous studies all involved a rectangular slot shape, but there is a wide range of conceivable shapes for use in the same manner. Slots were modified to have round, smooth terminations, triangular slots, circular slots, slots with cavities at the end, and multiple slots in the patch surface as shown in Figure 43.
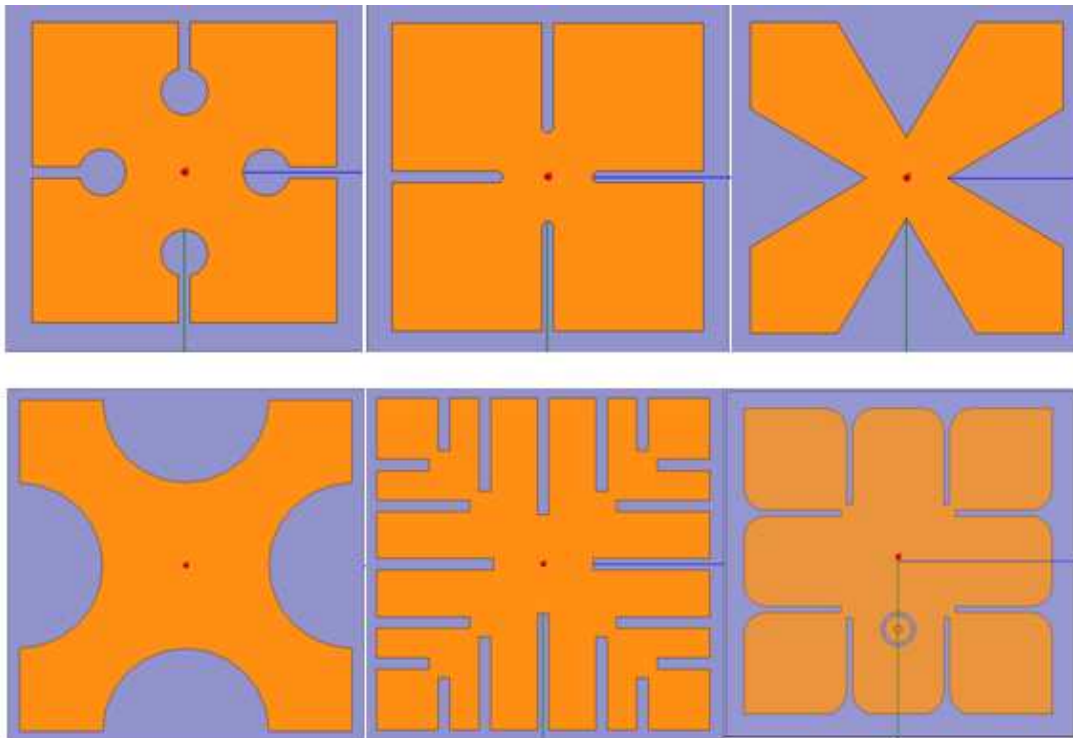
Figure 43 - Various slot shapes studied to determine the performance compared to a rectangular slot.

Three cases are compared – circular slots, as shown in the bottom left of Figure 43; slot with circular cavities, shown in top left of Figure 43; and triangular slots, shown in the top right of Figure 43. The dimensioned antennas are shown in Figure 44.
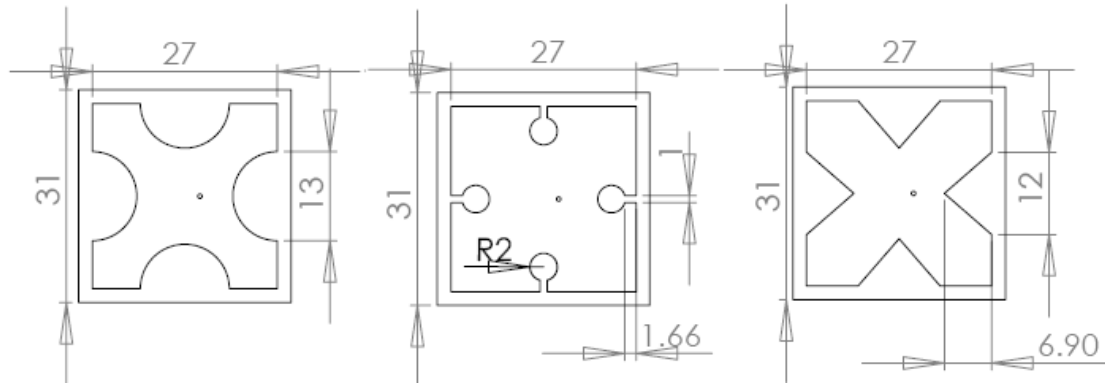
Figure 44 - Dimensioned drawings of the three slot shapes compared to observe effect of slot shape on bandwidth.

Slot Shape	f_o [GHz]	2:1 VSWR B [MHz]
Circular Slots	1.601	8
Slots with Circle Termination	1.598	8
Triangular Slots	1.606	8

Table 1- Comparison of the 2:1 VSWR bandwidth for three different slot shapes.
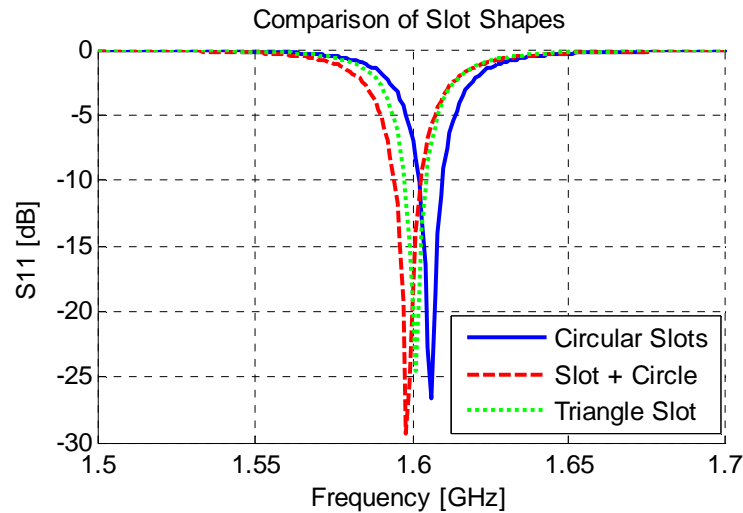
Figure 45 - Return loss of the simulated antennas with different slot shapes for comparison of bandwidth performance.

All three of the antennas were tuned to approximately 1.6GHz, and Table 1 shows that the 2:1 VSWR bandwidth is the same for each antenna. No shape was found to provide an improved impedance bandwidth compared to simple rectangular slots.

However, some slot shapes provide advantages in frequency tuning. For example, multiple slots can be cut into a patch surface, such as in Figure 43, which allows the patch antenna to be tuned to a lower resonant frequency than what is possible with a single slot. Also, Figure 44 shows that for the same resonant frequency, the edge of the triangular slot is closer to the center than the edge of the slot terminated in the circular cavity. Therefore, the slot with the circular cavity termination is less likely to interfere with the feed probe placement than the triangle-shaped slot. Some shapes may allow easier placement of the feed probe than others. Also, another use of multiple slots is to place two slots off-center from the central axis, shown in Figure 46, which allows the centerline to be completely unobstructed for maximum flexibility in feed probe placement, removing an impedance tuning obstacle while retaining the frequency tuning performance.
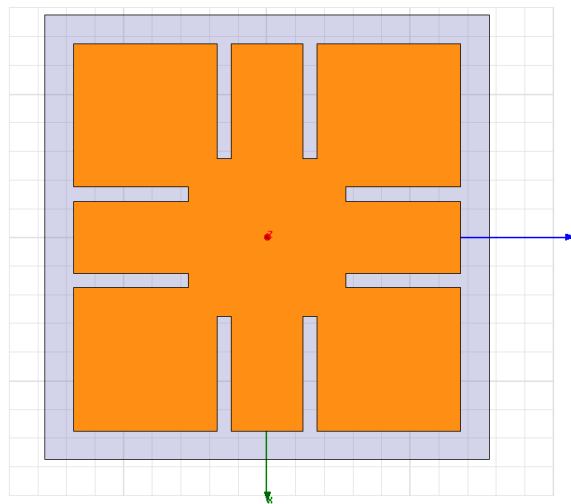
Figure 46 - Patch antenna using two slots to achieve the desired resonant frequency, while leaving the centerline of the patch free for the feed probe.

The slot study results can be summarized as follows:

- The slots decrease the resonant frequency of the patch antenna by diverting the current to a longer path, resulting in an effect analogous to that of an inductor placed in series between two halves of the patch.

- The slots have the most impact on performance when placed in areas of high current on the patch surface, which for the dominant TM_{100} mode is along the center of the patch length.

- For narrow rectangular slots, the resonant frequency decreases approximately linearly in direct relation to the length of the slot.

- Increasing the width of the rectangular slots further decreases resonant frequency, although in a nonlinear manner.

- For substrate thicknesses less than the slot width, the frequency is decreased further by capacitance developed between the ground and the patch.

- The shapes of the slots cut into the patch layer do not have any bandwidth performance benefits with respect to one another. Some shapes might allow for easier feed probe placement.

- Multiple slots can be cut into a patch to obtain further frequency reduction, although at no benefit in bandwidth or gain. Multiple slots can also be used to free the patch area along the center axis, allowing more convenient feed probe placement.

- Slot loading can be used to allow the use of low permittivity substrates while obtaining the same frequency tuning of much higher permittivity materials. This allows the high loss and high permittivity tolerances to be avoided.

3.2.2   Optimized Slotted, Stacked Patch Design

The slot study data provides insight and trends on how the various slot parameters affect the antenna performance. To illustrate the use of slot loading in reducing the size of an antenna, a design that uses slots is presented that was optimized according to the design specifications that motivated this study. This design consists of two stacked patches, the top patch is 30×30mm square with four 12mm long slots 1mm wide along each of the main axes of the patch, and the bottom patch is 27.5×27.5mm square, Figure 47 and Figure 48. The bottom patch is placed on a 36×36×3.5mm TMM10 substrate, and between the bottom and top patch is a 36×36×3mm TMM10 substrate.   The structure is fed via an L-shaped probe placed through a clearance hole in the bottom patch with the 4mm long horizontal section placed between the two patches with 0.75mm separation between the top patch and the probe.
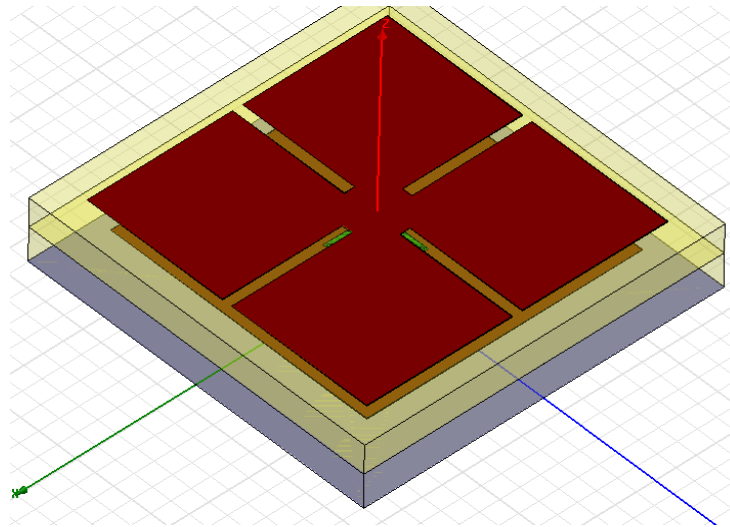
Figure 47 - Isometric view of the optimized slotted, stacked patch antenna.
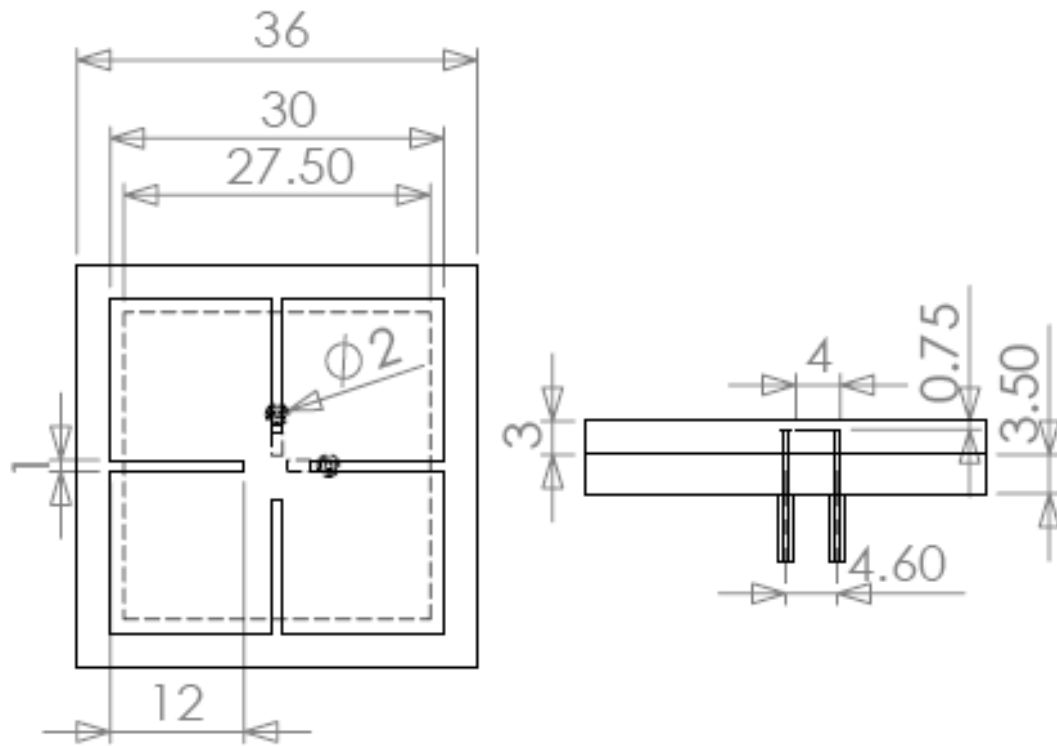
Figure 48 – Dimensioned drawing for the optimized slotted, stacked patch antenna. All dimensions are in millimeters.

The structure was simulated in Ansoft HFSS using PEC patch material and TMM10 dielectric material. The antenna is impedance matched at each band, with a 2:1 VSWR bandwidth of 6MHz at the L2 band, and 10MHz at the L1 band, Figure 49, satisfying the matching requirements of the design that motivated this study. The isolation is better than 20dB across both bands, indicating good cross-pol and low loss due to coupling. Figure 50 shows the impedance loci and the impedance match obtained on the Smith chart.
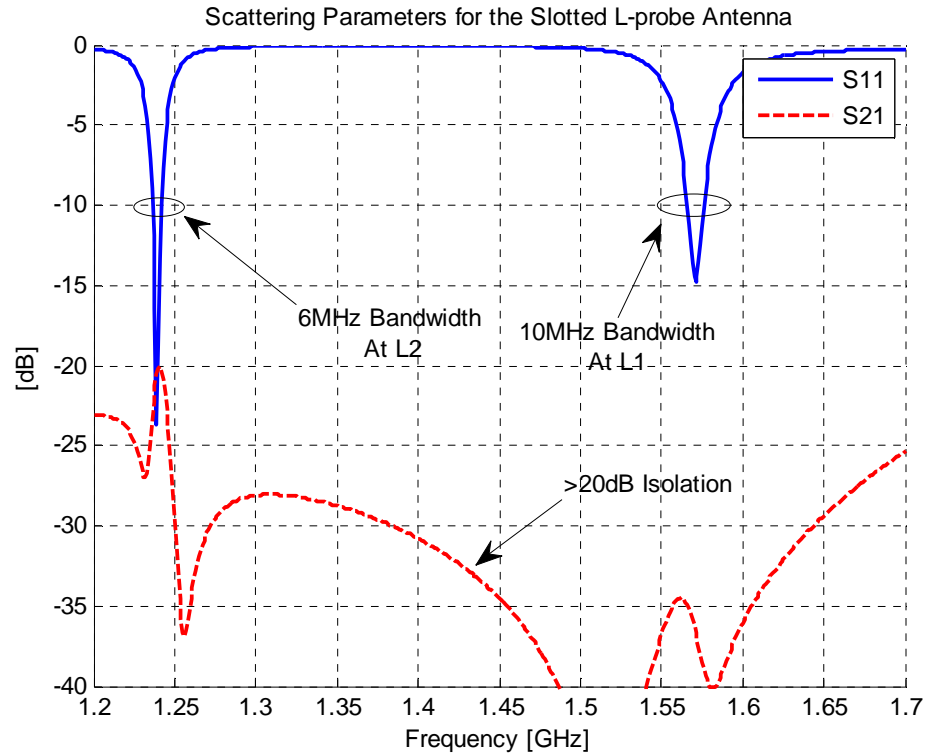
Figure 49 – Simulated return loss for the optimized slotted stacked patch design on TMM10 substrate material.
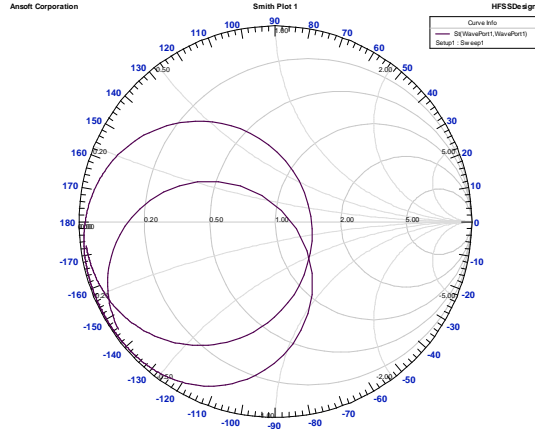
Figure 50 - Smith chart for the slotted stacked patch design, showing the matching of the impedance loci.

The gain performance was analyzed with the antenna placed on an infinite ground plane. The simulation results are expressed in "realized gain", which is the HFSS gain parameter that takes into account the impedance mismatch, which differs from the traditional IEEE definition of antenna gain. The excitations at each port were in quadrature phasing,

allowing circular polarization to be generated. The antenna was found to have a +/-1dB

gain flatness bandwidth of 28MHz at L1 and 15MHz at L2, with a gain above 3dB over

each band, although both bands have usable gain outside of this bandwidth if gain

flatness is not a priority, Figure 51.
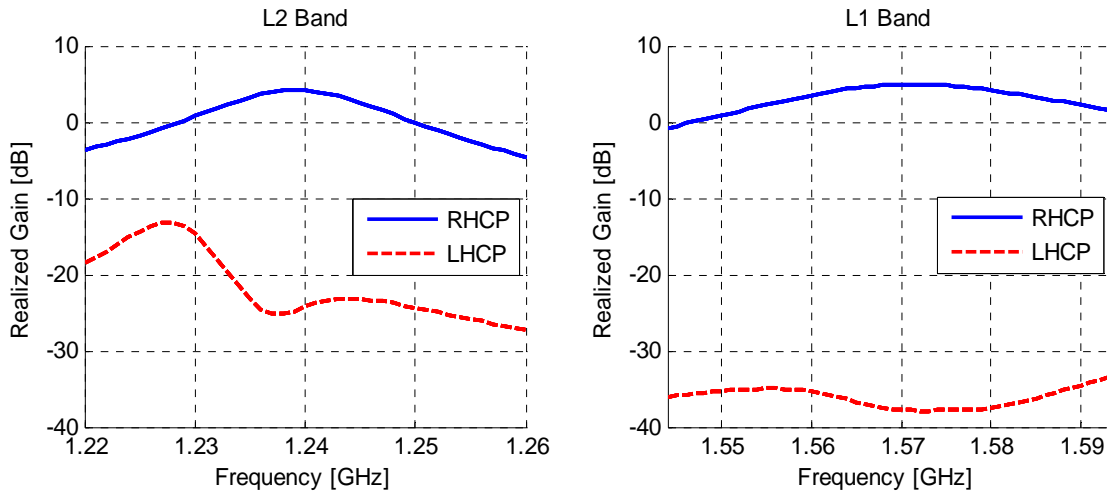
Figure 51 – Simulated maximum gain at broadside versus frequency at L1 and L2 for the slotted, stacked patch antenna.

The low LHCP levels indicate good cross-pol over each band, and the axial ratio was

calculated at broadside over the bands where gain flatness was obtained, Figure 52. At

L1, the axial ratio was below 0.4dB throughout the band, which is well below the typical

3dB axial ratio specification. For L2, the axial ratio was between 1 and 2dB except

towards the very lower end of the band, out of the gain flatness bandwidth, where the

axial ratio increases above the 3dB level. The performance met the desired 3dB axial

ratio specification over both bands L1 and L2.
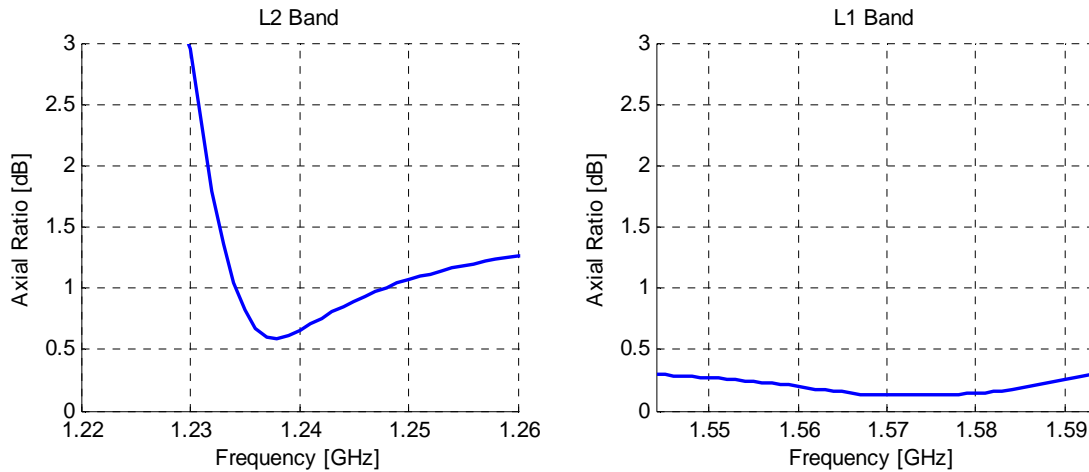
Figure 52 – Simulated Axial Ratio at L2 and L1 for the Slotted Stacked Patch Antenna.

This antenna performs satisfactorily, meeting the VSWR bandwidth requirements and approaches the gain bandwidth requirements, while occupying a small volume of 36×36×6.5mm (1.42×1.42×0.26"). The length of this antenna is on the order of $\lambda/6.7$, and has a thickness of only $\lambda/37$. The miniaturization achieved was due to the use of moderately high permittivity substrate (TMM10, $\varepsilon_r = 9.20$) and the slots that were used to reduce the size of the L2 patch without having to resort to either a larger size antenna or a higher permittivity substrate. Further, this design was the thinnest antenna designed during this study that met the impedance bandwidth specifications, resulting in a design that is closest to meeting the electrical specifications and the ultimate goal of 31×31×5mm total volume for the antenna.

3.3   Cavity Loading

Cavity loading offers some distinct advantages when designing a microstrip antenna. A cavity backing provides a metallic boundary around the antenna that can be

used to isolate the antenna from its surroundings. This allows close integration of an antenna onto circuit boards, or surfaces where the antenna must be placed near surfaces that might absorb or scatter energy. Also, a microstrip antenna is planar and can conform to the surface it is mounted on, providing compact and unobtrusive antenna placement on the exterior of automobiles, airplanes and other surfaces. When a cavity is placed around a microstrip antenna, this allows the antenna to be recessed into the mounting surface (the ground plane), flush with the surface.

The cavity also provides some electrical benefits. The walls of the cavity, if close to the patch antenna, load the edges of the patch similar to that of a lumped parallel plate capacitor, which lowers the overall resonant frequency of the patch. Often miniaturized patch antenna designs use thick, high permittivity substrates to reduce the resonant frequency while maximizing bandwidth for a given area. The side-effect of this method is the excitation of surface waves, which results in a loss of power out along the grounded substrate – lowering the efficiency of the antenna and/or distorting the radiation pattern. By placing a cavity behind the patch, surface waves are suppressed by the metallic walls, which essentially "short out" the TE/TM surface wave modes [31].

The cavity backing can also provide extra feeding options compared to a regular microstrip antenna. Since the cavity is essentially the ground plane for the antenna folded to form a cavity, a feed probe can be placed in a side wall to feed the antenna just as easily as on the bottom plane of the cavity. This can allow shorter paths to the antenna than from the bottom of the cavity, reducing the inductance introduced by feed probes in thick substrates.

One way of assessing the loading of the cavity is to look at the transmission line
model for a microstrip patch antenna, shown in Section 3.1.1 The cavity walls are part of
the ground system of the antenna, so the metallic walls load the antenna similar to a
capacitor in shunt from the edge of the patch to the ground, in parallel with the slot
admittance, shown in Figure 53.
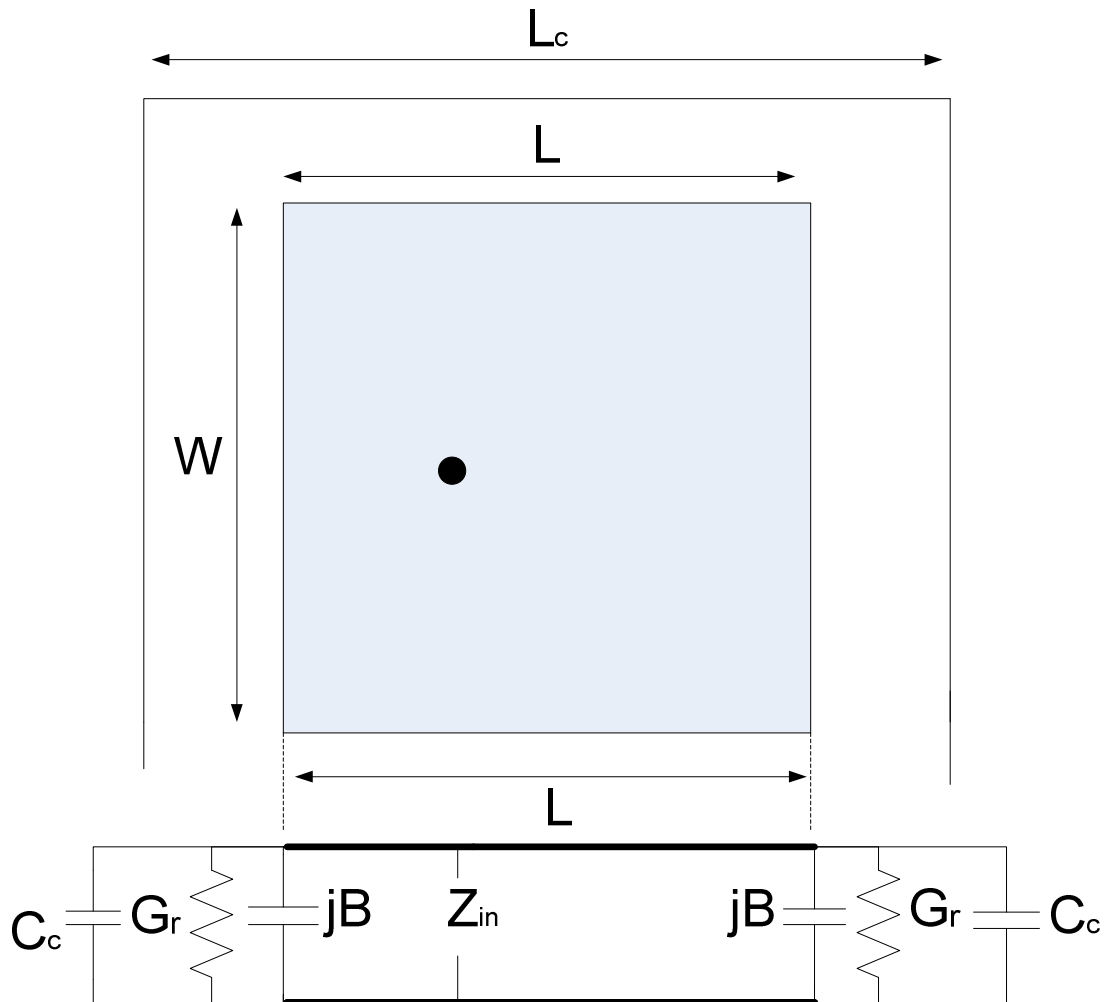
Figure 53 - Modified transmission line model for the microstrip patch antenna when a
cavity is placed behind it. C_C represents the effective capacitance of the cavity backing.

The capacitance in parallel with the slot admittance lowers the resonant frequency of the
patch antenna, similar to the lumped capacitor loading shown in Appendix G.

3.3.1   Cavity Loading Performance Trends

For a miniaturized patch antenna, increasing the substrate thickness will increase

the bandwidth, helping to compensate for the narrow bandwidths of the small antenna.

On substrates that extend well beyond the edges of the patch element, increasing the

thickness t of the substrate linearly decreases the resonant frequency, as predicted by

equations 3.2-3.5 (and shown in Appendix H).   However, small patch antennas often

have substrates not much larger than the patch itself, so an additional side effect of the

increased substrate thickness is an increase in resonant frequency with increasing

substrate thickness due to the fringing fields extending out the sides of the substrate.

With the fringe fields extending into air both above the substrate and on the sides of the

truncated substrate, the effective permittivity of the substrate dielectric decreases, which

equation 3.5 shows results in an increase in resonant frequency.

A 31.5×31.5mm square patch on a TMM10 (ε_r = 9.2) substrate of thickness t and

of width and length α, Figure 54, is used to illustrate this effect. The substrate size α is

varied between 31.5mm, where the substrate is truncated to the same size as the patch,

and 100mm, which is large enough to approach the performance of the antenna on an

infinite substrate for various thicknesses t. The simulated results are shown in Figure 55.
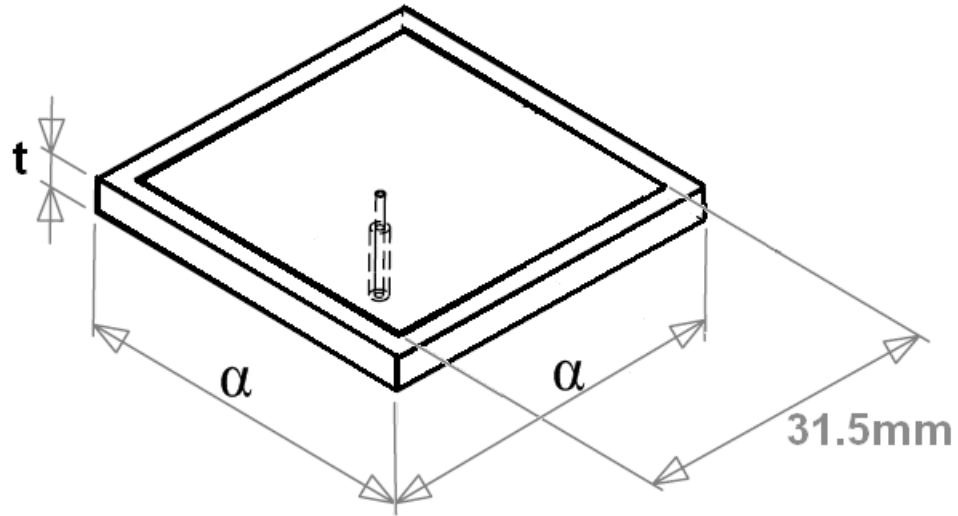
Figure 54 - 31.5×31.5mm square patch antenna on a TMM10 substrate of thickness t and length and width α. Antenna is mounted on an infinite ground plane.
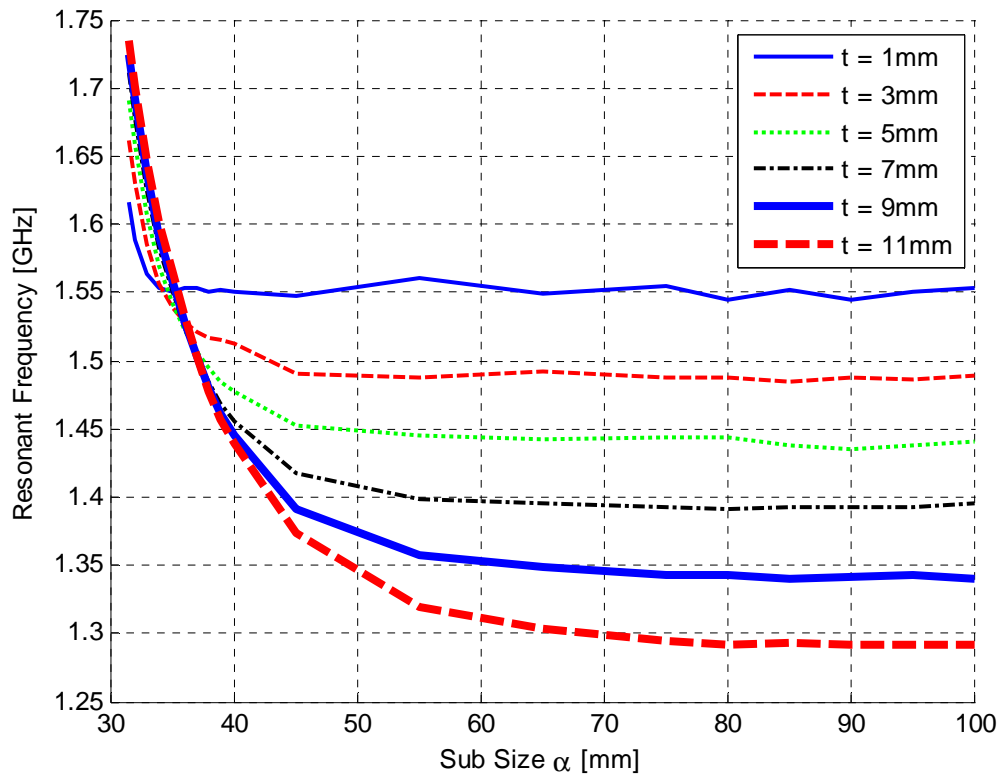
Figure 55 - Change in resonant frequency for 31.5×31.5mm patch on substrates of thickness t and length α, width α.

For α = 31.5, the antennas with thick substrates tune to a resonant higher frequency than the thin substrates, since all of the fringing fields extend outside of the substrate into the air, which lowers the effective permittivity of the substrate. This effect is more pronounced for thick substrates since more fields extend laterally from the thick substrates than for the thin substrates. For antennas with α = 100m, the substrate is large compared to the 31.5mm patch, and the antennas with thick substrates tune to a lower resonant frequency than the thin substrates, as theory predicts.

Figure 55 also shows that the resonant frequency decreases with increasing substrate size α until the substrate is large enough to contain the fringe fields for a particular thickness, after which the resonant frequency becomes approximately invariant with substrate size and the tuning curve approaches a horizontal line. The substrate size α = α_o at which this occurs varies depending on substrate thickness, where the thinnest substrate has the smallest α_o, and the thickest substrate has the largest α_o. This causes the tuning curves to crossover in the range of 34mm<α< 38mm, Figure 56.
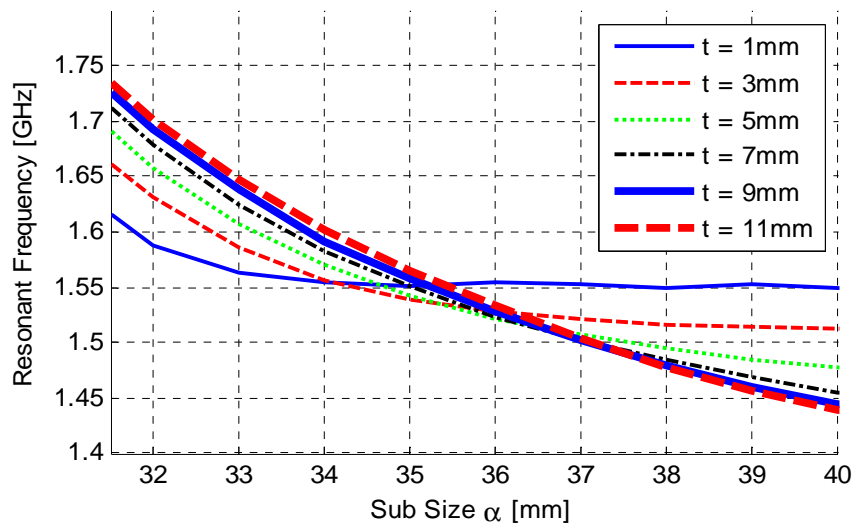
Figure 56 - Change in resonant frequency for 31.5×31.5mm patch on substrates of thickness t and length and width 31.5mm < α < 40mm.

For a particular resonant frequency, increasing the substrate thickness for a patch antenna with a small substrate size α will require increasing the area occupied by the antenna, which is counter-productive to the miniaturization effort.

Conversely, loading the patch with a backing cavity can alleviate this increase in resonant frequency. The antenna shown in Figure 54 was modified by cladding the substrate in metal on the vertical sides of the dielectric, as shown in Figure 57.
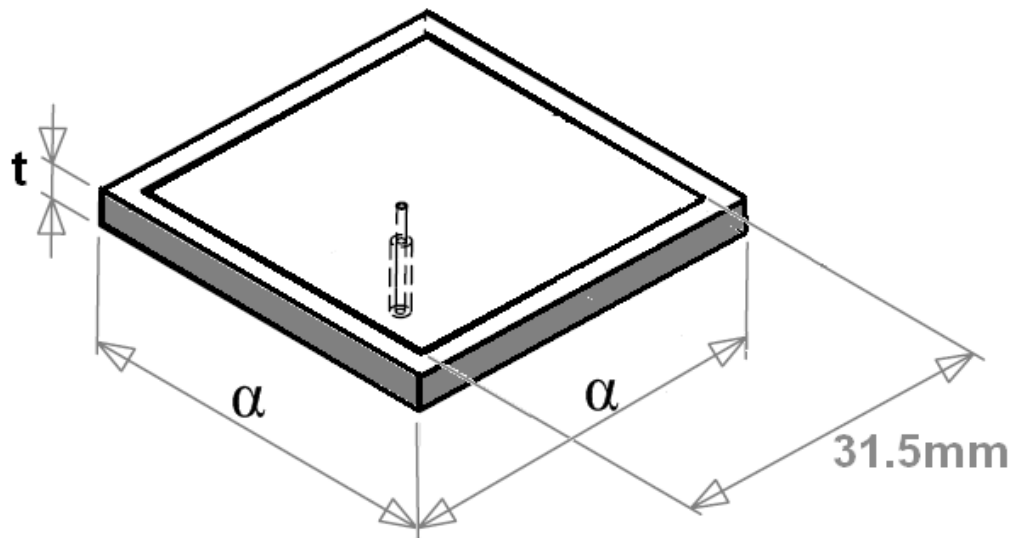
Figure 57 - Cavity backed 31.5×31.5mm square patch antenna on a TMM10 substrate of thickness t and length and width α. The gray represents the metallization on all four of the vertical walls of the substrate to form the cavity. The cavity is recessed in an infinite ground plane.

The thickness for the cavity backed antenna is chosen as t = 7mm, and the resonant frequency of the antenna is shown simulated for substrate sizes α over the range 32mm < α < 100mm, and is compared to the performance of the same size antenna of Figure 54, which does not have a cavity.
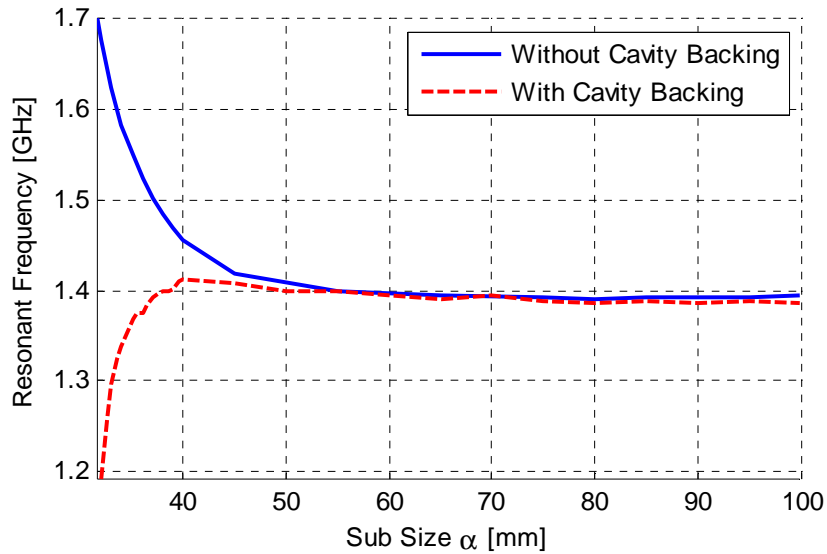
Figure 58 - Change in resonant frequency for 31.5×31.5mm patch antennas with carrying substrate size α. Antennas have TMM10 substrates of thickness t = 7mm, and the results are shown for antennas with and without a cavity backing.

For the substrate size α = 32mm, the cavity loading reduces the resonant frequency by 500MHz from 1.7GHz to 1.2GHz, which is also 200MHz below the resonant frequency of the same antenna on an approximately infinite substrate. As the size α increases, the cavity walls move further away from the patch and the capacitive loading is decreased, causing the resonant frequency to increase. This change in capacitance is analogous to a parallel plate capacitor, where increasing the separation between the plates decreases the capacitance. The resonant frequency of the cavity backed antenna continues to change with increasing α until the walls of the cavity are far enough away from the edges of the patch that they no longer have a loading effect. For the cavity backed antenna with substrate thickness t = 7mm, this occurs at approximately α = 55mm, beyond which the cavity backed antenna tunes to the same resonant frequency as the antenna without a cavity backing. Therefore, the cavity backing can be used to

lower the resonant frequency of the antenna when the cavity is close in size to the patch, even when the thickness of the substrate is increased.

The second study involves observing the effect on resonant frequency, gain, and bandwidth for a reduced size, cavity-backed patch antenna. Modifying the antenna in Figure 57, the patch size is reduced to 27×27mm, and the frequency reduction is accomplished by placing four 7mm long, 1mm wide slots in the patch surface.   The new antenna is shown in Figure 59. The cavity is formed by placing a metallic wall on each of the vertical walls of the TMM10 ($\varepsilon_r = 9.2$) substrate, of length and width α, and thickness t. Since this study deals only with a cavity backed antenna, the substrate thickness t will be referred to as cavity depth t. Four values of α were chosen - two values that place the cavity walls close to the patch (α = 27.5mm, 28.5mm) and two values that place the cavity walls a few millimeters beyond the patch edges (α = 30mm, 31mm).
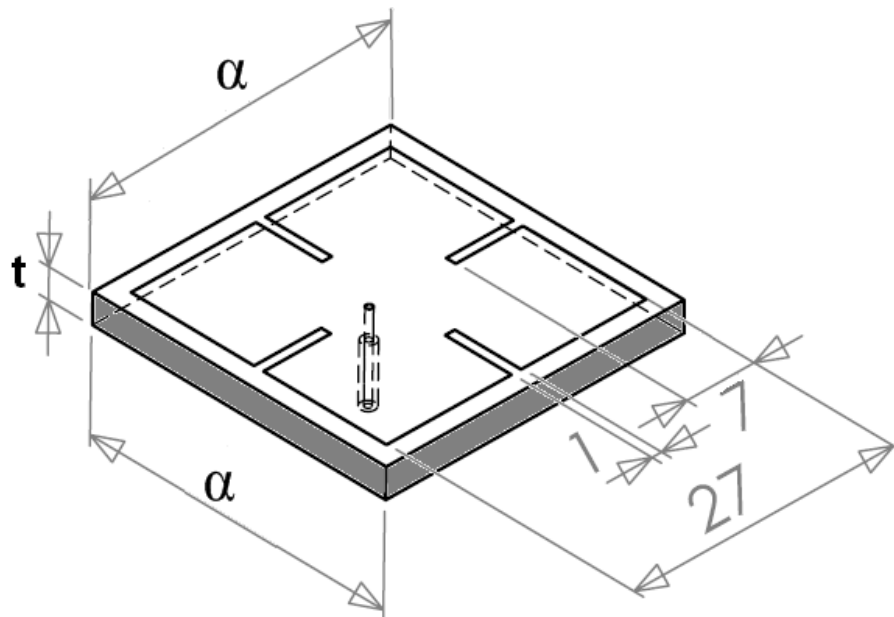
Figure 59 - 27×27mm patch antenna with four 7mm long, 1mm wide slots. The TMM10 ($\varepsilon_r = 9.2$) substrate has a thickness t and length α and width α, and is clad with metal on all four of the vertical walls of the substrate to form the cavity, represented in gray. The cavity is recessed in an infinite ground plane. All dimensions are in millimeters.

74

The resonant frequency is affected by changes in cavity depth t, as well as cavity size, α. With increasing cavity depth, the resonant frequency is decreased, Figure 60, as the taller cavity walls introduce a larger capacitance to the patch edges. This further validates the parallel plate analogy, since increasing the area of a parallel plate capacitor increase the capacitance, similar to increasing the area of the cavity walls increases the capacitance. Increasing the cavity size α results in an increase in resonant frequency, since the walls are moving further away from the patch edges, and the capacitance they introduce decreases. These two trends provide intuitive guidelines on how the cavity can be used to tune the resonant frequency of a patch antenna for a particular depth t or size α.
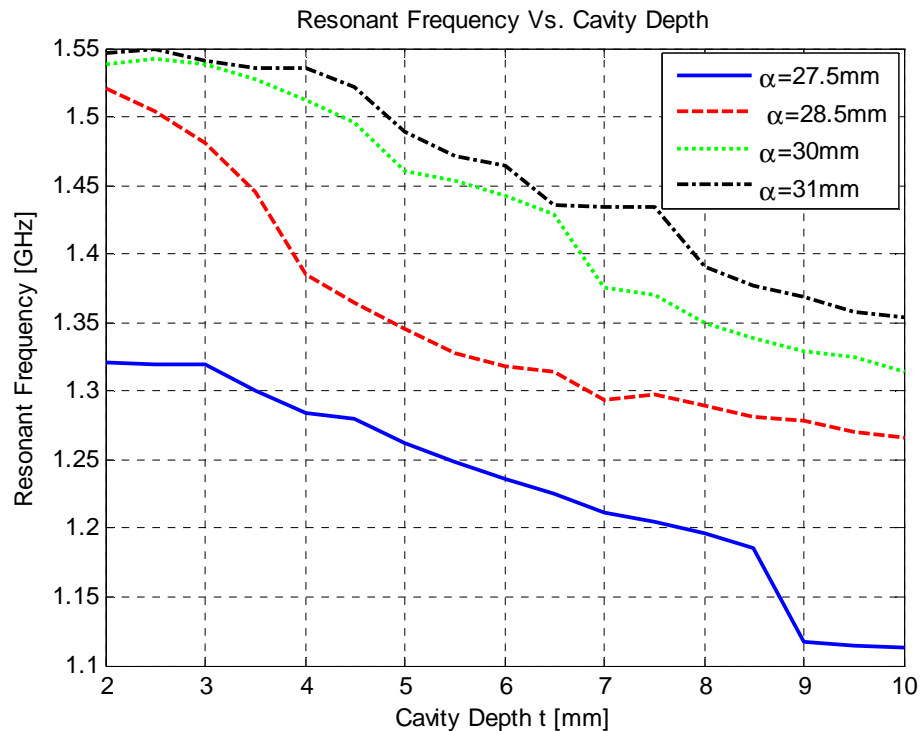
Figure 60 – Change in resonant frequency with variation in cavity depth t of a cavity backed, slotted microstrip patch antenna. Cavity sizes α are shown in the legend.

The cavity dimensions also affect the bandwidth of the patch antenna.   Figure 61

shows that increasing the cavity depth t leads to a larger fractional bandwidth, since the

volume of the antenna is increasing, which is directly related to the Q of the antenna. As

the cavity size α is increased, the fractional bandwidth also increases due to an increase in

antenna volume. Therefore, antenna bandwidth can be increased by increasing either

depth t or size α, but increasing α raises the resonant frequency, whereas increasing t

decreases the resonant frequency.
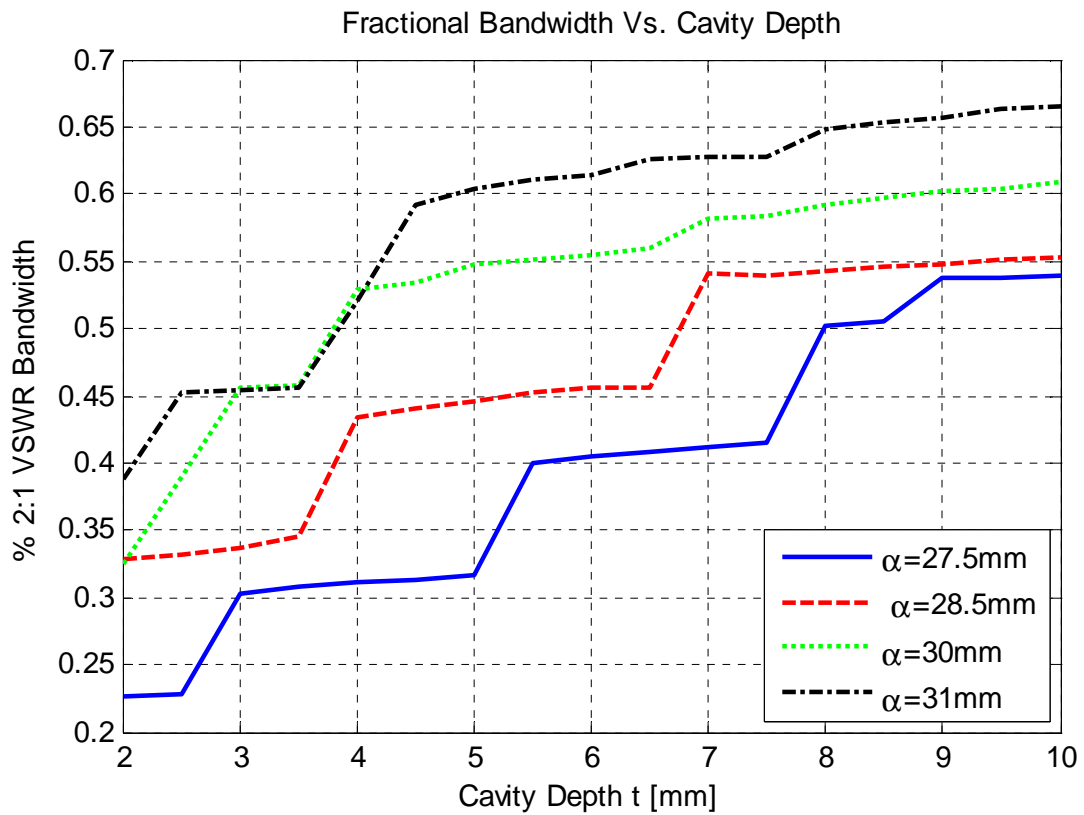
Figure 61 – Change in fractional 2:1 VSWR bandwidth with variation in cavity depth t of
a cavity backed, slotted microstrip patch antenna. Cavity sizes α are shown in the legend.
The stair step nature is due to bandwidth values in increments of 1MHz.
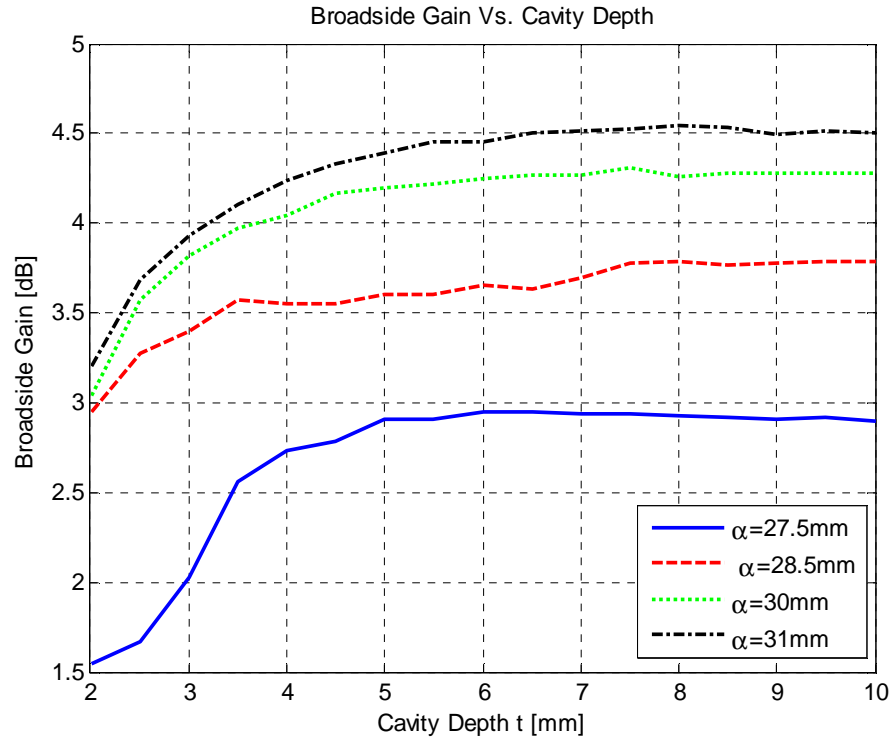
Figure 62 – Change in broadside gain with variation in cavity depth t of a cavity backed, slotted microstrip patch antenna. Cavity sizes α are shown in the legend.

Finally, the gain is shown to also vary with the size of the cavity. For small α, the gain is reduced due to the small aperture size of the antenna, and as α (and aperture size) is increased, the gain also increases, Figure 62. For small cavity depth t, the volume of the antenna is small, leading to low gain, and increasing the cavity depth t increases the volume of the antenna, resulting in increased gain. Figure 62 does not account for the change in resonant frequency which is different for a particular cavity depth t and size α. Since the resonant frequency is also changing with cavity depth t and cavity size α, the gain was normalized to the operating frequency to show more clearly the effects of aperture size and volume on gain, in Figure 63.
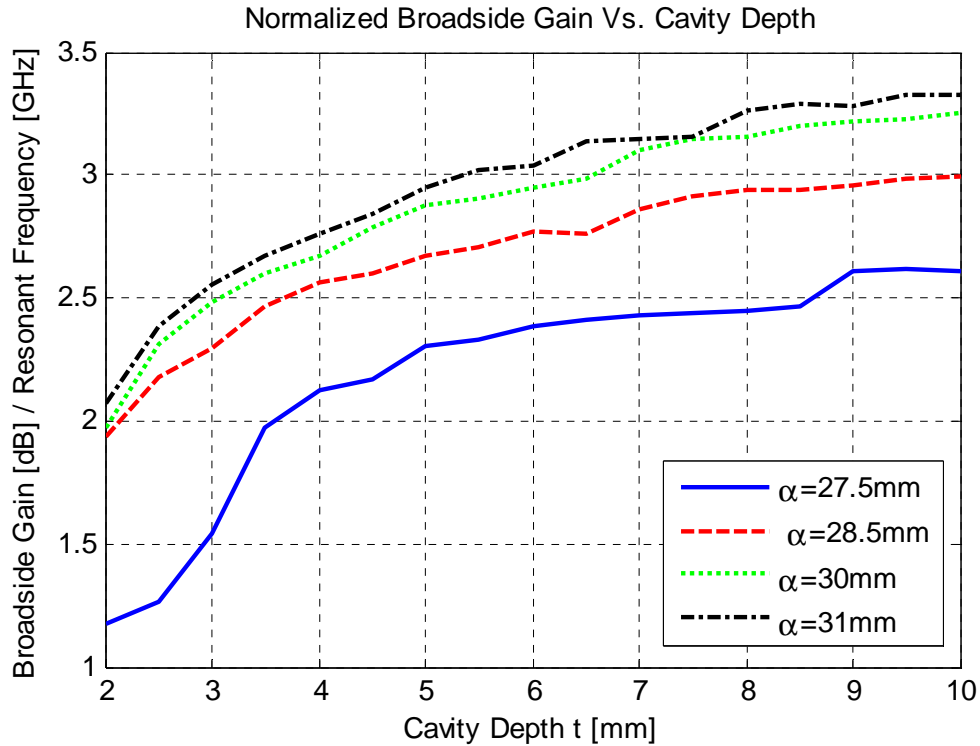
Figure 63 - Change in broadside gain normalized to resonant frequency with variation in cavity depth t of a cavity backed, slotted microstrip patch antenna. Cavity sizes α are shown in the legend.

For a particular resonant frequency, increasing the cavity depth t will result in higher gain. Increasing the cavity size α will result in higher gain, but note that the difference in gain between α=27.5mm and α = 28.5mm is much greater than the difference in gain between α=30mm and α = 31mm, which indicates that cavity size α will impact the gain more significantly when the cavity is close to the patch antenna.

Some design guidelines for the cavity backed antenna can be summarized as:

- Cavity backing allows thick substrates to be utilized without the loss in efficiency due to surface wave excitation, and without the increase in frequency resulting from a truncated substrate.

- The cavity backing allows the antenna to be isolated electrically from its surroundings, making it possible to mount the antenna in closer proximity to other components or surfaces.

- The cavity allows the antenna to be recess mounted, flush with a surface. This provides a low profile, unobtrusive microstrip patch antenna design.

- The cavity walls act like parallel plate capacitors connected in shunt with the radiating edges of the patch – increasing the depth of the cavity increases the effective capacitive loading (by increasing area of the walls), and increasing the separation between the patch edges and the cavity walls decreases the capacitive loading.

- Probe feeding can be accomplished via a side wall, instead of the bottom of the cavity, potentially reducing the inductance incurred by the use of a long feed probe by shortening the distance the probe travels to reach the antenna.

- The size of the cavity α and the depth of the cavity t can be used to tune the resonant frequency of the antenna, and can be optimized to provide the best compromise between bandwidth and gain.

This section has explored the effect of loading a patch antenna with a cavity to create the capacitive loading of the patch antenna. Another form of capacitive loading is illustrated by the stacked patch antenna shown in Appendix I. Vertical walls extend from the edges of the patch toward the ground plane, creating a capacitor loading very similar to the cavity. The resonant frequencies of this antenna are adjusted with the height of the walls on the edge of the patch, and the separation between the patch and the ground

plane. Additional tuning options are available by changing the width of the wall, or changing the shapes of the walls.

3.3.2   Optimized Cavity Backed, Stacked Patch Design

A stacked patch design is presented that operates with dual polarization (CP capability) and dual frequency performance to cover both L1 and L2 bands, and utilizes L-shaped probes to proximity couple to the antenna. The antenna was designed with a depth of 7mm (close to original design goals of 0.2" thickness), and the cavity length was chosen to be 34mm to achieve the desired bandwidth of 5MHz at 2:1 VSWR at the L2 band.   The cavity length was initially chosen as 31mm (due to original design specs of 1.25" length) but was increased in length until the desired minimum bandwidth of 5MHz at 2:1 VSWR was achieved at L2. The design is a variation on the stacked patch design with the feed extending through a circular opening in the lower patch, and the horizontal section of the L probe situated between the patches.
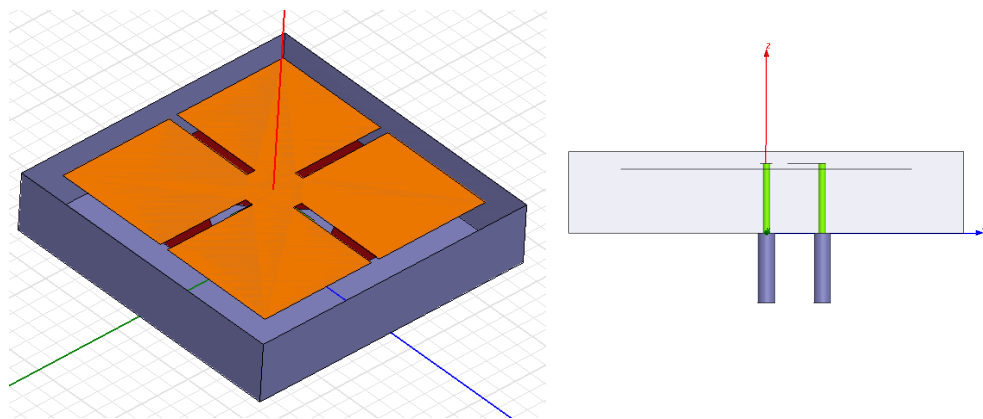
Figure 64 - Optimized design of the cavity backed stacked patch GPS antenna on TMM10 (ε_r = 9.2) dielectric substrate.
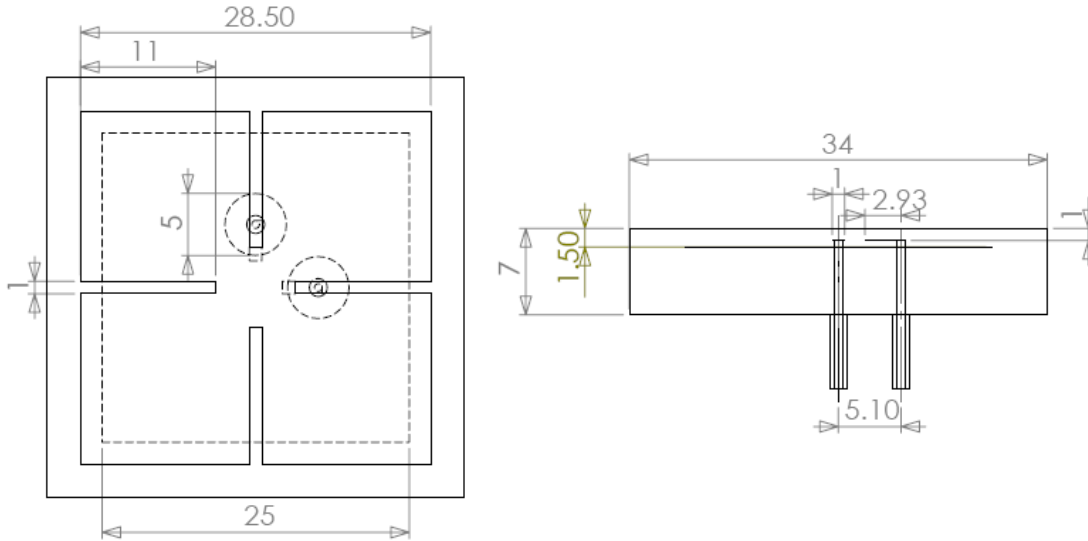
Figure 65 - Dimensioned drawing for the optimized cavity backed dual band, CP, stacked-patch GPS antenna. Horizontal "L" probes are 2.93×1mm. All dimensions are in millimeters.

The top patch is 28.5×28.5mm with four 11mm long, 1mm wide slots to provide additional loading to tune it down to the L2 band. Once again, placing the L2 band patch on top increased the bandwidth at L2 by increasing the size of the substrate below the patch. The bottom patch is 25mm×25mm with two 5mm diameter holes to allow the vertical sections of the L probes to pass through. The total antenna volume is 34×34×7mm, contained fully inside the metallic cavity. The antenna was modeled using PEC surfaces, and the antenna was modeled with the infinite ground plane flush with the top of the cavity, giving this antenna a recessed mounting platform.

The results of the simulations, Figure 66, show that the antenna exhibits a 5MHz 2:1 VSWR bandwidth at L2, and an 8MHz 2:1 VSWR bandwidth at L1. This is adequate bandwidth to meet the performance specifications of dual band GPS systems on both L1 and L2, and was obtained by use of the L-shaped feed probe, which allowed both bands to be matched through the extra degrees of freedom the L probe permits. The isolation

between the probes is also better than 20dB at both bands of interest, indicating good

cross-pol and very low power lost through coupling between the ports. The simulated

gain at L2 and L1 is shown in Figure 67.
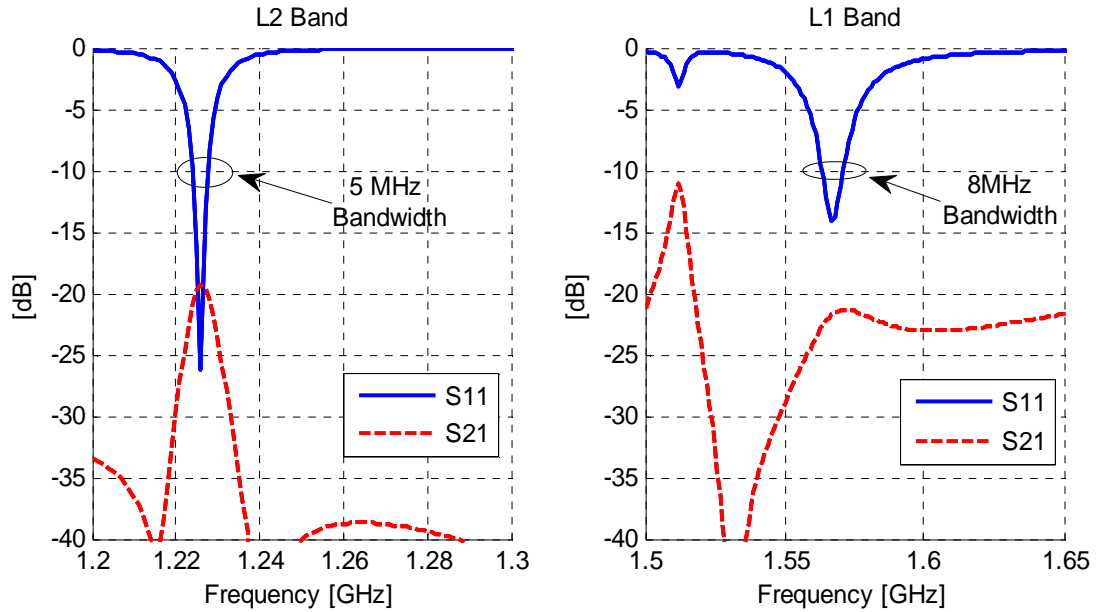
Figure 66 - Return Loss for the optimized cavity backed CP, dual frequency antenna.
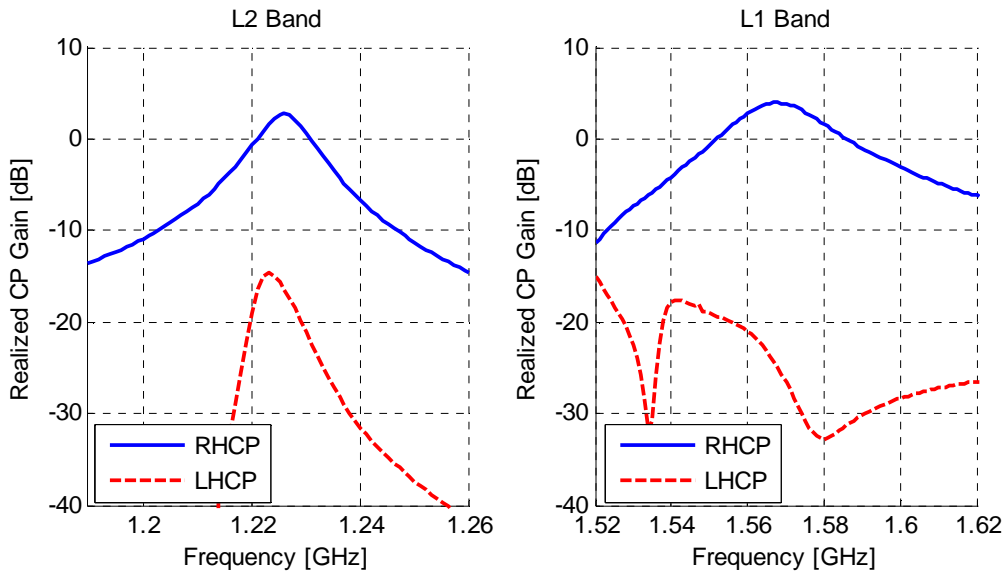
Figure 67 – Simulated realized gain at L1 and L2 for optimized cavity backed CP, dual frequency antenna.

The gain at L2 has a +/-1dB gain flatness bandwidth of 11MHz, which is approximately half of the desired bandwidth. This gain flatness bandwidth could be increased with a larger cavity size (depth or length), or can be used when gain flatness is not critical. At L1, however, the +/-1dB gain flatness bandwidth is 23MHz, and for gain above isotropic the gain bandwidth is 34MHz – both of which are wide enough for proper GPS signal reception. Figure 67 shows that over the L2 band the LHCP component of radiation below -15dB, indicating good cross-pol, and at L1 shows the LHCP component also below -15dB. The axial ratio is shown over both bands in Figure 68.
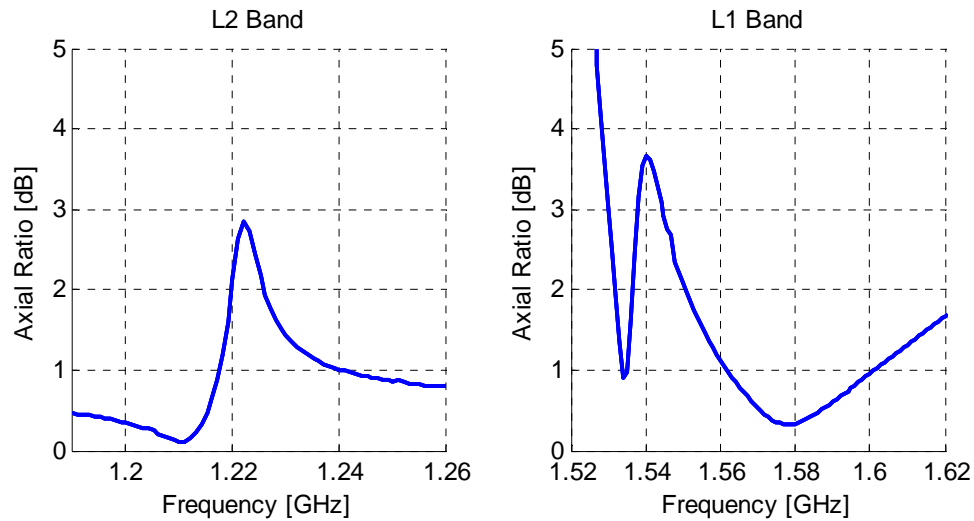
Figure 68 - Axial ratio over the L1 and L2 band for the optimized cavity backed antenna.

Both L1 and L2 have better than 3dB axial ratio over their operating bands, which is a desirable limit for maximum signal reception and rejection of reflections of LHCP signals. These low axial ratios are the result of the low cross-pol shown in the gain patterns.

This optimized antenna meets the VSWR and gain bandwidth goals at the L1 band, and meets the VSWR bandwidth at L2, but only approaches the gain bandwidth

goal at the L2 band. For most GPS applications, reception of the L1 band information is of primary importance, whereas the L2 band is secondary. As indicated, the gain bandwidths have been defined by a +/- 1dB flatness specification, but each band has wider, usable gain bandwidths above isotropic if the variation in amplitude with frequency can be tolerated. This makes this antenna viable for applications where low profile is the priority specification, and the sacrifice in gain performance is acceptable. This optimized antenna utilizes a cavity backing, which reduces the operating frequency of the antenna while making it very low profile, allowing it to be mounted flush in a metal surface, in a recess, making this a candidate for applications where it is desired to have the antenna built into a structure.

CHAPTER 4

CONCLUSION

This thesis set out to explore appropriate miniaturization methods for reducing the size of antennas for GPS systems. The motivation for this study stems from the desire to develop a miniature GPS microstrip patch antenna that would provide 20MHz bandwidth at both L1 (1.575GHz) and L2 (1.227GHz) bands, while occupying a volume of 1.25×1.25×0.2" (31.8×31.8×5mm). Circular polarization was desired with an axial ratio of less than 3dB over each band, with a minimum gain of 0dBi. Due to the requirements of bandwidth, circular polarization with low axial ratio, and gain, many miniaturization methods fail to meet the required performance. Three main methods were found to be viable solutions: the use of high permittivity dielectric materials, inductive loading of the patch element via slots cut into the surface, and capacitive loading via a cavity backing. Each method allows for two-axis rotational symmetry, required to produce circular polarization with good axial ratio, and provides reduction in size.

Some of the trade-offs involved when using each of the loading methods were explored, providing guidelines on how these loading methods can be used in patch antenna designs. Each loading method was then applied in an optimized design that approaches the desired specifications. Two of the optimized designs were built and tested: a linear antenna covering both bands and occupying a volume of 29×20.9×12mm (1.14×0.82×0.47"), and a CP stacked patch design that met all electrical specifications and occupied a volume of 41.5×41.5×6.5mm (1.63×1.63×0.26"). Additionally, other designs were presented that achieved similar performance. A slotted, stacked patch was designed to meet the VSWR specifications, and approached the gain flatness

specifications in a volume of 36×36×6.5mm (1.42×1.42×0.26"). This was the smallest

antenna found in this study that approached the electrical specifications. Finally, a cavity

backed stacked-patch configuration was used to design an antenna that once again met the

VSWR specifications but fell short of the gain flatness bandwidth goals. This antenna

was 34×34×7mm (1.33×1.33×0.28") in size, and allowed for recessed mounting if

desired.

Literature searches failed to find antennas that were as compact in size while

achieving the 2:1 VSWR bandwidths of these antenna designs. Many designs found in

the literature sacrificed the impedance match to achieve their operating bandwidth.

Additionally, the use of the "L" probe feed structure, which was used in most of the

designs presented, provided the ability to tune to both L1 and L2 in the stacked patch

configurations. The extra degrees of freedom, such as probe width, length, and proximity

to each patch allowed for a good impedance match of 2:1 to be achieved on both patches

at once. Additional size reduction was accomplished for each antenna by feeding the L

probes through clearance holes in the lower patch for the stacked patch configuration,

instead of proximity feeding the patches from the side, as in traditional proximity

coupling.

APPENDIX A

DERIVATION OF MINIMUM Q LIMITS

Based on [15]

Single Polarized, Omnidirectional Antenna – TM$_{10}$ mode only

First, to compute the fields of the TM$_{01}$ spherical mode, an r-directed magnetic vector potential is given as a linear electric current element

$$A_r = -\cos\theta\left(1 - \frac{j}{kr}\right)e^{-jkr}$$

The fields from which are

$$H_\phi = \sin\theta\left(\frac{j}{kr^2} - \frac{1}{r}\right)e^{-jkr}$$

$$E_\theta = \frac{1}{j\omega\varepsilon}\sin\theta\left(-\frac{1}{r^2} - \frac{jk}{r} + \frac{j}{kr^3}\right)e^{-jkr}$$

$$E_r = \frac{2}{\omega\varepsilon}\cos\theta\left(\frac{j}{r^2} + \frac{1}{kr^3}\right)e^{-jkr}$$

From the field components, the total stored electric energy density can be computed as

$$w_e = \frac{1}{2}\varepsilon\vec{E}\bullet\vec{E}^* = \frac{1}{2}\varepsilon\left(\left|E_\theta\right|^2 + \left|E_r\right|^2\right)$$

$$= \frac{1}{2\omega}\eta\left[\sin^2\theta\left(\frac{1}{k^3 r^6} - \frac{1}{kr^4} + \frac{k}{r^2}\right) + 4\cos^2\theta\left(\frac{1}{k^3 r^6} + \frac{1}{kr^4}\right)\right]$$

As the limit $r \to \infty$ is taken, the E$_r$ term goes to zero, and the radiated fields become

$$H_\phi^{rad} = -\sin\theta\frac{e^{-jkr}}{r}$$

$$E_\theta^{rad} = -\eta\sin\theta\frac{e^{-jkr}}{r}$$

87

The radiated electric energy density can be computed as

$$w_e^{rad} = \frac{1}{2}\varepsilon \vec{E}\cdot\vec{E}^* = \frac{1}{2}\varepsilon\left|E_\theta^{rad}\right|^2 = \frac{1}{2}\varepsilon\frac{\eta^2}{r^2}\sin^2\theta$$

McLean then used the difference between the total electric energy density and the radiated electric energy density to find the non-propagating electric energy density as

$$w_e' = w_e - w_e^{rad} = \frac{1}{2\omega}\eta\left[\sin^2\theta\left(\frac{1}{k^3r^6}-\frac{1}{kr^4}\right)+4\cos^2\theta\left(\frac{1}{k^3r^6}+\frac{1}{kr^4}\right)\right]$$

Then, to find the total non-propagating energy, the energy density is integrated over a volume between a sphere of radius a and an infinitely large sphere to get

$$W_e' = \int_0^{2\pi}\int_0^\pi\int_a^\infty w_e' r^2 \sin\theta drd\theta d\phi$$

$$= \int_0^{2\pi}\int_0^\pi\int_0^\infty \frac{1}{2\omega}\eta\left[\sin^2\theta\left(\frac{1}{k^3r^6}-\frac{1}{kr^4}\right)+4\cos^2\theta\left(\frac{1}{k^3r^6}+\frac{1}{kr^4}\right)\right]r^2\sin\theta drd\theta d\phi$$

$$= \frac{4\pi\eta}{3\omega}\left(\frac{1}{k^3a^3}+\frac{1}{ka}\right)$$

Next, the total radiated power can be found by integrating the real part of the Poynting vector over a spherical surface of an arbitrary radius

$$P_{rad} = \int_0^{2\pi}\int_0^\pi \text{Re}\left(\vec{E}\times\vec{H}^*\right)\cdot\hat{u}_r r^2 \sin\theta d\theta d\phi$$

$$= \int_0^{2\pi}\int_0^\pi \text{Re}\left(\frac{\eta\sin^2\theta}{r^2}\hat{u}_r\right)\cdot\hat{u}_r r^2 \sin\theta d\theta d\phi$$

$$= \int_0^{2\pi}\int_0^\pi \eta\sin^3\theta d\theta d\phi = \frac{8\pi}{3}\eta$$

The Quality factor can then be calculated as

$$Q = \frac{2\omega W_e'}{P_{rad}} = \frac{1}{k^3 a^3} + \frac{1}{ka}$$

Circularly Polarized Omnidirectional Antenna – TE$_{01}$ and TM$_{01}$ modes excited

Much of the derivation is the same, so details are omitted for operations that are the same. For the TE case, an electric vector potential and its fields are given as the dual of the TM case as:

$$F_r = -\cos\theta\left(1 - \frac{j}{kr}\right)e^{-jkr}$$

$$E_\phi = \sin\theta\left(\frac{j}{kr^2} - \frac{1}{r}\right)e^{-jkr}$$

$$H_\theta = \frac{1}{j\omega\mu}\sin\theta\left(-\frac{1}{r^2} - \frac{jk}{r} + \frac{j}{kr^3}\right)e^{-jkr}$$

$$H_r = \frac{2}{\omega\mu}\cos\theta\left(\frac{j}{r^2} + \frac{1}{kr^3}\right)e^{-jkr}$$

In order to get CP, an amplitude adjustment of jη is applied to F$_r$, and the TE fields and

TM fields are combined. The field components then become, where $k = \omega\sqrt{\mu\varepsilon}, \eta = \sqrt{\dfrac{\mu}{\varepsilon}}$

$$H_\phi = \sin\theta\left(\frac{j}{kr^2} - \frac{1}{r}\right)e^{-jkr}$$

$$E_\theta = \frac{1}{j\omega\varepsilon}\sin\theta\left(-\frac{1}{r^2} - \frac{jk}{r} + \frac{j}{kr^3}\right)e^{-jkr}$$

$$E_r = \frac{2}{\omega\varepsilon}\cos\theta\left(\frac{j}{r^2} + \frac{1}{kr^3}\right)e^{-jkr}$$

$$E_\phi = j\eta\sin\theta\left(\frac{j}{kr^2} - \frac{1}{r}\right)e^{-jkr}$$

$$H_\theta = \frac{1}{k}\sin\theta\left(-\frac{1}{r^2} - \frac{jk}{r} + \frac{j}{kr^3}\right)e^{-jkr}$$

$$H_r = \frac{2j}{k}\cos\theta\left(\frac{j}{r^2} + \frac{1}{kr^3}\right)e^{-jkr}$$

89

The total electric energy density of this field distribution can be found as

$$w_e = \frac{1}{2}\varepsilon \vec{E} \cdot \vec{E}^* = \frac{1}{2}\varepsilon \left(|E_\theta|^2 + |E_r|^2 + |E_\phi|^2 \right)$$

The same method is applied as in the linear polarization case, and it is found that

$$W_e' = \frac{4\pi\eta}{3\omega}\left[\frac{1}{k^3 a^3} + \frac{2}{ka} \right]$$

It is found that the radiating power is twice that of the linear case, since here power is exciting both modes equally, and is then

$$P_{rad} = \frac{16\pi}{3}\eta$$

The quality factor Q is then computed as

$$Q = \frac{2\omega W_e'}{P_{rad}} = \frac{1}{2}\left(\frac{1}{k^3 a^3} + \frac{2}{ka} \right)$$

The Q is approximately half that of the linear case.

ADDITIONAL ANTENNA DESIGNS

Antenna B1: Modified from the antenna found in 3.1.3, the stacked patch L-probe GPS antenna, this design was reduced in size to 36×36×10mm, and achieved similar bandwidths of 8MHz at L2 and 16MHz at L1 with a smaller area, but a larger thickness.
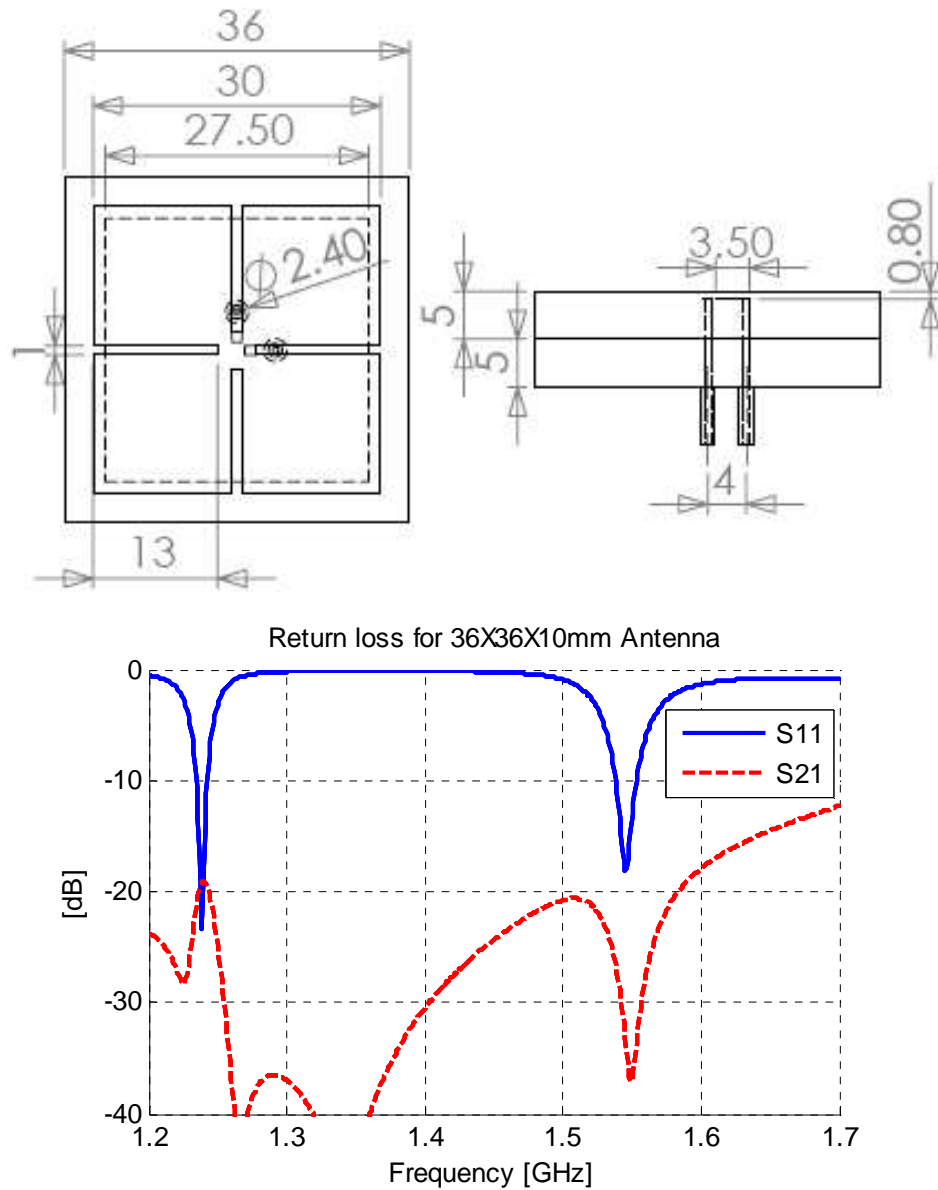
Figure 69 – Dimensioned drawing and return loss for the 36×36×10mm antenna. All dimensions are in millimeters.

Antenna B2: Modified from the antenna found in 3.1.3, the stacked patch L-probe GPS antenna, this design was reduced in size to 31×31×10mm, with slots in both the top and the bottom patches.   The antenna achieves smaller bandwidths of 7MHz at L2 and at L1 a match that gives approximately 50MHz 3dB bandwidth, with no match at 2:1 VSWR, and a larger thickness. This antenna would require further tuning to get L2 tuned down to the proper range, and L1 needs better impedance matching.
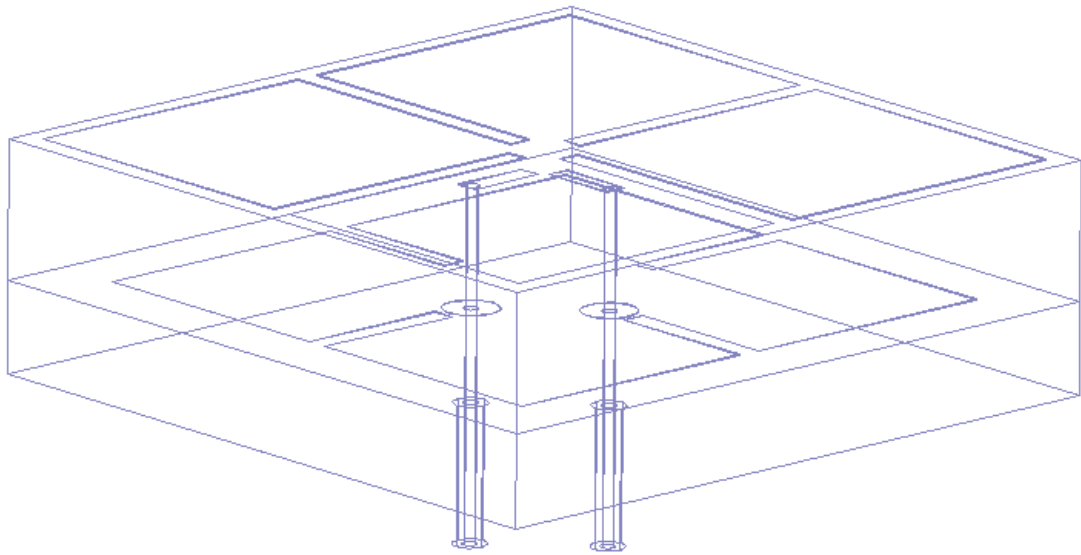
Figure 70 - Wireframe drawing of the 31×31×10mm stacked patch antenna, showing the location of slots in both the top and bottom patch layers.
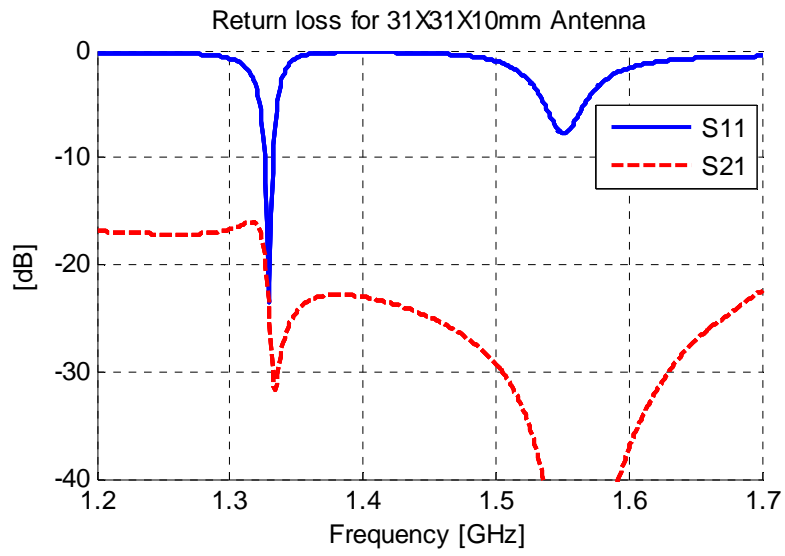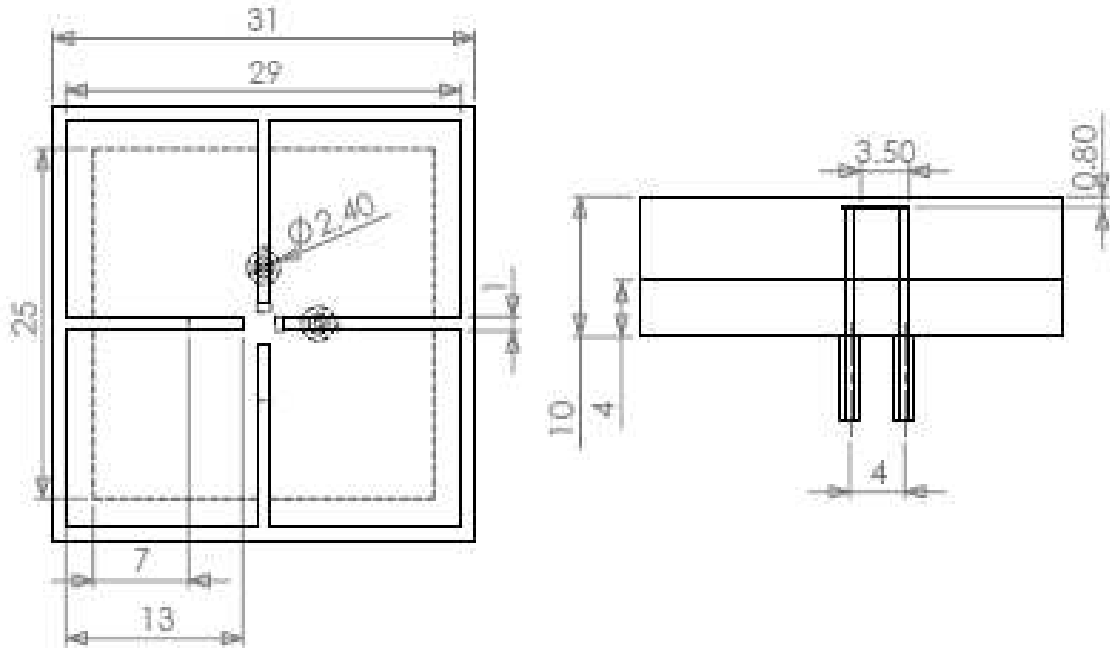
Figure 71 – Dimensioned drawing and return loss for antenna comparison with the theoretical Q limits. All dimensions are in millimeters.

APPENDIX C

HFSS CONDUCTIVITY CONSIDERATIONS

Finite Conductivity Study

Over the course of this research project, attempts were made to take advantage of the finite conductivity simulation options in Ansoft HFSS (High Frequency Structure Simulator) to better estimate performance of realistic antennas. The HFSS software offers multiple options to handle the surface boundary conditions for a conductive patch:

- **Finite Conductivity Impedance -** models the surface as an impedance boundary condition where the tangential E field is related by

$$\hat{n} \times \vec{E} = Z_o (\hat{n} \times \hat{n} \times \vec{H})$$
$$where:$$
$$Z_o = \sqrt{\frac{1+j}{\delta\sigma}}$$
$$\delta = skin\ depth = \sqrt{\frac{2}{\omega\sigma\mu}}$$

  A patch simulation, using this method, is defined as an infinitely thin sheet with this boundary condition assigned. Also allows an equivalent thickness to be assigned to the surface that attempts to model the effects of a finite thickness conductor.

- **PEC Boundary Condition** – models surface as having zero loss, and no tangential electric field. Patch antennas are usually modeled with a sheet layer assigned with a Perfect Electric Conductor boundary condition.

- **Copper Volume** – defines a copper volume as copper material with conductivity of $\sigma = 5.8 \times 10^7$ S/m. Provides the option to solve on the surface only or to include the interior of the volume in the solution.

In addition, there are meshing options:

- **Max Element Size** – restricts the element size on a given surface to a maximum size, allowing the meshing to be set as desired.

- **Skin Depth Mesh** – Allows a mesh to be developed to one skin depth thickness, while choosing the number of meshing layers used to mesh the skin depth.

To compare these different options, two of the prototype antennas were simulated using various settings for conductivity in HFSS. These results are compared to simulations using CST, and measured results.

The first comparison involves the antenna built on Rogers 5880 ($\varepsilon_r = 2.2$) for use as the transmit antenna in Appendix E, shown in Figure 89.
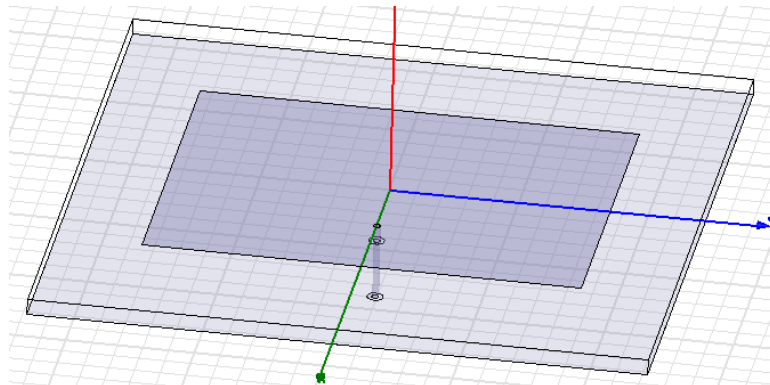
Figure 72 - Patch antenna built for use as transmit antenna in far-field range. Patch is 66×85mm on a 120×120×3.175mm Rogers 5880 substrate.

The simulations were carried out using:

1. a copper volume

2. a copper volume with a 1mm maximum element size

95

3. a copper volume with a skin depth mesh using 3 layers of mesh

4. a finite conductivity surface of copper with zero equivalent thickness

5. a finite conductivity surface of copper with 1mil equivalent thickness

6. a PEC sheet

7. CST copper surface

Figure 73 shows the return loss results for all seven methods, including the measured

results. For an antenna of this size, all of the HFSS simulations matched up well, with

very little variation among them, despite the different methods employed. The CST

simulation also showed good agreement, with a slightly lower resonant frequency and

approximately the same bandwidth. The measured results show a resonant frequency

very close to the simulation, although at a reduced bandwidth. It is possible that the

impedance match is affected by the 12×12" ground plane this antenna is mounted on,

compared to the infinite ground plane used in the simulations.
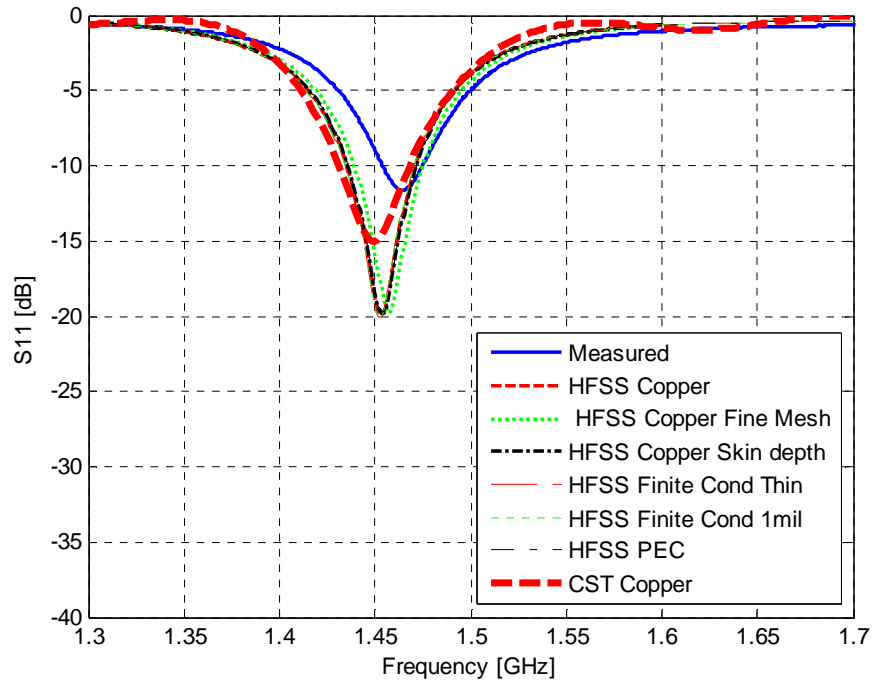
Figure 73 – Comparison of the return loss results for all 8 methods.

The results of the simulations and measurements are summarized in Table 2. The HFSS

simulations have little variation in bandwidth and resonant frequency, but vary

considerably both in memory usage and simulation time.

	Solution Method	B [MHz]	fo [GHz]	Memory	# Tetrahedra	Solution Time hr:min:sec
	Measured	25	1.464			
HFSS	Copper	36	1.453	712MB	21,826	0:13:26
	Copper 1mm mesh	35	1.454	2.14GB	115,076	1:26:21
	Copper Skin Depth	35	1.454	1.52GB	43375	0:37:10
	FC infinite thin	38	1.452	315MB	17,631	0:08:51
	FC 1mil thickness	38	1.452	314MB	17,631	0:09:36
	PEC	36	1.454	365MB	22,321	0:09:08
	CST	40	1.448			

Table 2 – Summarized results of the measured and simulated data. All simulations run on 64 bit WinXP, 2.4GHz Intel Core 2 Duo system (two active cores) with 4GB of RAM.

It is seen that there is little benefit gained by using the finite conductivity surfaces, compared to the PEC modeling, since the computational cost rose considerably while generating almost identical results.

Another example is the simulation of the patch antenna with four 9mm long, 1mm wide slots, on TMM10 dielectric material, Figure 74.
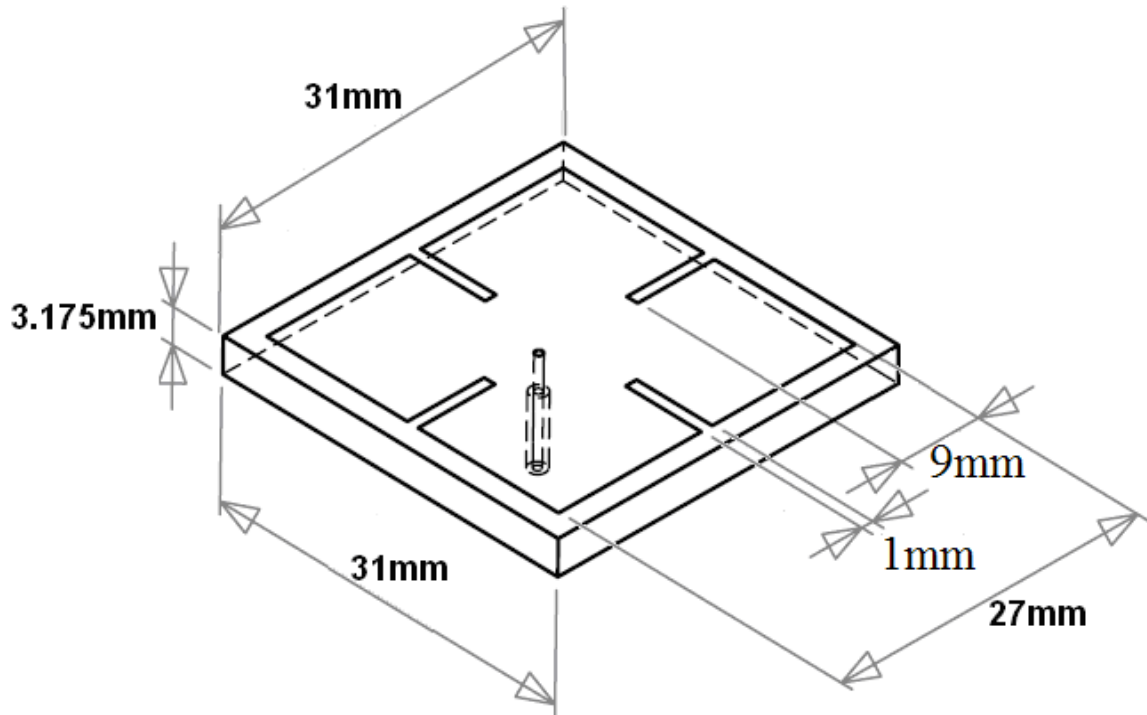
Figure 74 – 27×27mm patch on 31×31×3.175mm TMM10 substrate, with four 9mm long, 1mm wide slots.

The simulations were carried out using:

1. a copper volume

2. a copper volume with a 2mm maximum element size

3. a copper volume with a 0.5mm maximum element size

4. a copper volume with a skin depth mesh using 5 layers of mesh

5. a finite conductivity surface of copper with zero equivalent thickness

6. a finite conductivity surface of copper with 1mil equivalent thickness

7. a PEC sheet

8. CST copper surface

The various conductivity methods are compared to CST and measured data, in Figure 75, and summarized in Table 3. The gain of the antennas simulated using HFSS are shown in Figure 76 and summarized in Table 3.

Figure 75 – Comparison of simulation and measured data for the antenna with 9mm long, 1mm wide slots in the patch surface.
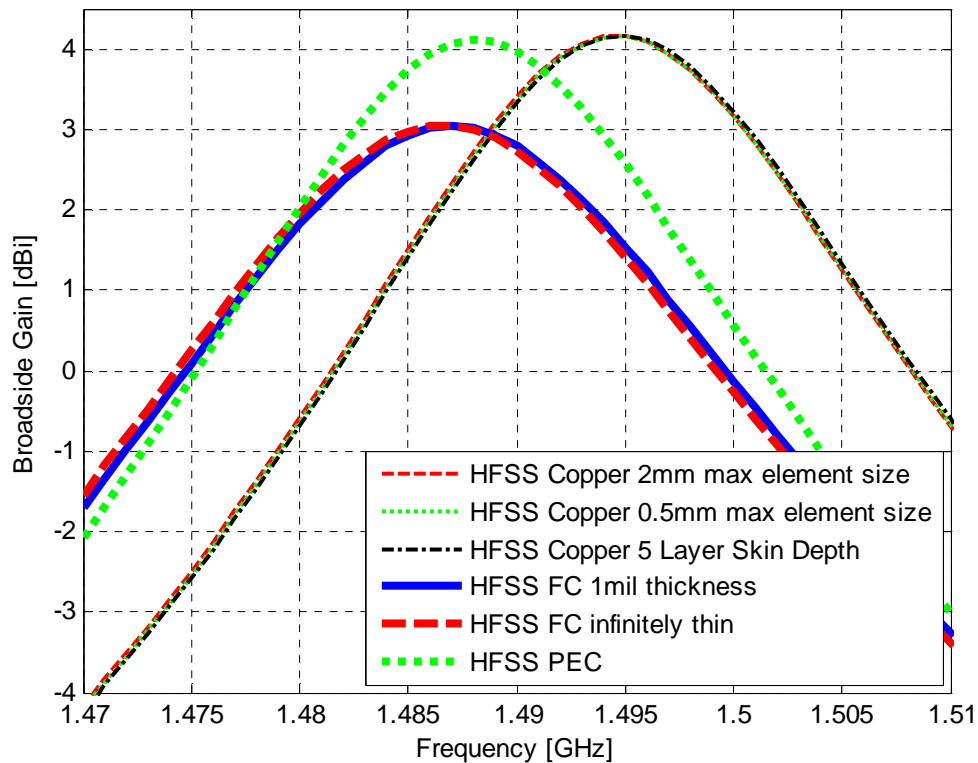
Figure 76 - Comparison of HFSS simulation gains for the antenna with 9mm long, 1mm wide slots in the patch surface.

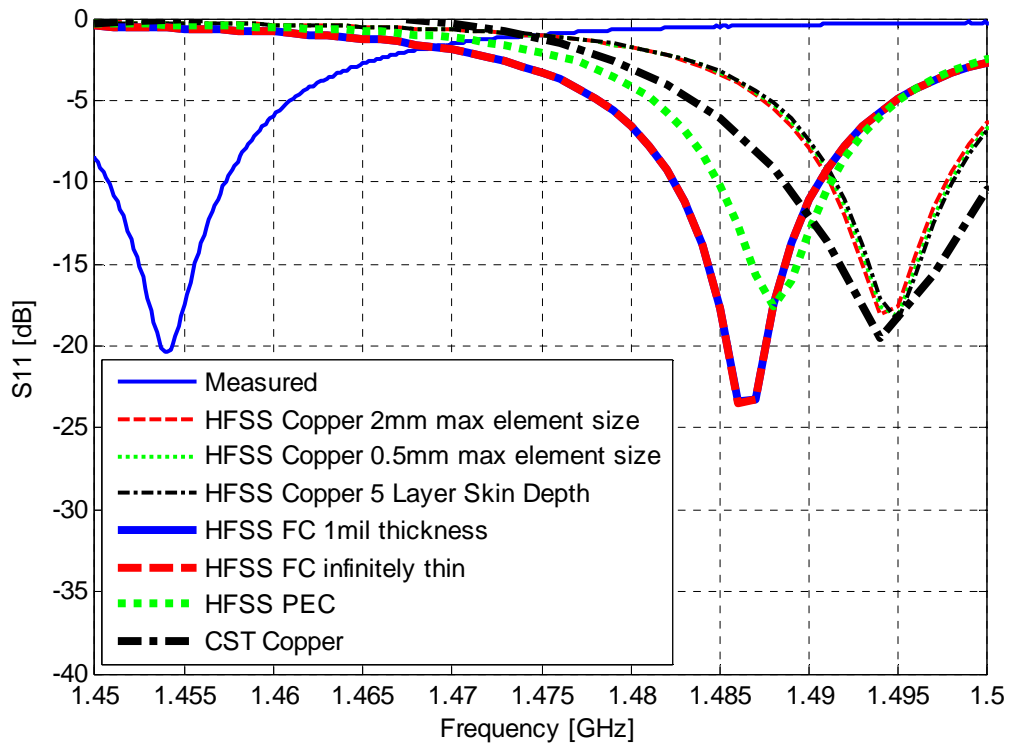| Solution Method		B [MHz]	fo [GHz]	Max Gain [dB]	Memory	# Tetrahedra	Solution Time hr:min:sec
	Measured	7	1.454				
HFSS	Copper*	7	1.494	4.1	1.98GB	31,940	0:47:08
	Copper**	7	1.494	4.1	3.58GB	40,852	1:52:36
	Copper - 5 layer skin depth*	7	1.495	4.1	3.15GB	34,736	1:45:23
	FC infinite thin*	9	1.487	3	2.5GB	36,031	1:02:19
	FC 1mil thickness*	9	1.488	3	3.55GB	54,704	2:55:01
	PEC	6	1.488	4.2	1.52GB	23,210	0:26:52
	CST	11	1.494				

Table 3 – Summary of comparison between simulated and measured data using different HFSS conductivity settings. * indicates 2mm maximum element size, **indicates 0.5mm maximum element size. All simulations run on 64 bit WinXP, 2.4GHz Intel Core 2 Duo system (two active cores) with 4GB of RAM.

All of the simulated resonant frequencies are within 8MHz, which is good agreement

amongst the different methods. All of the simulation methods show a resonant frequency

on the order of 40MHz higher than that measured, which is within 3%. This offset in

resonant frequency is also shown for many slot lengths, in section 3.2.1. One explanation

might be tolerances in the milling process that was used to fabricate the antennas.

The simulated bandwidths are all within a few MHz of the measured antenna.

The CST bandwidth is greater than the HFSS simulations, mainly due to the time domain

solver used and the difficulties that arise when simulating high Q resonant structures.

The infinitely thin finite conductivity layer showed the highest bandwidth out of the

HFSS simulations, while the PEC simulation had the lowest. Regardless, these

bandwidth values are all very close, and once again the computational costs for the

various conductivity methods do not produce a benefit for these antenna structures.

The maximum gain values vary between 4dBi for the PEC and copper cases and

3dBi for the finite conductivity cases, shown in Figure 76. The difference in efficiency is

also reflected in the bandwidths, where the finite conductivity cases show an increased

bandwidth compared to the PEC and copper cases. The finite conductivity boundary

condition results in too much loss on the patch, more than what is expected with a copper

surface.

Considering the results of the large microstrip patch antenna on low permittivity

material, and the small slotted patch antenna on TMM10, for this study it was determined

that modeling using PEC surfaces suffices in predicting the performance of the antennas

while using less computer resources. Throughout this thesis, all simulation results use PEC patch surfaces.

Size of Radiating Air Volume

Finally, concern was raised over size of the radiation air box volume used in the HFSS simulations and the impact on antenna performance.   The antenna in Figure 74 was simulated for an air box of volume 2a×2a×a, as shown in Figure 77. Ansoft HFSS recommends a radiating box that extends at least $\lambda_o / 4$ from the structure when using the radiation boundary condition.

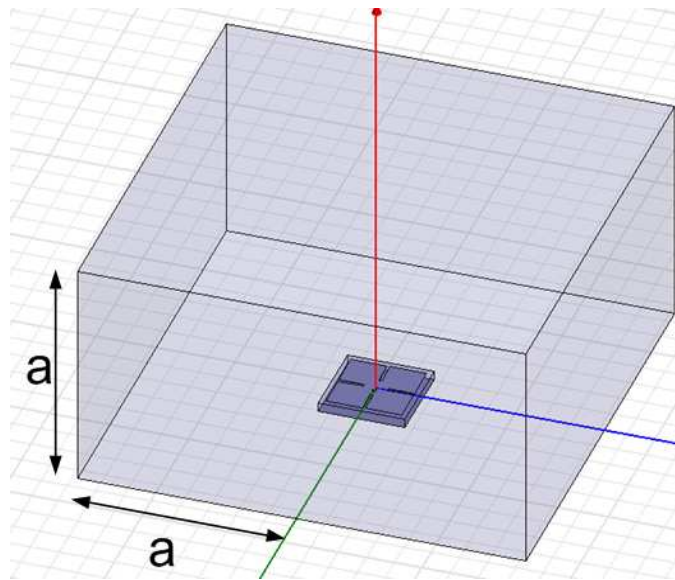**Figure 77** – 27×27mm patch antenna with four 9mm long, 1mm wide slots on TMM10 substrate of size 31×31×3.175mm, with an air box of size 2a×2a×a.

The results of the simulations are shown in Figure 78. For a small air box where a = 30mm, which places the radiating boundary at approximately $\lambda_o / 8$ from the antenna structure, the impedance match of the antenna is shown to suffer, although the -10dB

bandwidth is nearly the same as the other cases. As the air box size a is increased, the

impedance match is approximately the same for each simulation.

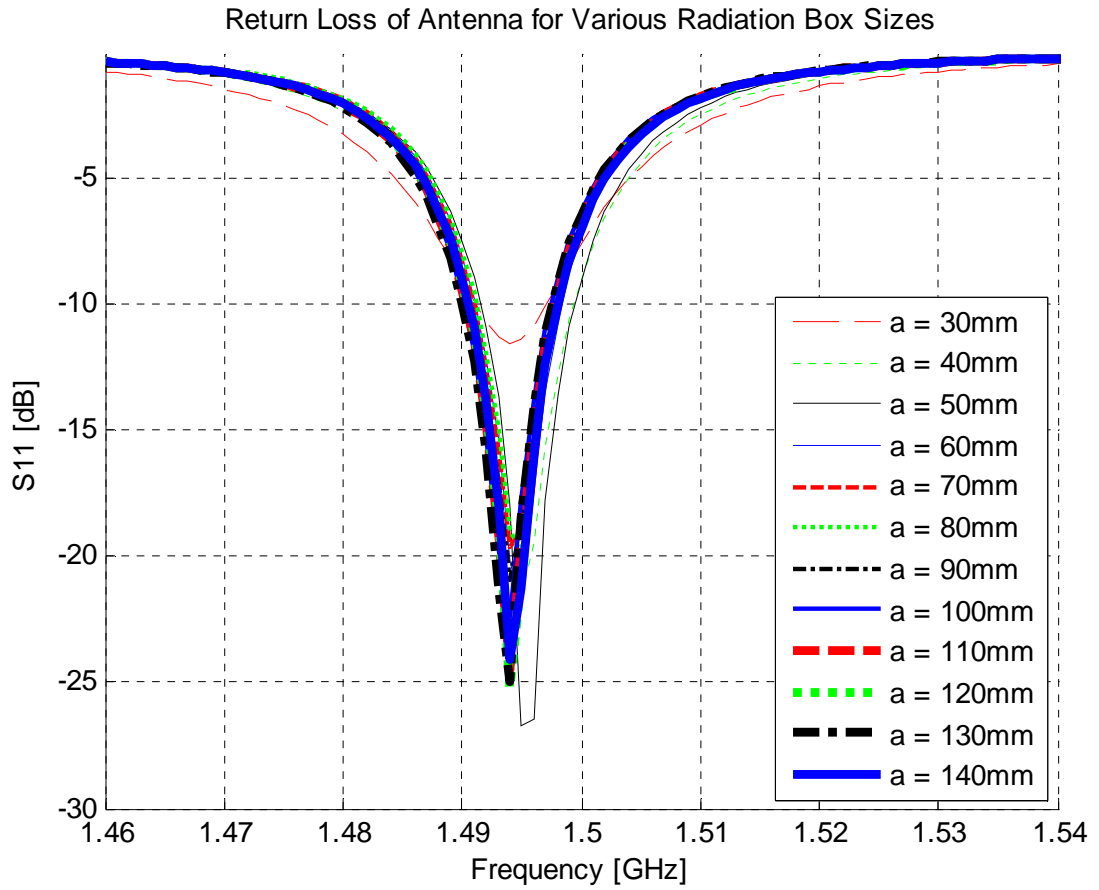**Figure 78** – Simulated return loss for air box volumes of size a=30mm to a=140mm.

For all simulations in this study, an air box of at least 160×160×80mm was used to ensure

a large enough distance between the antenna and the radiation boundary.

APPENDIX D

SLOT MAGNETIC FIELD VECTOR PLOTS

The Ansoft HFSS simulations allow for visualization of the fields on the antenna, which were used to observe the effect of the slots on the fields. Specifically, the magnetic field (H) was of interest in the slot, as well as the currents on the patch surface supporting this magnetic field. These fields are shown in Figure 79, Figure 80 and Figure 81.
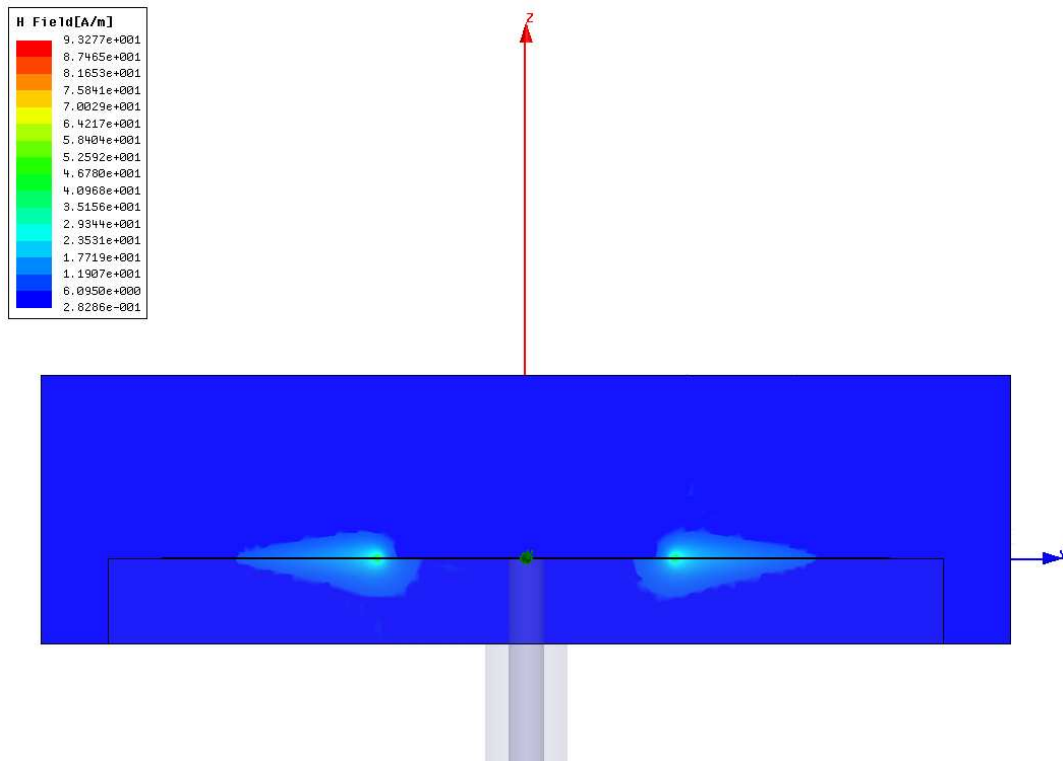

Figure 79 - Plot of the magnitude of the H field at x=0 plane of the patch in Figure 34b, showing the concentration of field in the slots.

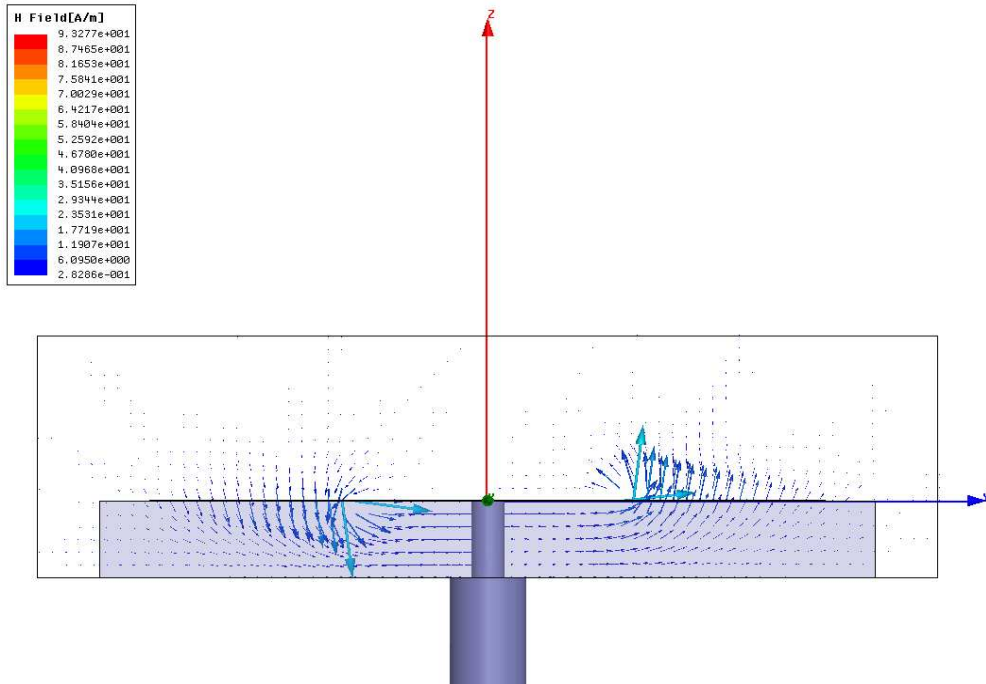**Figure 80** - Vector field plot of the magnetic field in the x=0 plane of the patch in Figure 34b, showing the field penetrating the patch through the slot.
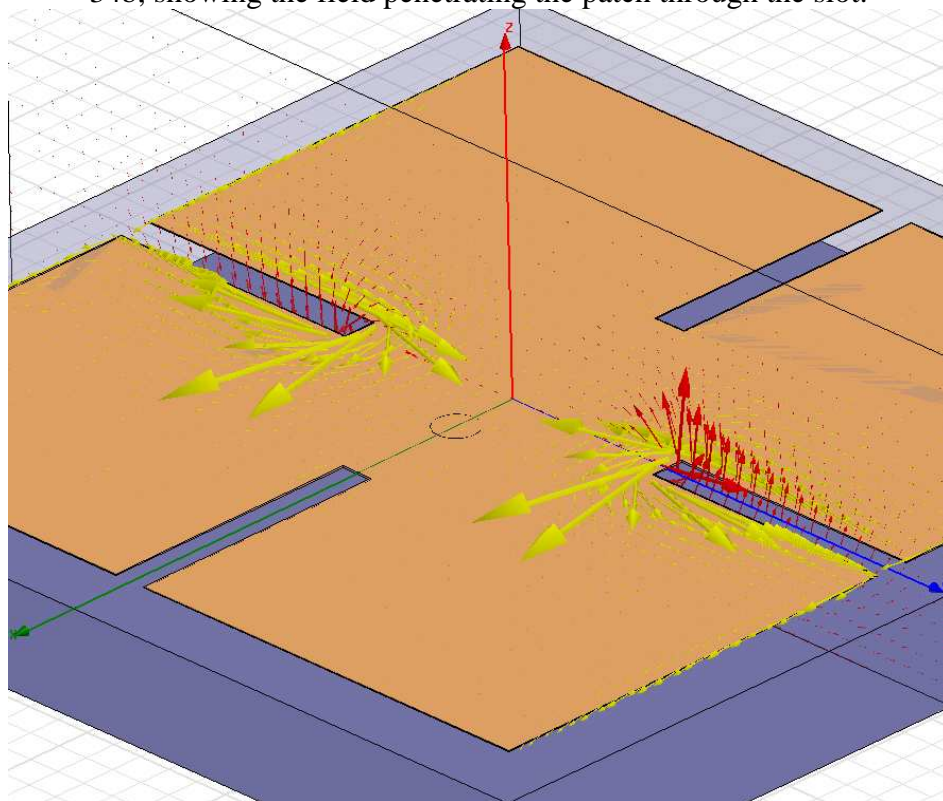

Figure 81 - Vector plot showing the currents (YELLOW) on the patch surface around the slots, and the magnetic field (RED) inside the slot. This shows the concentration of currents at the end of the slot producing the strongest magnetic field.

MEASURED SLOTTED PROTOTYPE ANTENNAS

Six antennas were fabricated at UMASS Amherst in order to validate the studies performed on the slot loading of the patch antennas. The antennas were milled on 31×31×3.175mm TMM10 substrates, with 2oz copper plating on both sides of the substrate material. The antennas were probe feed using SMA connectors, and all of the antennas were mounted on 12×12" metallic ground planes for impedance measurements, and a pattern measurement was taken for the patch antenna with 9mm long, 1 mm wide slots.
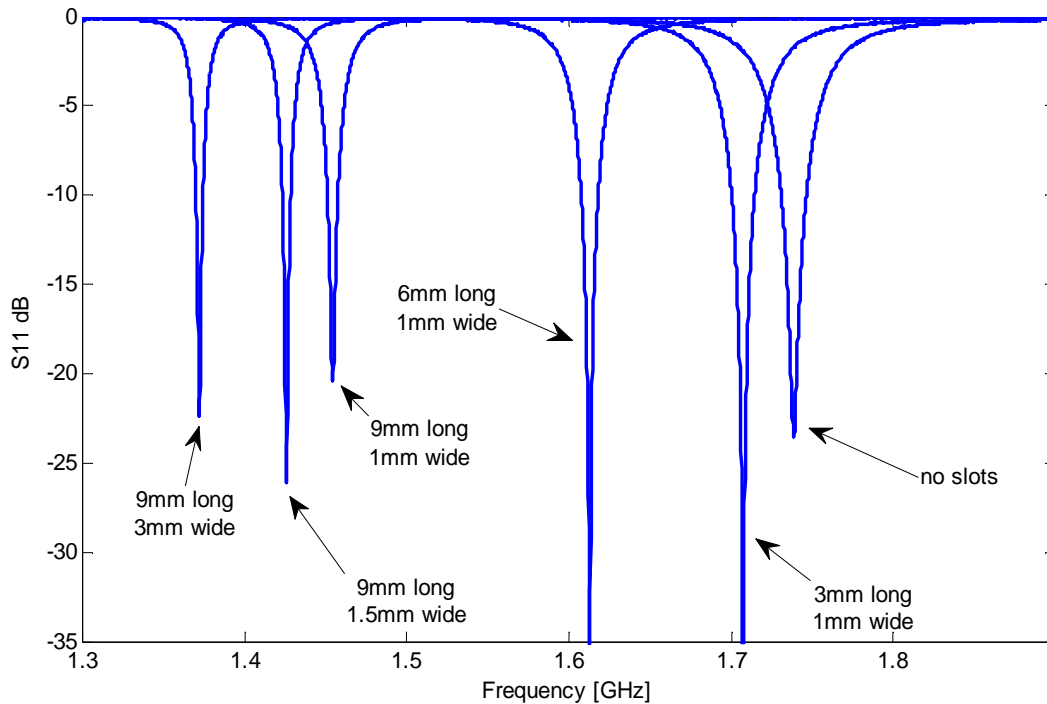
Figure 82 - Measured return loss for the 6 prototype slotted antennas. The dimension on the first line of each label denotes the slot length, and the second line denotes the slot width. All antennas were mounted on a 12×12" ground plane.

Figure 83 - Built 27×27mm Patch Antenna on 31×31×3.175mm TMM10 substrate, with no slots.

Figure 84 - Built 27×27mm Patch Antenna on 31×31×3.175mm TMM10 substrate, with 3mm long, 1mm wide slots.

Figure 85 - Built 27×27mm Patch Antenna on 31×31×3.175mm TMM10 substrate, with 6mm long, 1mm wide slots.

Figure 86 - Built 27×27mm Patch Antenna on 31×31×3.175mm TMM10 substrate, with 9mm long, 1mm wide slots.

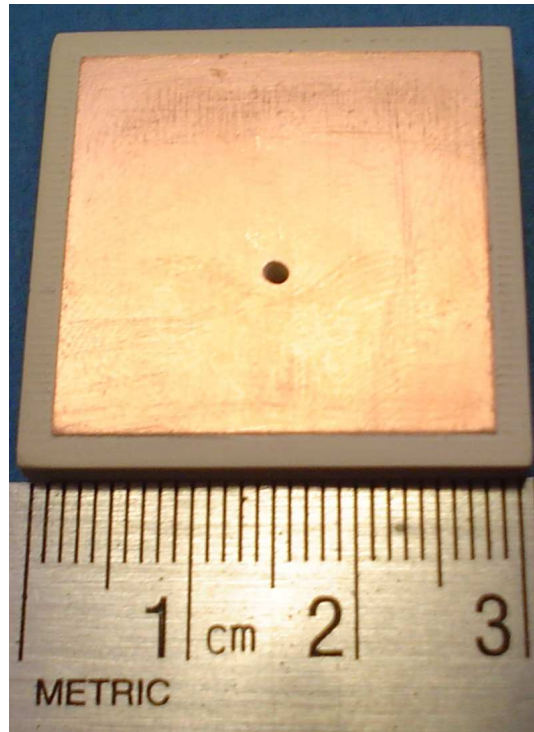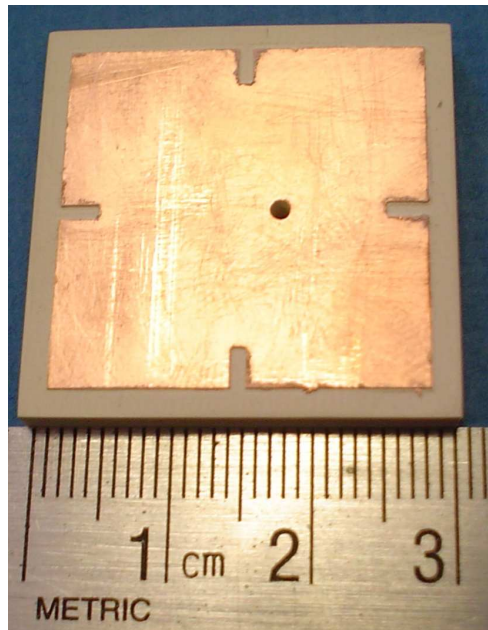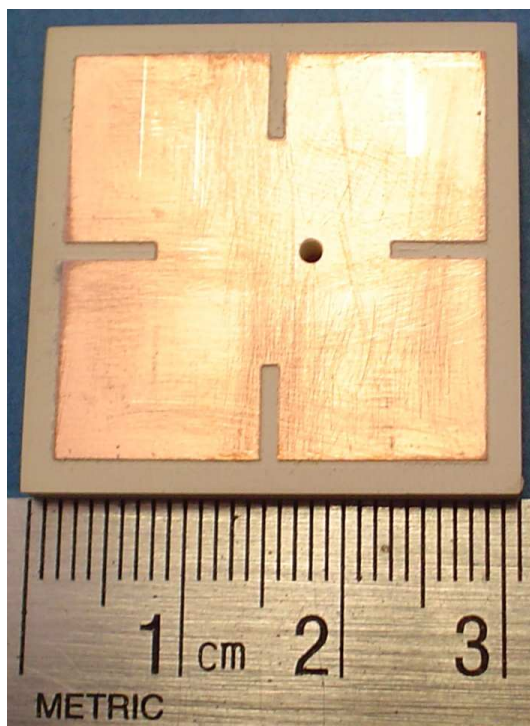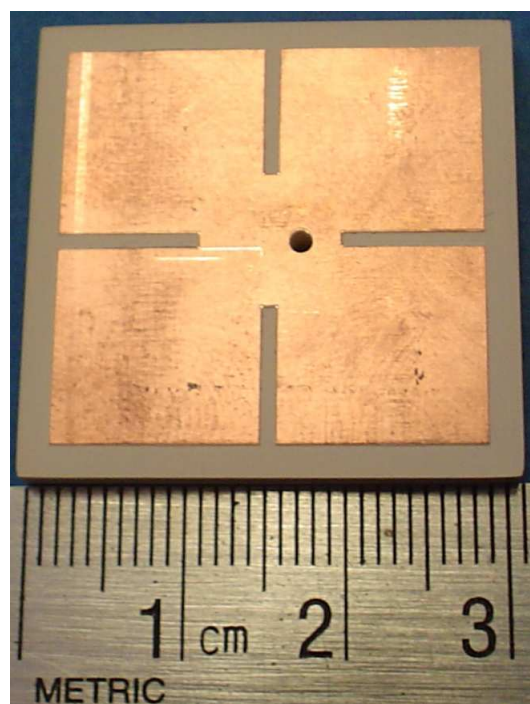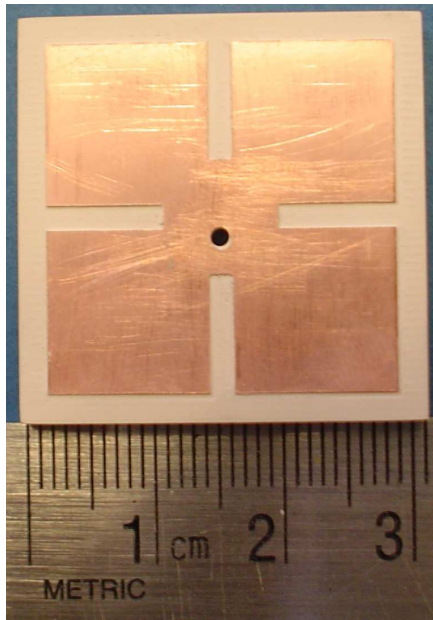**Figure 87** - Built 27×27mm Patch Antenna on 31×31×3.175mm TMM10 substrate, with 9mm long, 1.5mm wide slots.
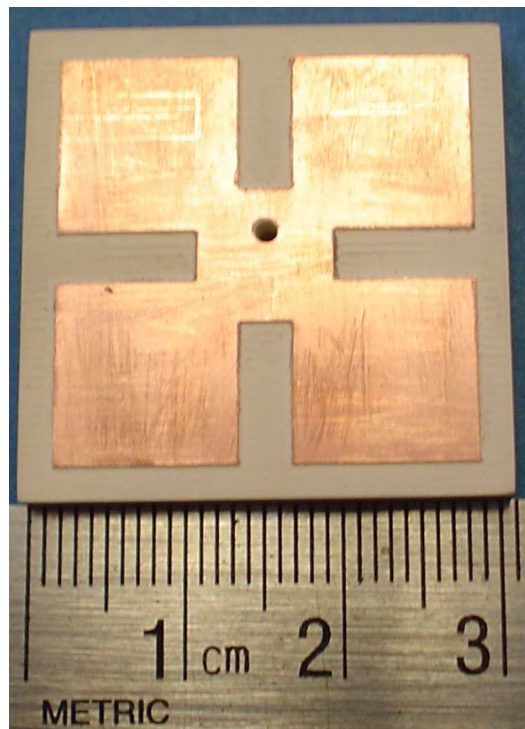
Figure 88 - Built 27×27mm Patch Antenna on 31×31×3.175mm TMM10 substrate, with 9mm long, 3mm wide slots.

Also, radiation patterns were measured for the antenna shown in Figure 86. The

far-field range at UMASS Amherst is not equipped with standard gain horns at 1.5GHz,

so a 66×85mm (L×W) patch was fabricated on 125mil thick Rogers 5880 substrate

material to be used as the transmit antenna, and is shown in Figure 89 and Figure 90.
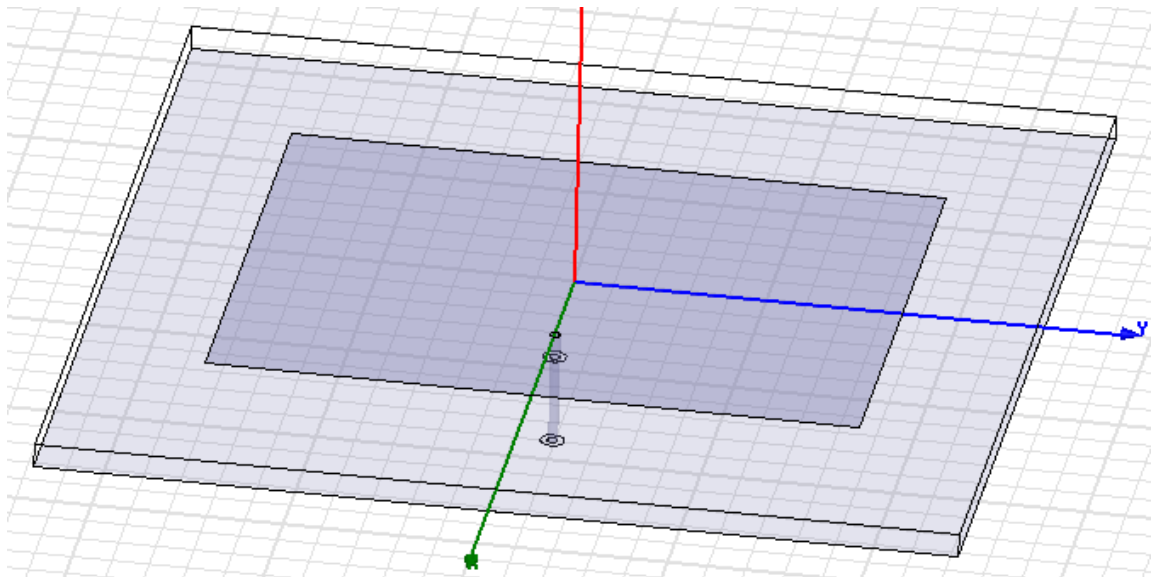
Figure 89 - Patch antenna built for use as transmit antenna in far-field range. Patch is 66×85mm on a 120×120×3.175mm Rogers 5880 substrate.

Figure 90 - Built transmit antenna for use in the far-field range.

The antenna used for transmit was designed to have the same resonant frequency

as the slotted patch with four 9mm long, 1mm wide slots, and was mounted on a 12×12"

ground plane. The patterns for the antenna for the antenna with 9mm, 1mm wide slots

are shown in Figure 91 and Figure 92, the principle plane pattern cuts.
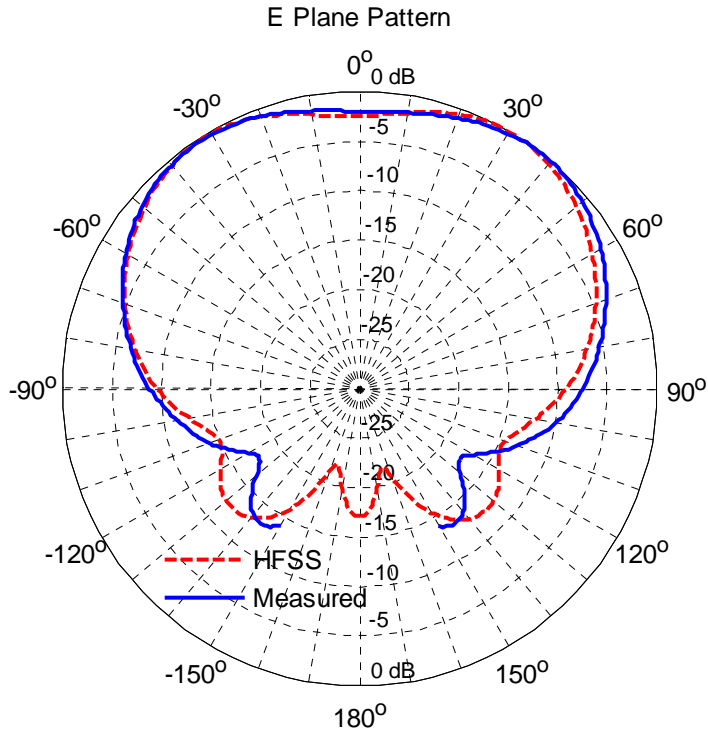
E Plane Pattern

Figure 91 - E-plane pattern for the slotted patch antenna with four 9mm long, 1mm wide slots.
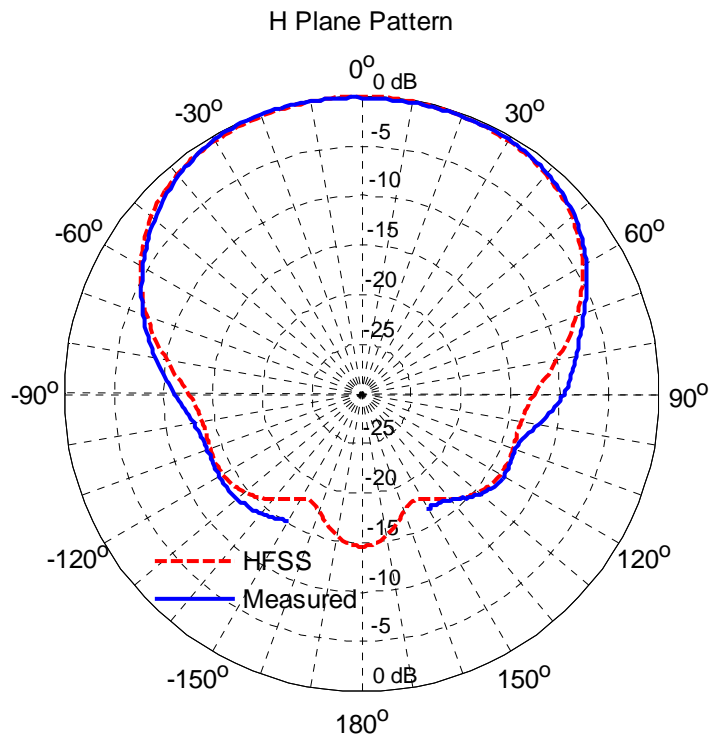
H Plane Pattern

Figure 92 - H-plane pattern for the slotted patch antenna with four 9mm long, 1mm wide slots.

Figure 93 – Patch with four 9mm long, 1mm wide slots mounted on AUT positioner in the far field range. The ground plane is 12×12".
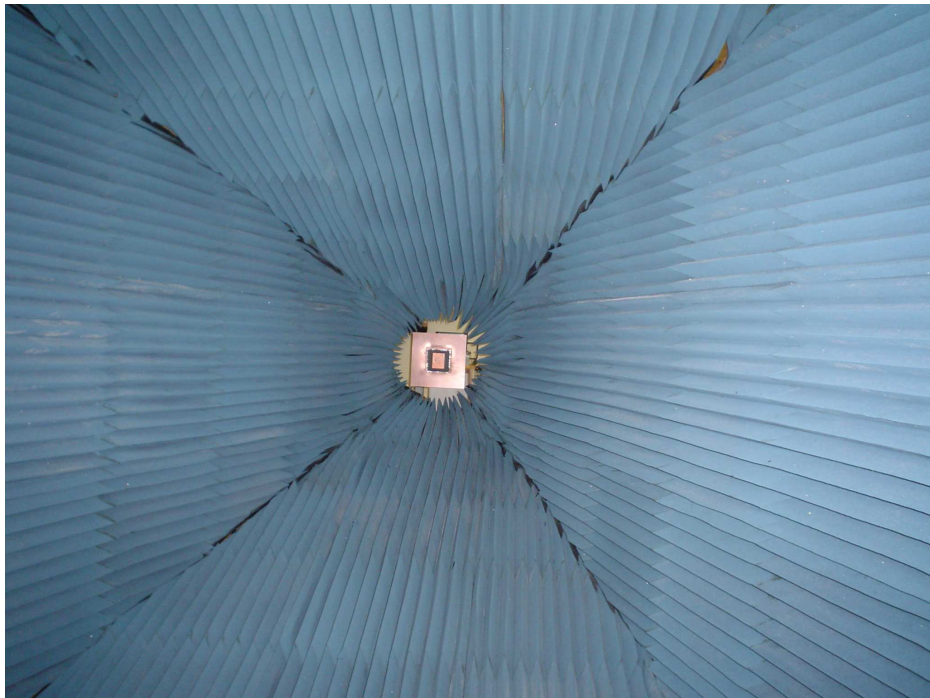
Figure 94 - Transmit antenna mounted on tapered end of the far field range.

APPENDIX F

EQUIVALENT CIRCUIT FOR WIDE SLOTS

As the slot width increases, the circuit model is changed to take into account the

capacitance loading both between the patch and the ground and across the slot itself,

Figure 95.
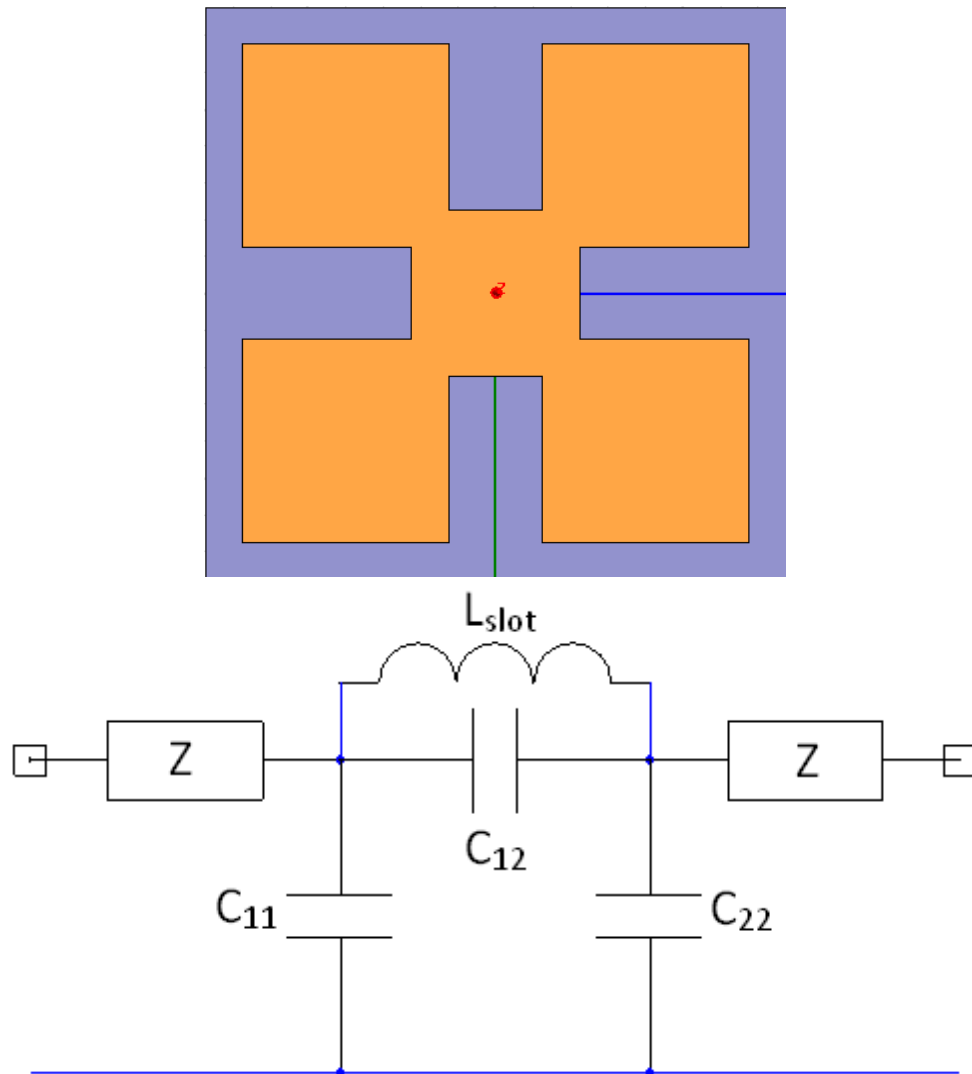
Figure 95 - Transmission line model for slot cut in a patch surface when the width of the slot is much greater than the substrate thickness. The patch shown is on a 3mm thick substrate with 5mm wide slots.

CAPACITOR LOADED PATCH ANTENNA

The transmission line model is useful for predicting the resonant frequency

performance of a microstrip antenna, and a modified form from section 3.1 is presented.
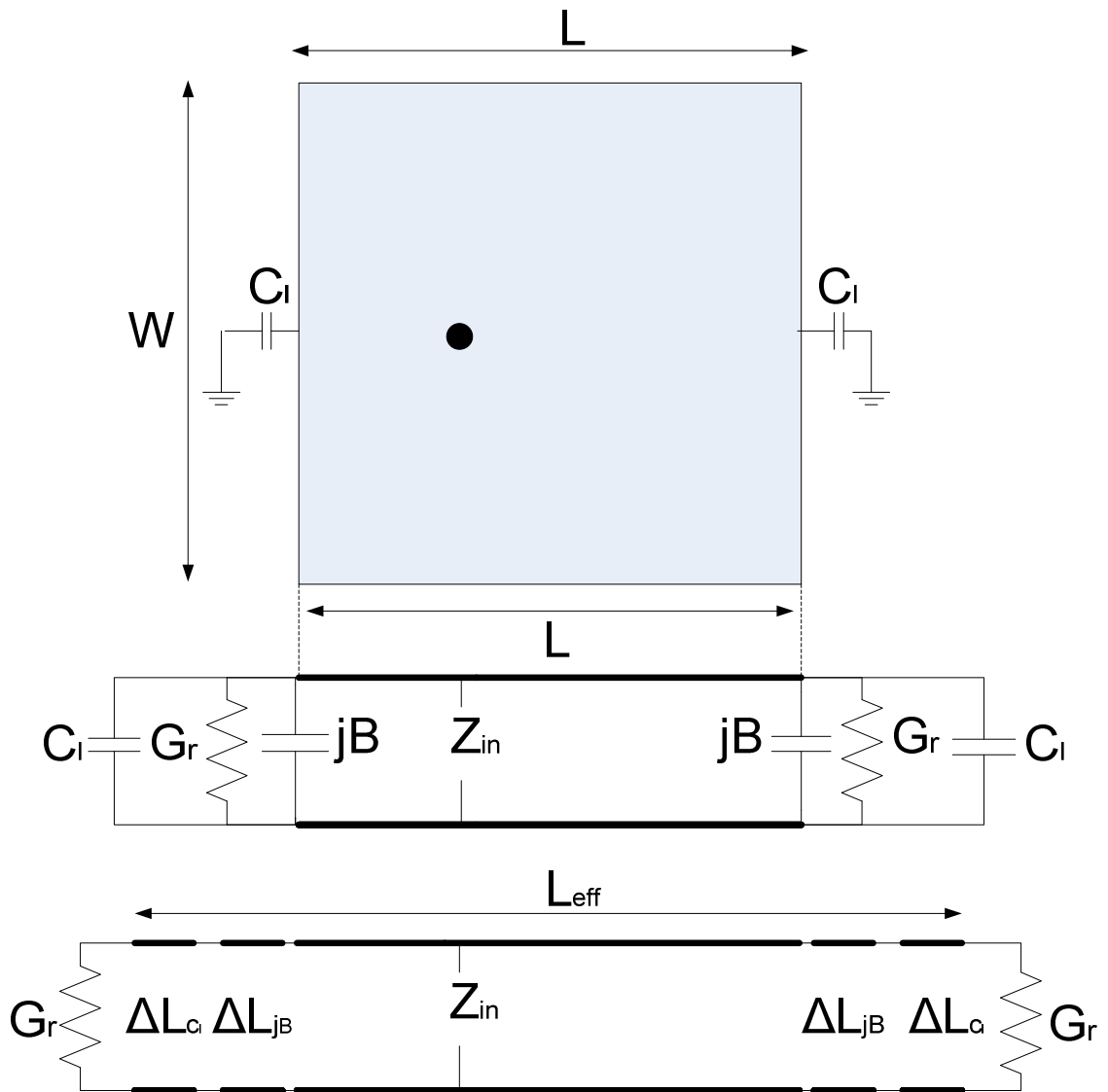
Figure 96 - Transmission line model modified with the addition of a 2 lumped capacitors on the radiating slots of the microstrip patch antenna.

The modified model in Figure 96 allows for calculation of the resonant frequency of the antenna when the radiating edges are loaded with lumped capacitors, connected between the patch and ground. The analysis makes use of equations 3.2 and 3.3, as well as the equations included specifically for capacitive loading on the radiating edges of the patch [2].

The equivalent length added by the shunt capacitance can be found using equation G.1 [32].

$$\Delta L_{C_l} = \frac{c}{\omega\sqrt{\varepsilon_e}} \tan^{-1}\left(\omega C_l Z_o\right) \approx \frac{c C_l Z_o}{\sqrt{\varepsilon_e}}, \qquad \omega C_l Z_o \ll 1 \qquad \text{(G.1)}$$

Where Z_o is defined as [9]

$$Z_o = \frac{377}{\sqrt{\varepsilon_{reff}}\left\{\dfrac{W}{t} + 1.393 + 0.667\ln\left(\dfrac{W}{t} + 1.444\right)\right\}} \qquad \text{(G.2)}$$

and the new effective length is found using equation G.3.

$$L_{eff} = L + 2\Delta L_{jB} + 2\Delta L_{C_l} \qquad \text{(G.3)}$$

Note that ΔL_{jB} is the same ΔL calculated in equation 3.4. Finally, the resonant frequency is found using equation 3.5, included again as G.4.

$$f_r = \frac{c_o}{2\left(L_{eff}\right)\sqrt{\varepsilon_{reff}}} \qquad \text{(G.4)}$$

For a square patch with L=W=27mm on an infinite substrate of TMM10 ($\epsilon_r = 9.2$) of thickness t = 3mm, the resonant frequency can be approximated using the analytic equations, with shunt capacitances ranging from 0-10pF.
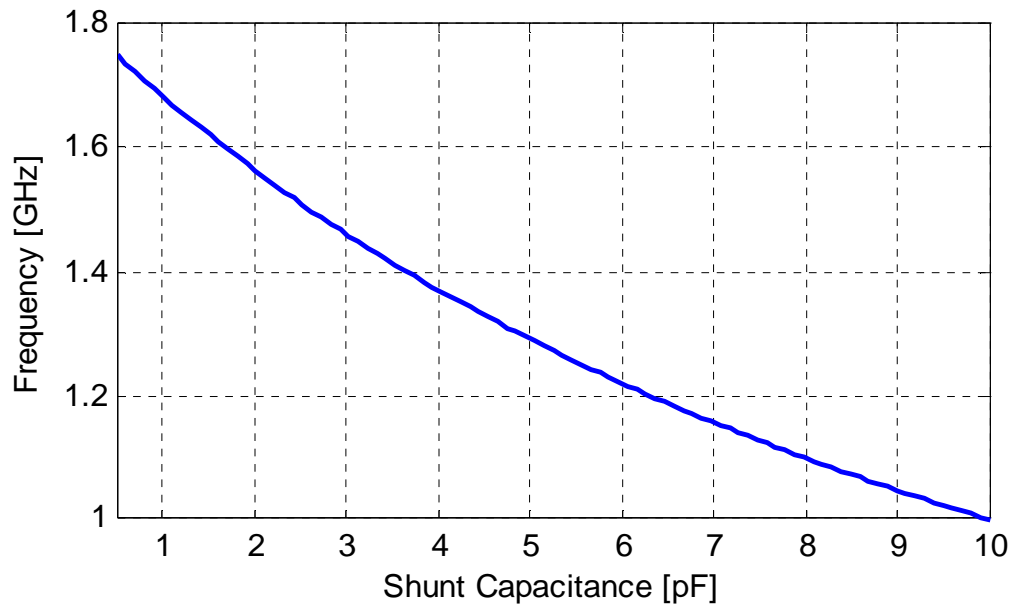
Figure 97 – Resonant frequency behavior for varying the value of the lumped loading capacitor, calculated using the modified transmission line model shown in Figure 96.

APPENDIX H

EFFECT OF SUBSTRATE THICKNESS ON RESONANT FREQUENCY

Using equations 3.2-3.5, the resonant frequency of a 27×27mm square patch (Figure 98) on an infinite substrate of TMM10 ($\epsilon_r = 9.2$) is calculated for various thicknesses t, shown in Figure 99.
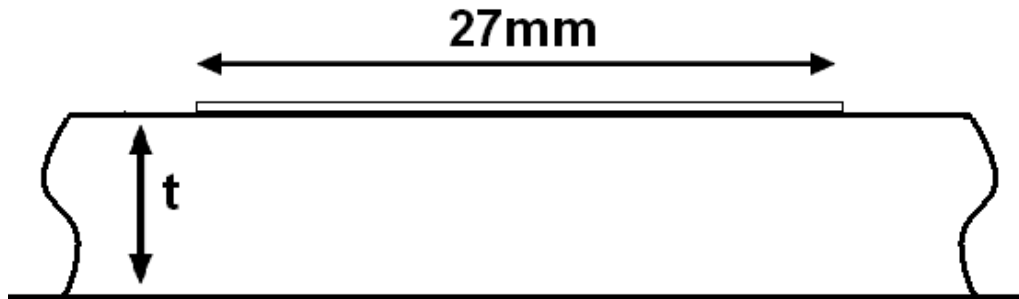
Figure 98 - Square 27×27mm patch antenna on an infinite substrate, thickness t, of TMM10 dielectric material.
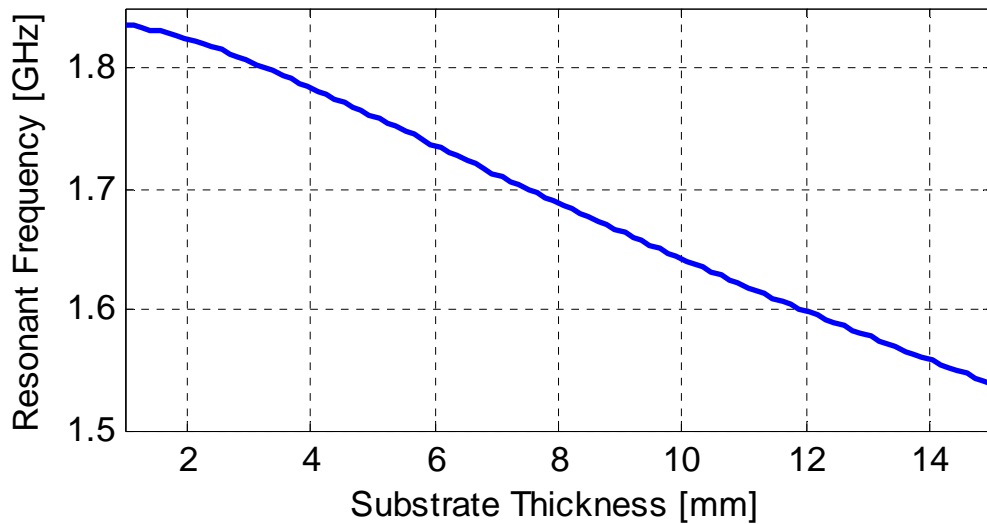
Figure 99 - Change in resonant frequency with substrate thickness for 27×27mm patch on an infinite substrate of TMM10 dielectric material.

APPENDIX I

VERTICAL WALL LOADED ANTENNA

An additional example of capacitive loading is a patch antenna loaded with bent

sections in the patch surface. This antenna was explored and shows another application

of the capacitive loading without using lumped element capacitors. The antenna is

formed by bending down the edges of a patch to lower the resonant frequency for one of

the fundamental (TM_{010}, TM_{100}), modes on each of the patches.

- Flat plate along patch's radiating
edges makes the patch look longer by
adding a capacitor, allowing patch to
resonate at a lower frequency

Figure 100 - Capacitively loaded antenna utilizing bent capacitive sections of the patch to
generate a lower resonant frequency.

L1 and L2 were then split between the two stacked patches, as shown in Figure 101. The

combination of resonant mode directions allowed for circular polarization to be obtained

when the ports were fed in quadrature.

By feeding the antenna with 0 degree phase shift on port 1 and 90 degree phase shift on port 2, LHCP circular polarization is achieved:

$$(L2_x + jL1_y) + (L1_x + jL2_y) = L1_x + jL1_y + L2_x + jL2_y$$

L1 LHCP   L2 LHCP
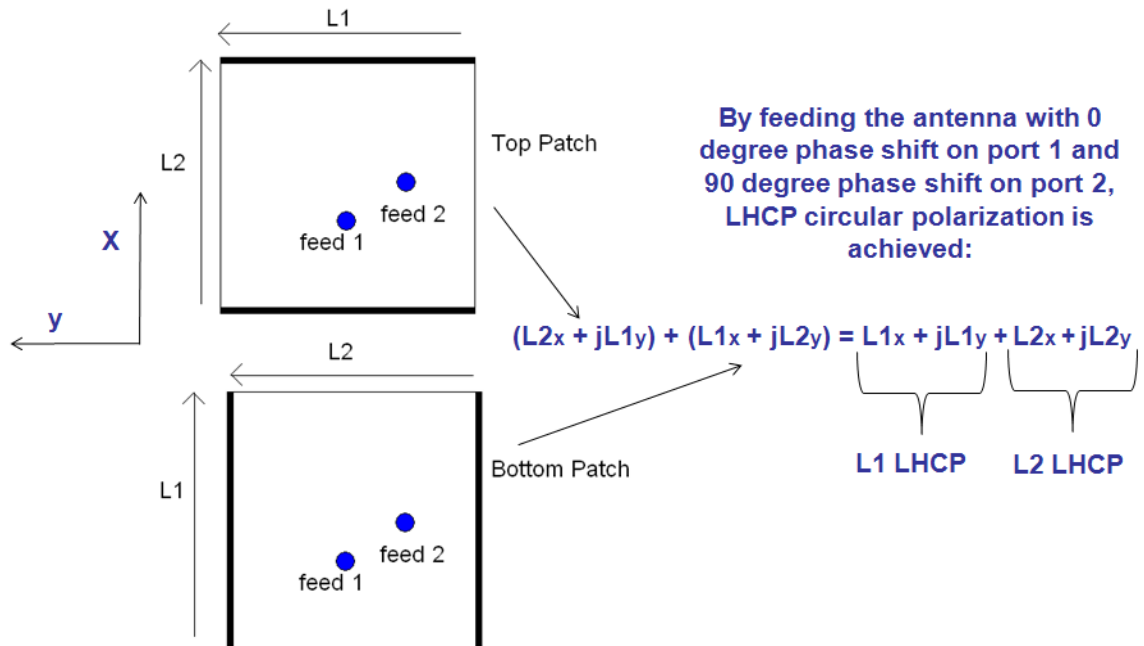
Figure 101 - Diagram of the tuning of both bands in both orthogonal directions when both patches were excited. Shown are the field components at L1, L2 bands in the x, y directions and how when fed with 90° phase difference (j) generate proper CP at both bands.
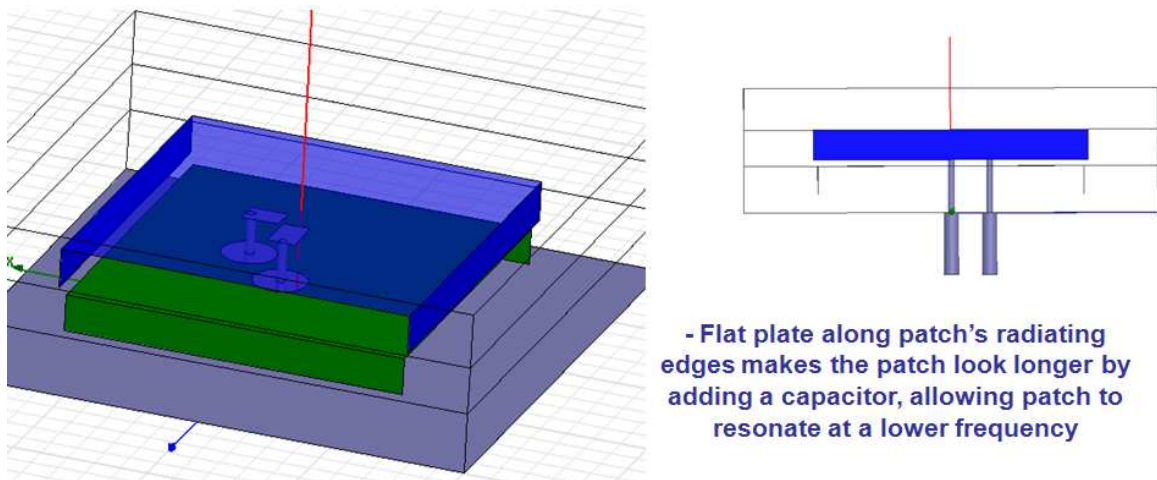
Ultimately, many tuning difficulties arose due to the asymmetries in the structure, which was very sensitive to changes in any of the feed positions or dimensions. The best case return loss tuned for the antenna at L2 is shown in Figure 102. This was obtained only after finely tuning the probe dimensions and placement, which showed large changes in tuning with very small changes in the physical parameters. The main difficulty was tuning each polarization of each band to have the same RL response (to have equal amplitude), where the coupling mechanism is drastically different between the two modes. A proper match in return loss for port 1 and port 2 was not obtained for both L1 and L2 at the same time.

Figure 102 - Return loss of the side wall loaded stacked patch antenna with L-probe feeds.

BIBLIOGRAPHY

[1]   Howell, J., "Microstrip antennas," *Antennas and Propagation, IEEE Transactions on*, vol.23, no.1, pp. 90-93, Jan 1975.
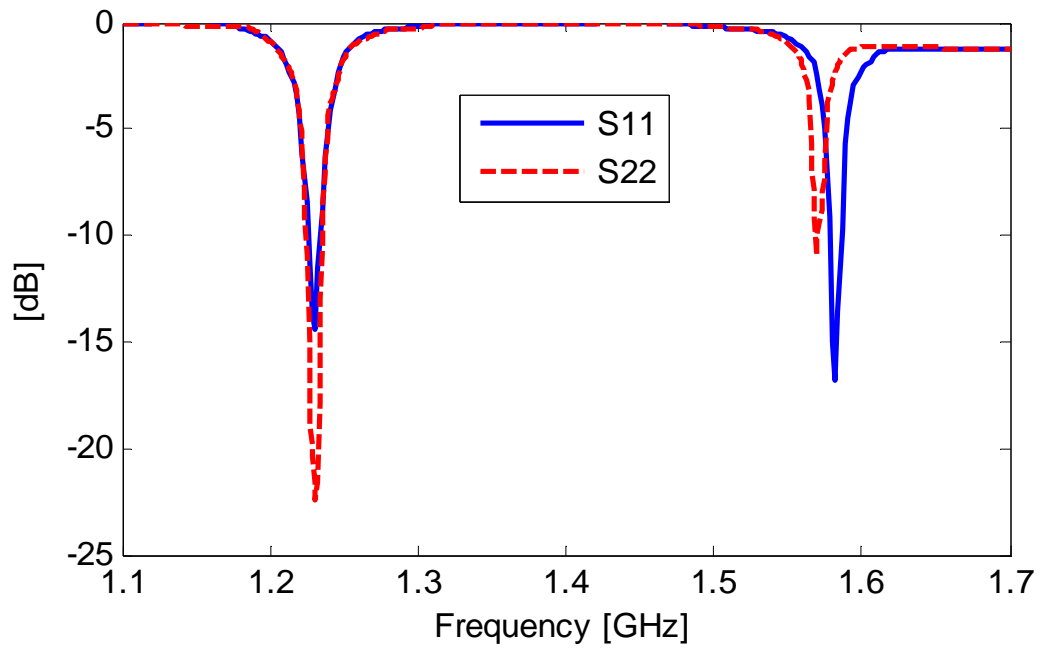
[2]   G. A. Deschamps, "Microstrip microwave antennas," presented at the Third USAF Symp. on Antennas, 1953.

[3]   Pozar, D.M., "Microstrip antennas," *Proceedings of the IEEE*, vol.80, no.1, pp.79-91, Jan 1992.

[4]   C.A. Balanis, "Antenna Theory Antenna Analysis & Design", 2nd edition, John Wiley& Sons, Inc. 1993.

[5]   Enge, P.; Misra, P., "Special Issue on Global Positioning System," *Proceedings of the IEEE*, vol.87, no.1, pp.3-15, Jan 1999.

[6]   Zhou, Y.; Chen, C.-C.; Volakis, J. L., "Dual Band Proximity-Fed Stacked Patch Antenna for Tri-Band GPS Applications," *Antennas and Propagation, IEEE Transactions on*, vol.55, no.1, pp.220-223, Jan. 2007.

[7]   Yijun Zhou; Kiziltas, G.; Koulouridis, S.; Volakis, J.L., "A miniature four-arm antenna for tri-band GPS applications," *Antennas and Propagation Society International Symposium, 2005 IEEE* , vol.3A, no., pp. 872-875 vol. 3A, 3-8 July 2005.

[8]   Yong-Xin Guo; Hwee Siang Tan, "New compact six-band internal antenna," *Antennas and Wireless Propagation Letters* , vol.3, no., pp. 295-297, 2004.

[9]   D. M. Pozar, *Microwave Engineering*, 3rd ed. New York:Wiley, 2005.

[10]   J. D. Krauss, *Antennas*, 3rd ed. New York: McGraw-Hill, 2002.

[11]   R. F. Harrington, *Time-Harmonic Electromagnetic Fields* (IEEE: Wiley-Interscience, New York, 2001).

[12]   Collin, R.; Rothschild, S., "Evaluation of antenna Q," *Antennas and Propagation, IEEE Transactions on*, vol.12, no.1, pp. 23-27, Jan 1964.

[13]   Wheeler, H.A., "Fundamental Limitations of Small Antennas," *Proceedings of the IRE* , vol.35, no.12, pp. 1479-1484, Dec. 1947.

[14]   L. J. Chu, "Physical limitations on omni-directional antennas," *J. Appl. Phys.*, vol. 19, pp. 1163–1175, Dec. 1948.

[15] McLean, J. S., "A re-examination of the fundamental limits on the radiation Q of electrically small antennas," *Antennas and Propagation, IEEE Transactions on* , vol.44, no.5, pp.672-, May 1996.

[16] Best, S.R. "A Study of the Performance properties of small antennas," *2007 Antenna Applications Symposium, Allerton Park, Monticello, Illinois,* pp. 193-211 , 18-20 September, 2007.

[17] Yaghjian, A.D., "Internal Energy, Q-Energy, Poynting's Theorem, and the Stress Dyadic in Dispersive Material," *Antennas and Propagation, IEEE Transactions on* , vol.55, no.6, pp.1495-1505, June 2007.

[18] Yaghjian, A.D.; Best, S.R., "Impedance, bandwidth, and Q of antennas," *Antennas and Propagation, IEEE Transactions on* , vol.53, no.4, pp. 1298-1324, April 2005.

[19] Geyi, W., "Physical limitations of antenna," *Antennas and Propagation, IEEE Transactions on* , vol.51, no.8, pp. 2116-2123, Aug. 2003.

[20] Hum, S.V.; Chu, J.; Johnston, R.H.; Okoniewski, M., "Improving the bandwidth of microstrip patch antennas using resistive loading," *Antennas and Propagation Society International Symposium, 2003. IEEE* , vol.2, no., pp. 276-279 vol.2, 22-27 June 2003.

[21] Karmakar, N.C., "Investigations into a cavity-backed circular-patch antenna," *Antennas and Propagation, IEEE Transactions on* , vol.50, no.12, pp. 1706-1715, Dec 2002.

[22] Chien-Jen Wang and Wen-Tsai Tsai, "Small Microstrip Antennas for Mobile Communications," *Microwave and Optical Technology Letters,* vol.43, no.3, pp. 207-210, Nov 2004.

[23] Yijun Zhou,; Chi-Chih Chen,; Volakis, John L., "Tri-band miniature GPS Array with a single-fed CP antenna element," *Antennas and Propagation International Symposium, 2007 IEEE* , vol., no., pp.3049-3052, 9-15 June 2007.

[24] Munson, R., "Conformal microstrip antennas and microstrip phased arrays," *Antennas and Propagation, IEEE Transactions on [legacy, pre - 1988]* , vol.22, no.1, pp. 74-78, Jan 1974.

[25] Hammerstad, Erik O., "Equations for Microstrip Circuit Design," *European Microwave Conference, 1975. 5th* , vol., no., pp.268-272, Oct. 1975.

[26]   Hwang, Y.; Zhang, Y.P.; Zheng, G.X.; Lo, T.K.C., "Planar inverted F antenna loaded with high permittivity material ," *Electronics Letters* , vol.31, no.20, pp.1710-1712, 28 Sep 1995.

[27]   Hoefer, W.J.R., "Equivalent Series Inductivity of a Narrow Transverse Slit in Microstrip," *Microwave Theory and Techniques, IEEE Transactions on* , vol.25, no.10, pp. 822-824, Oct 1977.

[28]   Zachou, V.; Mayridis, G.; Christodoulou, C.G.; Chryssomallis, M.T., "Transmission line model design formula for microstrip antennas with slots," *Antennas and Propagation Society International Symposium, 2004. IEEE* , vol.4, no., pp. 3613-3616 Vol.4, 20-25 June 2004.

[29]   Zhang, X.; Yang, F., "Study of a slit cut on a microstrip antenna and its applications," *Microwave and Optical Technology Letters,* vol.18, no.4, pp.297-300, *1998.*

[30]   Benedek, P.; Silvester, P., "Equivalent Capacitances for Microstrip Gaps and Steps," *Microwave Theory and Techniques, IEEE Transactions on* , vol.20, no.11, pp. 729-733, Nov 1972.

[31]   Aberle, J.T., "On the use of metallized cavities backing microstrip antennas," *Antennas and Propagation Society International Symposium, 1991. AP-S. Digest* , vol., no., pp.60-63 vol.1, 24-28 Jun 1991.

[32]   P. Bhartia and I. J. Bahl, "Frequency agile microstrip antennas," *Microwave J.,* vol. 25, pp. 67-70, Oct. 1982.